Clean Surfaces, Dirty Water:

Topography and Chemistry in the Wetting of Superhydrophobic Surfaces by Pure Liquids and Surfactant Solutions

by 

Andrew James Barnabas Milne

A THESIS
SUBMITTED TO
THE FACULTY OF GRADUATE STUDIES AND RESEARCH
IN PARTIAL FULFILMENT OF
THE REQUIREMENTS FOR THE DEGREE OF
MASTER of SCIENCE

DEPARTMENT OF MECHANICAL ENGINEERING
UNIVERSITY of ALBERTA
EDMONTON, ALBERTA

Spring 2008

Your file Votre référence
ISBN: 978-0-494-45858-7
Our file Notre référence
ISBN: 978-0-494-45858-7

Abstract

The effects of surface chemistry and topography on the wetting of smooth and superhydrophobic surfaces (SHS) by pure liquids and surfactant solutions were studied. SHS of aluminum, PTFE and alkyl ketene dimmer (AKD), and smooth coated silicon wafer were probed with four pure liquids (surface tensions ~27-73 mN/m), and aqueous solutions of sodium dodecyl sulphate, hexadecyltrimethylammonium bromide and n-decanoyl-n-methylglucamine at three concentrations below Critical Micelle Concentration (CMC). Surfaces had either fluorinated or saturated hydrocarbon coatings. Surfaces were characterized by SEM, AFM, and XPS analysis, and wettability was probed using Axisymmetric Drop Shape Analysis. On SHS, surfactant solution advancing contact angles (CA) remained hydrophobic near CMC while results for pure liquids with surface tensions similar to the solutions decreased 20-120°. Solution contact angles on coated silicon were slightly higher than pure liquid contact angles for pure liquid advancing contact angles less than 90°. For low intrinsic CA, the receding CA is zero on most SHS. Dual-scale topography (aluminum) gave higher CA for all pure liquids, with the dense spiked pattern of PTFE next highest. Results were reversed for solutions. It is hypothesized that surfactant films cover the surface pores, promoting 'metastable' Cassie wetting. Saturated hydrocarbon chemistry is shown to give lower advancing and much lower receding CA. The main finding is that dependent on topography, surfaces can remain superhydrophobic for surfactant solutions of high concentration (low surface tension).

To Sarah Andrea Milne,

My love, my life, my wife.

Thank you for all your support, love, and encouragement throughout this time and always.

I love you so much, my words cannot express it.

Preface

The work for this thesis was conducted in two locations. Testing of fluorinated aluminum was done in Dresden, Germany, by the author, at the Leibniz Institute of Polymer Research. Samples of PTFE and aluminum were brought back to Edmonton for further testing, along with fluorinated and uncoated samples of alkyl ketene dimmer as well as coated silicon, by the author at the University of Alberta. This necessitated two sets of surfactant solutions and two experimental rigs. Surface tension measurements were made for each set of solutions and results are presented for each set as applicable.

Acknowledgements

First and foremost, I would like to thank my supervisor, Dr. Alidad Amirfazli, for his help, support, and patience as I have completed this work, and also for all the opportunities he has given me during my time at the University of Alberta.

Second, but no less important, I thank my wife, Andrea, for love, support, and encouragement, and excusal from regular chores during the busy times.

To my family and friends for their support, especially in coming to Edmonton. To my lab mates, who are also friends, in the Surface Engineering and Instrumentation Lab, for all of their help. To all the front of office staff, IT staff, and machine shop technicians at the University of Alberta and the Leibniz Institute of Polymer Research (IPF), for performing small miracles with no complaint.

To Kristian Olsen and all the NanoFab staff for their training and expertise, and to the staff of the Alberta Centre for Surface Engineering Science, for their assistance with characterization. To Barnabas, Nick, and Marta for helping with work.

I wish to thank the Natural Science and Engineering Research Council of Canada (NSERC) for their support (I held a Julie Payette NSERC Post

Graduate Scholarship for the project). I also thank the University of Alberta International Office Research in Germany Award and IPF for financial assistance in conducting research in Dresden. Thanks also to Nicole Petong, Stefan Michel, Frank Simon and others of the Leibniz Institute of Polymer Research, Dresden, Germany, for sample preparation and characterization. Specifically, to the Institut für Werkstoffwissenschaft at the Technical University of Dresden, for the high quality, high magnification SEM images in Figure 2-1 b, c, d, e. Finally, to Pedro J Ramón-Torregrosa for sample characterization.

To all those who have helped in my past schooling, especially Bruce Cameron at S.M.H., Kitchener, and Dr. Beth Weckman at the University of Waterloo. I wouldn't be here if it weren't for you.

Finally, to all the people I've missed. Thank you.

Table of Contents

List of Tables

List of Figures

List of Symbols, Nomenclature and Abbreviations

γ_{xy} – Surface tension between the materials x and y (in this thesis, x, y can be l, v, s denoting liquid, vapor, and solid phases, respectively)

θ – Intrinsic contact angle, thermodynamically derived from Young's Equation

θ_A – Advancing contact angle

θ_C – Cassie contact angle

θ_{CR} – The critical intrinsic contact angle for a transition from the Cassie to the Wenzel wetting state or vice versa

θ_R – Receding contact angle

θ_W – Wenzel contact angle

f – The solid fraction of the surface. A topographical parameter used in the Cassie equation

fluorinated surface - a surface chemistry with CF_3 and CF_2 terminated surface groups

r – The roughness parameter, sometimes called rugosity. A topographical parameter used in the Wenzel equation

ra – average height or centre line average roughness

rq – root mean square roughness

saturated hydrocarbon surface - a surface chemistry with CH_3 and CH_2 terminated surface groups

sccm – standard cubic centimeters per minute

water – ultrapure distilled deionized water (unless otherwise noted)

ADSA – Axisymmetric Drop Shape Analysis

AKD – Alkyl Ketene Dimer

BN – 1-bromonaphthalene

CA – Contact angle

CAH – Contact angle hysteresis

CL – Contact line

CMC – Critical Micelle Concentration

DI – De-ionized

EG – ethylene glycol

HD – Hexadecane

HTAB – hexadecyltrimethylammonium bromide, sometime called cetyltrimethylammonium bromide (CTAB)

MEGA 10 – n-decanoyl-n-methylglucamine

OTS – octadecyltrichlorosilane

probe liquid – Liquid or solution used to study the wettability of a surface

PTFE – poly(tetrafluoroethylene)

SDS – sodium dodecyl sulphate

SHS – Superhydrophobic surface(s)

Chapter 1 - Introduction

1.1 What is a Superhydrophobic Surface?

A superhydrophobic surface (SHS) is a surface that repels water very well. Water drops bead up on the surface, rolling with slight applied force, and bouncing if dropped on the surface from a height. A common definition delineating hydrophobic surfaces from superhydrophobic ones is that a water drop on a SHS has an advancing contact angle (CA) greater than 150° and low contact angle hysteresis (CAH). Contact angle hysteresis is the difference between advancing and receding contact angle. A surface is considered hydrophilic if the contact angles (CA) are below 90° and hydrophobic if the CA's are between 90° and 150°. Contact angle is the angle measured from the baseline of the drop (the macroscopic liquid-solid interface), through the liquid to the tangent of the liquid-air interface at the three phase contact line (CL). An illustration of CA and the CL is shown in Figure 1-1. The terms advancing or receding refer to the CA's taken by a drop as the CL advances or recedes across the surface (e.g. due to an increase or decrease of drop volume). It is assumed in this thesis that the drop is sitting so that its center of mass is stationary on a flat surface and the drop is axisymmetric about the vertical, such that the contact angle is the same at all points on the contact line.

Alternative definitions of superhydrophobicity exist. If CA's are close to 150° the surface might still be considered a SHS. If only advancing CA is important in a situation the CAH condition might be relaxed. Definitions

may also include information on the height the drop bounces on impact or the necessary force to move a drop on the surface. In this thesis we will mainly take the first definition outlined (advancing CA greater than 150° and low CAH). We will, at times, relax the CAH condition, especially when receding contact angle is not reported in literature (which is unfortunately common). A SHS is sometimes called an ultrahydrophobic, super-water repellant, or lotus-effect surface, if a surface behaves as a SHS for liquids other than water the surface is sometimes referred to as superlyophobic, superoleophobic (or similar) surface. In this thesis, the term superhydrophobic/superhydrophobicity will be used for all liquid/surface combinations showing the definition of superhydrophobicity or superlyophobicity etc. outlined above.

Superhydrophobic surfaces have evoked great interest in researchers for both purely academic pursuits and industrial applications. As explained in Section 1.2, SHS result from the interplay of liquid with a generally low energy surface topographically modified on the micron and sub-micron scale. The exact physics of this is not fully understood, and thus SHS provide a fascinating tool for their study. Potential industrial applications are plentiful; SHS have shown antifouling and self cleaning properties [1-5]. As well, they are of interest for drop and liquid actuation in microfluidics [6-10]. Research is ongoing in the use of SHS to decrease fluid friction on bodies and in channels [11-15], as well as using them to decrease the impact of icing/snow accumulation on structures [16,17].

This brief, partial list of possible applications should serve to explain the interest these surfaces are generating in the research environment.

Considering the interest in industrial applications, many studies to date are of limited use for industry because they are conducted with ultra-pure, distilled, deionized water as the probe liquid. Industrial applications are unlikely to use such ideal liquid. Non-ideal liquids could impact surface wetting, so the study of superhydrophobicity with other liquids is needed.

The topic of this thesis is the study of how topography and surface chemistry affect the wetting of smooth surface and SHS by liquids/solutions other than pure water. Besides water, SHS could be used with non-aqueous pure liquids and impure liquids, which can be modeled by the addition of surfactants to pure liquids. In the remainder of this chapter, the theories explaining superhydrophobicity are outlined, with emphasis on what is and is not understood about SHS (especially regarding topography and chemistry effects). Following this, the relevant literature of pure liquids and surfactant solution wetting of hydrophobic surfaces and SHS is reviewed. Finally, the approach, scope and outline of the remaining thesis chapters are given.

1.2 The Theory of Superhydrophobic Surfaces

A SHS is presently understood to be the phenomenon of topographically enhanced liquid repellency of a chemically hydrophobic (or slightly

hydrophilic) surface. The generally accepted models for explaining this phenomenon have been developed for the case of pure liquid wetting on surfaces. The application of these equations for impure liquid wetting is questionable because the impurities could change the interactions of the surface, solid, and surrounding vapor, but in the absence of analogous equations for impure solutions, the equation for pure liquid wetting will be applied in this thesis for both pure liquids and surfactant solutions.

When a drop of pure liquid rests on a smooth, flat and homogeneous surface, Young's equation relates the intrinsic contact angle (θ) the drop makes to the interfacial tensions γ_{lv}, γ_{sl} and γ_{sv}, where *l*, *v* and *s* represent liquid, vapor and solid phases, respectively. These interfacial tensions depend upon solid and liquid chemistry and purity. The vapor phase is normally air. Young's equation is:

$$\cos\theta = \frac{\gamma_{sv} - \gamma_{sl}}{\gamma_{lv}} \qquad 1\text{-}1$$

The lowest possible surface energy has been reported [16,18] to be for closest packed, hexagonal, CF_3 groups. This coating on a smooth surface yields a contact angle of ~120°, which is presently the maximum attainable thermodynamically relevant contact angle on a smooth surface. To achieve higher contact angles, the surface must be non-smooth. For non-smooth surfaces, prediction of contact angle is much more difficult. Traditionally, the two equations of Wenzel [19] and Cassie [20] have been used to

understand superhydrophobicity. These equations are described below and the states they describe are illustrated in Figure 1-2.

If the liquid completely wets the surface by contacting the entire solid interface beneath the drop, Wenzel's equation describes the Wenzel contact angle (θ_w) as:

$$\cos\theta_w = r\left(\frac{\gamma_{sv} - \gamma_{sl}}{\gamma_{lv}}\right) = r\cos\theta \qquad 1\text{-}2$$

where the effect of topography is modeled by r, the roughness factor (sometimes called rugosity), which is the ratio of actual surface area to projected surface area. By Equation 1-2, it is seen that for hydrophobic surfaces ($\theta>90^o$), roughness increases the apparent contact angle by increasing the contact area of the drop on the surface, and therefore the energy for wetting the surface, whereas for hydrophilic surfaces ($\theta<90^o$) roughness decreases the apparent contact angle in a similar manner. The term, 'apparent contact angle' is used to describe the contact angle on a rough surface, and refers to the fact that the macroscopic contact angle measured on a rough surface (or SHS) may not be the same as the microscopic contact angle that exists at the microstructure of the surface.

If the drop is instead assumed to sit on top of the pores/crevices in the surface, leaving vapor in the low regions, the Cassie equation can be written as:

$$\cos\theta_c = f(\cos\theta + 1) - 1 \qquad 1\text{-}3$$

where θ_c is the Cassie contact angle (θ_c), and the effect of topography is modeled by *f*, the solid fraction, which is the ratio of the surface area that is wetted by the drop compared to the total surface area under the drop. For simplicity, this equation is usually used with projected surface areas, which neglects the curvature of the air-liquid interface beneath the drop, and also neglects the curvature or roughness of the solid asperity tops wetted by the liquid. The first omission, (curvature of the air-liquid interface) is generally considered negligible, but could lead to the interface touching the bottom of the air-filled regions, and triggering a collapse to the Wenzel state [21,22]. The second omission (roughness of the asperity tops) can be thought of as a mixed Cassie/Wenzel mode, or as a Cassie mode with partial penetration of the liquid into the surface. The author of this thesis has found few studies [23], and no rigorous investigations of this concept in the literature, though Cassie himself noted the possibility.

A given surface topography will have both an *f* and *r* value, corresponding to the Cassie and Wenzel states that a drop could take on the surface, respectively. The question of which state a drop will take is an interesting one. Quéré et al. [24] have studied the problem; combining equations 1-2 and 1-3, to yield:

$$\cos\theta_{cr} = \left(\frac{f-1}{r-f}\right) \qquad 1\text{-}4$$

They suggest that the state will be Cassie/Wenzel depending whether Young's contact angle (controlled by liquid chemistry for a given surface chemistry) is greater/less than the critical contact angle (θ_{cr}, constant for a given surface topography). 'Metastable' Cassie states have been suggested for surfaces which should exhibit the Wenzel state [23,25,26], suggesting energy barriers that must be overcome for this transition to take place.

Both Wenzel's and Cassie's equations describe how the intrinsic equilibrium value of contact angle is modified by topography. However, the act of advancing a drop across a surface increases the contact angle to a higher metastable state compared to the Wenzel or Cassie angle. This is termed the advancing contact angle. Likewise, receding a drop across a surface decreases the contact angle to a lower metastable state, resulting in the receding contact angle [Chapter 3 of reference 27]. The difference between these two contact angles is termed the contact angle hysteresis (CAH). Prediction of the advancing and receding contact angles *a priori* based on the intrinsic contact angle is difficult, and has been the study of much work and debate, e.g. [28-30]. The Wenzel wetting state is assumed to have a higher CAH due to the increased work of adhesion necessary to recede the drop due to the increased solid-liquid interface whereas the Cassie wetting state is assumed to have a lower CAH [31] because of its reduced solid-liquid interface compared to the Wenzel state. So, to design

a SHS, researchers try to roughen a low energy surface in such a way that the Cassie wetting regime is favored. Some studies have expressed this idea in more detail [28,30], but the understanding is still rudimentary and incomplete. Generally, on a smooth hydrophobic surface, the advancing contact angle is taken to be the intrinsic contact angle.

Several papers [e.g. 23,32-36] have showed that the classical Wenzel and Cassie models do not always predict observed contact angles. Likewise, many alternatives to/modifications of Wenzel's and Cassie's models have been proposed (involving, e.g., line tension [37], contact line effects [16,38-40], roughness scale/architecture [25], and penetration of liquid into the surface [21,23,28,33,34]). Researchers such as Extrand [41], and Gao and McCarthy [42], have recently argued that the area averages that Wenzel and Cassie present are erroneous. They argue that the area around the contact line is of more importance. McHale showed in his response [43] that for a homogeneous topography there is no difference in the two considerations, and that for the Cassie wetting state the contact line exists discontinuously at every pore/crevice under the drop, meaning that the whole area under the drop is important for contact angle calculations. Nosonovsky [44] agrees with the finding of McHale regarding homogeneous topographies, and with Gao and McCarthy's and Extrand's findings for heterogeneous topographies. Nosonovsky also goes into further detail determining when wetting equations are valid or not.

All of the theories presented above were derived considering pure liquids, usually water, on surfaces, and may not be applicable for wetting by impure liquids (modeled by surfactants). The focus of this thesis is not a detailed analysis of different wetting models, instead it focuses on the study of non-aqueous pure liquid and surfactant solution wetting on hydrophobic surfaces and SHS from an experimental perspective, examining how topography, surface chemistry, and liquid type/purity affect wetting. In the absence of relevant relations to describe the contact angle on rough surfaces with surfactant solutions, the Wenzel and Cassie models will be used as starting points and other considerations will be discussed as needed. The results of this thesis will be of interest to industry for application of SHS, and to academia as fundamental studies of surfactant solution interactions on smooth and topographically modified surfaces.

1.3 Literature Review

In the literature there is some work regarding the wetting of non-aqueous pure liquids or pure liquid combinations on smooth hydrophobic surfaces and SHS. Industrial applications can also involve impurities in the liquids, which can be modeled by the addition of surfactants to pure liquids, and for which there is much less literature available. The relevant literature for both cases will be reviewed below.

1.3.1 Pure Liquids

Zisman [e.g. 45-50] is generally considered a pioneer in surface science for his systematic study of pure liquid wetting on smooth surfaces. He has studied numerous hydrophilic and hydrophobic surfaces with several pure liquids. He concludes that solid surface tension is a material property and that generally, with decreasing liquid-vapor surface tension of pure liquids there comes decreasing contact angle (explained by Young's equation). He also proposed the idea of a critical surface tension below which spreading occurs and the contact angle is zero. This can be understood as the point at which the liquid vapor surface tension equals the difference between the solid-vapor and solid-liquid surface tensions. i.e.:

$$\gamma_{sv} - \gamma_{sl} = \gamma_{lv}$$

which gives:

$$\theta = \cos^{-1}\left(\frac{\gamma_{sv} - \gamma_{sl}}{\gamma_{lv}}\right) = \cos^{-1}(1) = 0$$

Kwok and Neumann [51] have reported on pure liquid contact angles on a variety of hydrophobic surfaces for the purpose of solid interfacial free energy calculation. They have found that for sufficiently smooth surfaces and well chosen liquids a smooth decreasing trend in contact angle is seen with decreasing pure liquid surface tension. They conclude that this supports the idea that solid interfacial free energy is a physical quantity, independent of liquid type.

Other researchers, such as van Oss [52], have argued that liquid type affects the solid free energy due to interactions (acid-base, van der Waals, etc.) between the liquid and the surface not considered by Kwok and Neumann [51], and have observed this in variations from the smooth curves seen by Kwok and Neumann.

All researchers agree that with decreasing liquid-vapor surface tension of a pure liquid, the contact angle that liquid takes on a smooth surface is generally decreased. For the application of smooth surface results to SHS, the idea of decreasing contact angle on smooth surfaces (decreasing intrinsic contact angle for SHS) is important. It impacts the wetting state that a drop will take on a surface (Cassie or Wenzel) and is therefore a controlling factor for superhydrophobicity. Based on traditional reasoning [24], the Cassie wetting state (desired for SHS) cannot exist for intrinsic contact angles below 90°. Considering the importance of intrinsic contact angle on the wetting of surfaces, in this thesis the effect of two different low surface energy surface chemistries (controlling intrinsic contact angle) on the wetting of SHS and smooth surfaces has been studied.

For SHS, Shirtcliffe *et al.* [53] and Rao *et al.* [54] both studied porous SHS for industrial applications. They did not measure contact angles with pure liquids but reported that for sufficiently low surface tension (surface tension was unreported for the ethanol-water mixture used in [53], surface tension was ~30 mN/mm for [54]) the non-aqueous pure liquids

penetrated the surfaces fully, while pure water did not. This shows that transition from the Cassie state to the Wenzel state is dependent on surface tension. Similarly, Fujita *et al.* [55] reported advancing contact angles above 150° for their bumpy SHS for water and water-glycerol mixtures, but a contact angle below 10° for ethanol (γ_{lv} = 22.3 mN/mm). Ultrasonic energy dissipation tests led them to conclude that the SHS was behaving in the Cassie mode for the water and water-glycerol, and the Wenzel mode for ethanol. These studies are incomplete (reporting single contact angles or no contact angles at all, and not reporting results for liquids of surface tension between those near water and the liquid that shows penetration) but demonstrate the idea of transitions from the Cassie to the Wenzel wetting state with decreasing surface tension.

Shibuchi *et al.* [56,57] studied two SHS. The first [56], was purified alkyl ketene dimer (AKD). They generated a dual-scale topography, and reported contact angles above 150° for water, decreasing with increasing dioxane fraction. They did not report receding contact angle. Contact angle for smooth and rough AKD were seen to cross at slightly under 90° at 85:15 water/dioxane (no surface tension given). The surface tension of dioxane is 33 mN/m at 20 °C [58]. The decline of contact angles on rough AKD (at 85:15 water/dioxane) was much more abrupt than on smooth AKD (from much higher contact angles to much lower contact angles). They gave a contact angle of 15° for maximum dioxane ratio (20:80). Shibuichi *et al.*'s results [56] can be interpreted as a switch from the Cassie

to the Wenzel mode and their results will be compared to AKD SHS and other SHS in Chapter 2 and 3.

With their second surface [57], Shibuichi *et al.* studied electrochemically etched aluminum, coated with in-house derived fluorinated compounds. They again reported high static contact angles, this time with a variety of oils with surface tensions as low as 21.6 mN/m (Octane), which produced an intrinsic contact angle of 46.6° and an apparent contact angle of 105.3° with their best fluorination treatment. With hexadecane they found angles of 75.5° and 135.5° on smooth and etched samples, respectively. They did not present receding contact angles but said that 'A rapeseed oil droplet having a surface tension of ~35 mN/m rolls around on the surface without attaching.' [57] This statement is of limited use for estimating CAH since they did not report how or how much they tilted the surface. Also, it has been shown [59] that receding contact angle measured by dynamic low rate receding of a sessile drop does not always compare with the contact angle difference between the leading and trailing edge of a drop on an inclined plane. Shibuichi *et al.* explained their results in terms of fractal dimension and differences in chemical structure on smooth and rough surfaces.

The work of Mohammadi *et al.* [60], studied pure liquids on SHS AKD. Because they also studied surfactant solutions this paper will be discuss in Section 1.3.2.

Chen *et al.* [40] have presented advancing and receding contact angles for a variety of rough and smooth surfaces and a variety of pure liquids. For packed spherical particles of PTFE they reported advancing/receding angles of 177°/177° with water, 140°/138° with methylene iodide (γ_{lv}= ~50.8 mN/m at 20 °C [58]) and 140°/125° with hexadecane. Chen et al.'s results with hexadecane are extraordinary, since Kwok and Neumann's results [51] (along with others) suggest that the intrinsic contact angle of hexadecane on smooth PTFE is about 70°. Based on standard analysis [24], the PTFE sphere SHS should show the Wenzel wetting state for hexadecane, but does not. This can possibly be explained by the work of Herminghaus [25] which suggests that re-entrant or overhanging structures (formed here by the packing of the PTFE spheres) can give high contact angles for low surface tension liquids. This concept is demonstrated schematically in Figure 1-3.

In all, for a given surface chemistry, non-aqueous pure liquids on SHS are seen generally to behave more and more poorly as liquid-vapor surface tension decreases, eventually loosing their superhydrophobic nature, generally with an abrupt transition from SHS to extremely hydrophilic. Considering the above literature, however, it is clear that topography can play an important role in controlling this transition. For this reason, topographic effects on superhydrophobicity is one of the areas of study in this thesis.

1.3.2 Surfactant Solutions

There is a great deal of research on the adsorption and wetting effects of surfactants on smooth hydrophilic surfaces. This work is of limited application to this thesis since it is seen that behaviors are very different on hydrophilic versus hydrophobic substrates when considering wetting by surfactant solutions. There is some information on the topic of surfactants on smooth hydrophobic surfaces [61-65]. Care must be taken when applying results to rough surfaces since the surfactant behavior might not be the same, but the works do serve as simplified control studies for SHS.

Starov et al. [61] presented a theoretical derivation of surfactant assisted spreading of drops on smooth hydrophobic substrates. Their predictions matched experimental data for spreading of sub and super Critical Micelle Concentration (CMC) solutions of SDS on PTFE and polyethylene, showing that the spreading is self limiting and is complete within 10-20 seconds. They continued their work [62], looking at surfactant solution imbibition into hydrophobic capillaries. Based on the time scales they showed, one could expect that penetration into a micron-scale SHS topography would be complete in under 30 seconds.

Kumar et al. [63] showed that non-ionic surfactants will adsorb on the solid-liquid and liquid-vapor interfaces, and even ahead of the advancing contact line on unwetted regions of the solid-vapor interface for

hydrophobic octadecyltrichlorosilane (OTS) monolayers on silicon. In each case the adsorption promotes spreading and Kumar *et al.* theorize that this will make the spreading greater than what would be expected based upon the changes in liquid-vapor and liquid-solid surface tensions alone. They term this behavior 'the autophilic effect' in analogy to the autophobic effect of surfactants on hydrophilic surfaces, but they did not study how the wetting of surfactant solutions would compare to the wetting by pure liquids of similar surface tension. Again they found that spreading was complete in a few tens of seconds.

In their work, Varanasi and Garoff [64] observed the receding contact line for non-ionic and cationic surfactant solutions on OTS monolayers on silicon. They showed that the surfactant assemblies on all three interfaces must interact and reform at the contact line. They found that they generally do so very quickly (0.002-0.2 s) but that pinning points form at locations where the surfactants cannot reform fast enough. These pinning points hold the local contact line and decrease the local contact angle. The frequency of occurrence of the points was found to be higher on hydrophobic surfaces compared to hydrophilic ones, and also higher with their non-ionic surfactant. The frequency increased with increasing withdrawal speed in a roughly linear fashion (the standard deviation of their data prevented them from determining if there were non-linearities).

Finally, Dutschk et al. [65] reported contact angles on Teflon coated smooth silicon wafer, paraffin wax, as well as several other smooth and hydrophobic substrates for anionic sodium dodecyl sulphate (SDS), cationic dodecyltrimethylammonium bromide (DTAB), and nonionic pentaethylene glycol monododecyl ether. They found that surfactant solution drops did begin to spread instantly upon contact with the surface, but that this spreading was complete in ~20 seconds or less. They found that drops spread more on less hydrophobic surfaces, and with greater concentration of surfactant. SDS was found to show practically no spreading, DTAB some, and their non-ionic surfactant by far the most. Further, they found that the variation in contact angle with surfactant concentration was smooth. Considering all the above studies, the time scale for surfactant interactions to be complete on SHS is likely under 30 seconds.

In all, the effect of surfactants on smooth hydrophobic surfaces can be seen to promote wetting by lowering the liquid-vapor surface tension. In addition, surfactant adsorption on the solid-liquid, and solid-vapor interfaces (the autophilic effect) further promotes wetting. The autophilic effect has been observed on smooth surfaces, but its importance in terms of wetting has not been experimentally verified by testing surfactant solutions and pure liquids of similar surface tension on the same smooth surface. Previously [60], surfactant solutions were seen to inhibit wetting of SHS compared to pure liquids of similar surface tension. Thus, this

thesis is of interest as it will directly compare wetting by pure liquid and surfactant solutions on the same smooth hydrophobic surface (and SHS's).

Little consideration has been given to the use of impure liquids on SHS; in total, three studies were found. In 2007, Shirtcliffe *et al.* [53] studied superhydrophobic porous sol-gels for their use as switches (switching from superhydrophobic to hydrophilic behavior based on temperature, liquid type, or impurity concentration). Their study examined the wetting of only one surfactant solution on a single SHS. They reported a decrease in advancing contact angle from 140° with water to about 120° for concentrations of SHS above CMC, and a decrease in receding contact angle of 140° for Critical Micelle Concentration (CMC) of SDS, but did not present corresponding results with non-aqueous pure liquids for comparison. As mentioned in Section 1.3.1, they did report that sufficiently low surface tension mixtures of ethanol in water penetrated the SHS. They suggested limited contact of the surfactant solution with the surface resulted in the high advancing angles, though they did not suggest why the solution did not penetrate the surface. They also suggest that surfactant films across the crevices could be bridging them and decreasing the receding contact angle due to pinning of the contact line.

Ferrari et al. [66], published in 2006 on non-ionic, semi-polar, and ionic (SDS and HTAB) surfactant solution wetting on a bumpy SHS. They created their SHS by roughening a glass slide, covering it with silica

nanoparticles, and coating them with saturated hydrocarbon and then fluorinated treatments. They tested a single concentration of four surfactant solutions far below (CMC) and at 2CMC, with no intermediate concentrations, with and without the addition of 20 mM NaCl. They found superhydrophobic behavior for low concentrations, and decreased but non-zero contact angles at 2CMC. Salt was seen to have little effect at low surfactant concentration, and was somewhat detrimental to repellency at 2CMC. They did not test pure liquids, and their explanation for the observed behavior suggested that self limiting surfactant adsorption (decreased surface tension) explained the results. If this were the case, the surfaces would be expected to behave at least as poorly with surfactant solutions as with pure liquids of similar surface tension. This was not seen by Mohammadi *et al.* when comparing the wetting results of surfactant solutions and pure liquids of similar surface tension [60].

Mohammadi et al. [60] studied a SHS produced by the natural formation of a rough microstructure on alkyl ketene dimmer (AKD), a wax that presents a saturated hydrocarbon surface. Mohammadi *et al.*'s paper was the progenitor of this thesis and their results are re-reported in Chapter 3. They found that pure liquids showed an abrupt drop in advancing contact angle around a surface tension of 45 mN/m, similar to the work of Shibuichi *et al.* [56], who also studied AKD SHS, but only with pure liquids. Surfactant solutions of the same and lower surface tensions did not show this same drop in Mohammadi *et al.*'s study, and instead

maintained high advancing contact angles (above 90° in nearly all cases). The receding angle data reported by Mohammadi *et al.* has been discovered to be erroneous; using the traditional definition of receding angle (a sustained and constant value while the contact line is receding) it is found that the receding angle for all liquids (pure and solution) is zero. Shibuichi *et al.* [56] did not measure receding contact angle and may be unaware if it was zero for their AKD surfaces. It is also possible that their more highly purified AKD would lead to a non-zero contact angle. The wetting of AKD samples tested in this thesis will be discussed in Chapters 2 and 3.

Overall, it seems that SHS show high advancing contact angles with surfactant solutions. Receding contact angles vary between high and low values between and within studies. Three surfaces have been tested so far in the literature. Two were fluorinated, and one was made up of mostly saturated hydrocarbons. Considering the small number of experimental or theoretical studies of surfactant wetting on SHS, more investigation is needed to study what effects (if any) liquid type and liquid impurities have on the wetting of topographically different SHS, and to investigate the influences of independently varied topographies and surface chemistries. The comparison of surfactant solution and non-aqueous pure liquid wetting on smooth surfaces is also of interest.

1.4 Experimental Approach

In this thesis, the wettability of smooth surfaces and SHS is studied by means of dynamic low rate advancing and receding contact angle measurements. These measurements are made by Axisymmetric Drop Shape Analysis (ADSA).

ADSA is a measurement technique developed at the University of Toronto by the group led by Dr. A. W. Neumann. It is described in detail elsewhere [Chapter 10 of reference 27, 51,67]. Briefly, the surface to be tested has a hole drilled through it, and a syringe is filled with the liquid to be used for probing the surface and mounted below the surface. The syringe is then driven to create a drop on the surface. It can then increase drop volume slowly (advancing the drop across the surface slowly to maintain quasi-equilibrium conditions and give rise to the advancing contact angle). The syringe can also be driven in reverse. In this case the drop volume is decreased (leading in a similar way to the receding contact angle). A CCD camera captures many back-lit images of the drop profile during both the advancing and receding stages, and a program performs edge detection on the image to determine the drop shape. This shape is fitted to a solution of the Laplace-Young equation of wettability and from this fit, the contact angle of the drop on the surface can be determined for each image. Other information (drop radius, volume, surface area and surface tension) are also calculated, however, they are not used in this thesis. ADSA depends

on the drop maintaining axisymmetry, which is not difficult if the surface is homogeneous, isotropic, flat and level.

There are other measures of wettability, including, e.g., drop tilt angles for rolling motion, drop impact and rebound measurement, and drop adhesion measurement under various applied forces (shear, vibration, gravity etc). These techniques are not explored in this thesis.

1.5 Scope of this Thesis

In this thesis, the wetting of four pure liquids of various surface tensions (~27-73 mN/m) and nine surfactant solutions of various polarities was studied on surfaces with four different topographies. These topographies were SHS of anodically oxidized aluminum, plasma etched PTFE and naturally rough alkyl ketene dimer, and smooth silicon wafer. These different topographies were chosen to compare how topography affects wetting for similar surface chemistries (controlled to be either fluorinated or saturated, i.e. CH_3/CH_2 terminated hydrocarbon chemistry).

The surfactants used as probe liquid solutions were sodium dodecyl sulphate, hexadecyltrimethylammonium bromide and n-decanoyl-n-methylglucamine at three concentrations below Critical Micelle Concentration (CMC). The three different surfactants, with different ionic properties, were chosen to examine possible effects of charge interactions on the surface and to relate to various possible types of liquid impurities in

industrial applications of SHS. The pure liquids used were water, ethylene glycol, bromonaphthalene, and hexadecane, chosen to yield a similar range of surface tensions to the surfactant solutions, and to provide comparison of wetting results for pure and impure liquids.

Surfaces were treated to either give a fluorinated surface chemistry, or a saturated hydrocarbon surface chemistry, in order to study the effect of different hydrophobic surface chemistries on wetting. In most cases, each of the topographies was tested with both chemistries. Wettability was studied by means of dynamic low rate advancing and receding contact angles, measured using Axisymmetric Drop Shape Analysis (ADSA).

1.5.1 Outline of Remaining Thesis Chapters

This thesis is presented in 'Mixed-Paper' format. The two body chapters have been written as papers, and will be submitted for publication in peer reviewed journals (likely Langmuir). For readers who wish to also read the peer reviewed publications, they will be listed with Milne, A. J. B., and Amirfazli, A. as authors, and titles will be similar to the chapter headings.

In Chapter 2, silicon, aluminum, PTFE and AKD surfaces are studied with surfactants and pure liquids. The surfaces are treated to give a fluorinated chemistry, which is found to be incomplete on the AKD. Analysis focuses on how topography, and also liquid/solution variation, affects wetting of SHS and smooth surfaces.

In Chapter 3, silicon, aluminum, and AKD surfaces are studied with surfactants and pure liquids. The surfaces all have a saturated hydrocarbon chemistry. The PTFE surfaces were not studied because they could not be coated. The AKD surface data is taken, in corrected form, from Mohammadi et al. [60]. With a new surface chemistry, the effects of topography and liquid/solution variation can be re-examined to test the hypotheses formed in Chapter 2. Comparison of the results of Chapter 3 to those of Chapter 2 allow for analysis of the effects of surface chemistry on the wetting of SHS and smooth surfaces.

Finally, in Chapter 4, the previous chapter's results are summarized, and conclusions are drawn as to the effects of surface chemistry, topography, and liquid type/surfactant type and concentration on wetting of smooth hydrophobic surfaces and SHS. Suggestions for future work are also presented including other surface topographies/chemistries to test, development of theoretical models, the addition of other impurities to liquids, and tests using other measures of wettability. Possible experiments to directly probe the liquid-vapor interface underneath the drop are proposed as a way to determine the mechanism by which surfactant solutions are evoking the wetting behaviors seen in Chapters 2 and 3. Following Chapter 4, the appendix gives details of experimental methods, etc. not fully discussed in previous chapters.

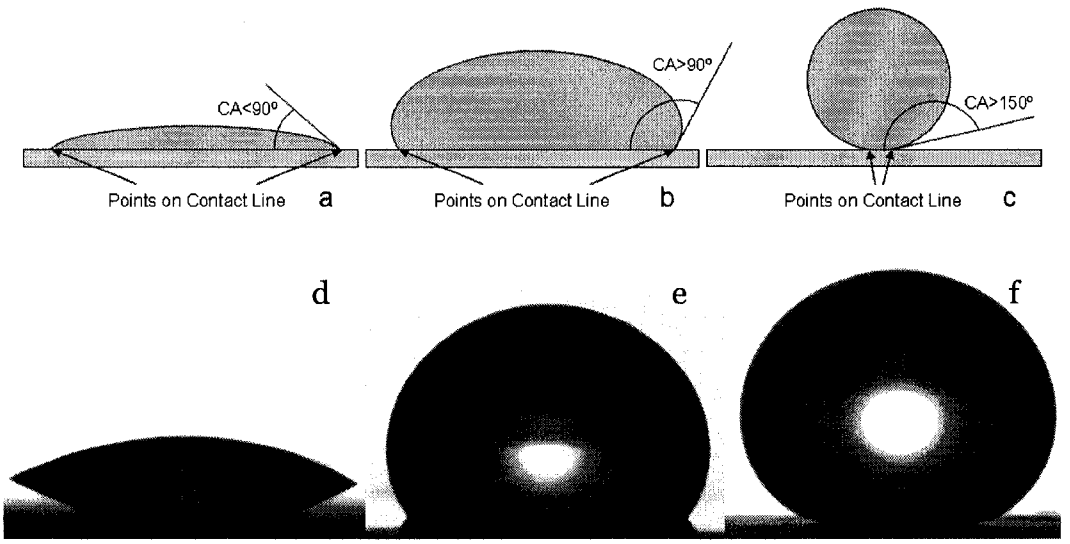

Figure 1-1: Schematic of contact angle (CA) and points on the contact line (CL) shown for a drop placed on a (a) hydrophilic, (b) hydrophobic and (c) superhydrophobic surface. Drop is on top of rectangular surface. Below each schematic is a picture of an actual drop of water on (d) hydrophilic silicon, (e) hydrophobic Teflon™ coated silicon, (f) superhydrophobic plasma etched PTFE. Note that the surface of the PTFE is grey in (f) which may obscure the contact line and contact angle in reproductions of this page.

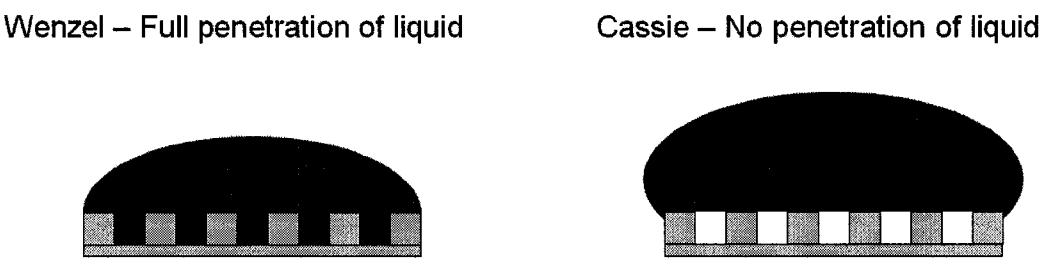

Figure 1-2: Schematic of Wenzel and Cassie wetting states. Drop is on top of surface. Yellow blocks denote surface topography and white denotes air around/under drop. Drop size not to scale, drop size (~1 mm - 1 cm) is normally several orders of magnitude larger than scale of topography (~nm - μm).

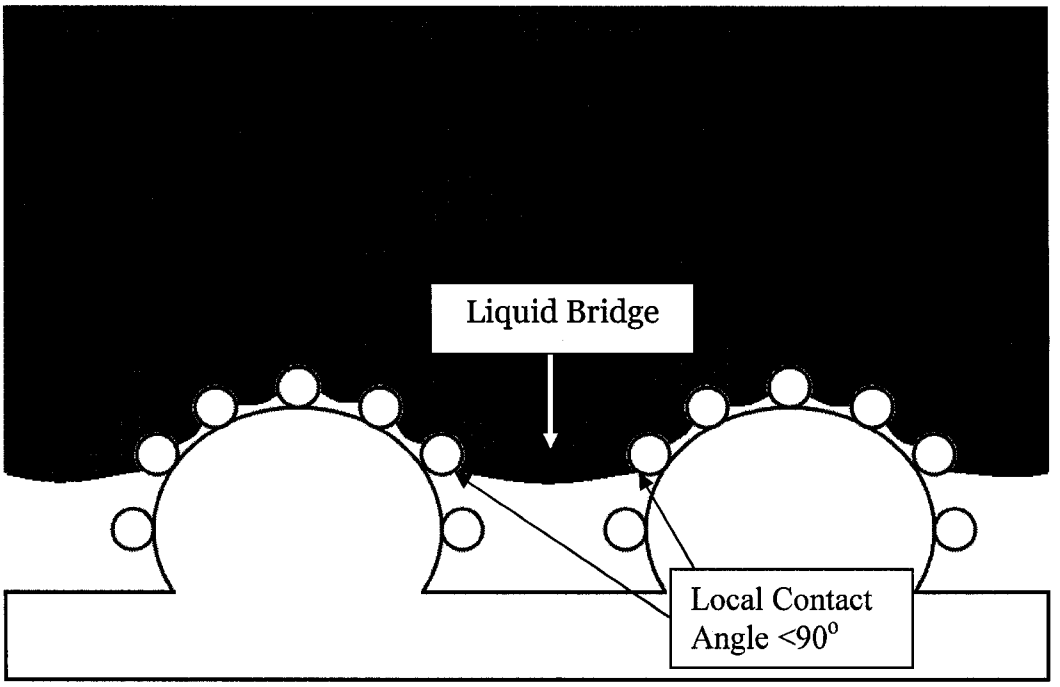

Figure 1-3: Schematic of topography resulting in overhanging (reentrant) liquid bridging for intrinsic contact angle less than 90°. Blue liquid is bridging topography of black outlined surface. White space between the outline and the liquid denotes trapped air, signifying the Cassie wetting state.

References

1. Carman, M. L.; Estes, E. G.; Feinberg, A. W.; Schumacher, J. F.; Wilkerson, W.; Wilcon, L. H.; Callow, M. E.; Callow, J. A.; Brennan, A. B *Biofouling* **2006**, 22, 11.
2. Cheng, Y. T.; Rodak, D. E.; Wong, C. A.; Hayden, C. A. *Nanotechnology* **2006**, 17, 1359.
3. Hoipkemeier-Wilson, L.; Schumacher, J. F.; Carmen, M. L.; Gibson, A. L.; Feinberg A. W.; Callow, M. E.; Finlay, J. A.; Callow, J. A. Brennan, A. B. *Biofouling* **2004**, 20, 53.
4. Shang, H. M.; Wang, Y.; Takahashi, K.; Cao, G. Z.; Li, D.; Xia, Y. N. *J Mat. Sci.* **2005**, 40, 3587.
5. Shang, H. M.; Wang, Y.; Limmer, S. J.; Chou, T. P.; Takahashi, K.; Cao, G. Z. *Thin Solid Films* **2005**, 472, 37.
6. Aussillous, P.; Quéré, D. *Nature* **2001**, 311, 924.
7. Shikida, M.; Ando, M.; Ishihara, Y.; Ando, T.; Sato, K.; Asaumi, K. *J. Micromech. Microeng.* **2004**, 14, 1462.
8. Ren, S.; Yang, S.; Zhao, Y.; Yu, T.; Xiao, X. *Surface Science* **2003**, 546, 64.
9. Ren, S.; Yang, S.; Zhao, Y. *Acta Mechanica Sinica* **2004**, 20, 159.
10. Zhai, L.; Berg, M. C.; Cebeci, F. Ç.; Kim, Y.; Milwid, J. M.; Rubner, M. F.; Cohen, R. E. *Nano Letters* **2006**, 6, 1213.
11. Choi, C.-H.; Ulmanella, U.; Kim, J.; Ho, C.-M.; Kim, C.-J. *Phys. Fluids* **2006**, 18, 087105.

12. Fukagata, K.; Kasagi, N.; Kououtsakos, P. *Phys. Fluids* **2006**, 18, 051703.
13. Gogte, S.; Vorobieff, P.; Truesdell, R.; Mammoli, A.; van Swol, F.; Shah, P.; Brinker, C. J. *Phys. Fluids* **2005**, 17, 051701.
14. Mamur, A. *Langmuir* **2006**, 22, 1400.
15. Ou, J.; Rothstein, J. P. *Phys. Fluids* **2005**, 17, 103606.
16. Nakajima, A.; Hashimoto, K.; Watanabe, T. *Chemical Monthly* **2001**, 132, 31.
17. Kako, T.; Nakajima, A.; Irie, H.; Kato, Z.; Uematsu, K.; Watanabe, T.; Hashimoto, K. *J. Mat. Sci.* **2004**, 39, 547.
18. Nishino, T.; Mefuro, M.; Nakamae, K.; Matsushita, M.; Ueda, Y. *Langmuir* **1999**, 15, 4321.
19. Wenzel, R. N. *J. Ind. Eng. Chem.* **1936**, 28, 988.
20. Cassie, A. B. D.; Baxter, S. *Trans. Faraday Soc.* **1944**, 40, 546.
21. Extrand, C. W. *Langmuir* **2004**, 20, 5013.
22. Zheng, Q.-S.; Yu, Y.; Zhao, Z.-H. *Langmuir* **2005**, 21, 12207.
23. Jeong, H. E.; Lee, S. H.; Kim, J. K.; Suh, K. Y.; *Langmuir* **2006**, 22, 1640.
24. Quéré, D.; Lafuma, A.; Bico, J. *Nanotechnology* **2003**, 14, 1109.
25. Herminghaus, S. *Euro. Phys. Lett.* **2000**, 52, 165.
26. Barbieri, L.; Wagner, E.; Hoffmann, P. *Langmuir* **2007**, 23, 1723.
27. Neumann, A. W.; Spelt, J. *Applied Surface Thermodynamics*; CRC Press: New York, **1996**.
28. Extrand, C. W. *Langmuir* **2002**, 18, 7991.

29. Gao, L.; McCarthy, T. J. *Langmuir* **2006**, 22, 6234.

30. Li, W.; Amirfazli, A. *Adv. Colloid Interface Sci.* **2007**, 132, 51, 2007.

31. Hennig, A.; Grundke, K.; Frenzel, R.; Stamm, M. *Tenside Surf. Det.* **2002**, 29, 243.

32. Shirtcliffe, N. J.; Aqil, A.; Evans, C.; McHale, G.; Newton, M. I.; Perry, C. C.; Roach, P. *J. Micromech. Microeng.* **2004**, 14, 1384.

33. Wagner, P.; Fürstner, R.; Barthlott, W.; Neinhuis, C. *J. Exp. Bot.* **2003**, 54 1295.

34. Yoshimitsu, Z.; Nakajima, A.; Watanabe, T.; Hashimoto, K. *Langmuir* **2002**, 18, 5818.

35. Shiu, J. Y.; Kuo, C. W.; Chen, P.; Mou, C. Y.; *Chem. Matter.* **2004**, 16, 561.

36. Jung, D. H.; Park, I. J.; Choi, Y. K.; Lee, S. B.; Park, H. S.; Ruhe, J. *Langmuir* **2002**, 18, 6133.

37. Drelich J.; Miller, J. D. *Langmuir* **1993**, 9, 619.

38. Li W.; Amirfazli A. *J. Colloid Surface Sci.* **2005**, 292, 195.

39. Roura, P.; Fort, J. *Langmuir* **2002**, 18, 566.

40. Chen, W.; Fadeev, A. Y.; Hsieh, M. C.; Oner, D; Youngblood, J.; McCarthy, J. *Langmuir* **1999**, 15, 3395.

41. Extrand, C.W. *Langmuir* **2003**, 19, 3793.

42. Gao, L.; McCarthy, T. J. *Langmuir* **2007**, 23, 3762.

43. McHale, G. *Langmuir* **2007**, 23, 8200.

44. Nosonovsky, M. *Langmuir* **2007**, 23, 9919.

45. Ellison, A. H.; Zisman, W. A. *J. Phys. Chem* **1954**, 58, 503.

46. Hare, E. F.; Zisman, W. A. *J. Phys. Chem.* **1955**, 59, 335.

47. Bernett, M. K.; Zisman, W. A. *J. Phys. Chem.* **1959**, 63, 1911.

48. Bernett, M. K.; Zisman, W. A. *J. Phys. Chem.* **1962**, 64, 1292.

49. Zisman, W. A. *Ind. Eng. Chem.* **1963**, 55, 19.

50. Jarvis, N. L.; Zisman, W. A. *Report of NRL Progress* **1965**, Sept., 1.

51. Kwok, D. Y.; Neumann, A. W. *Adv. Colloid Interface Sci.* **1999**, 81, 167.

52. van Oss, C. J. *J. Adhesion Sci. Technol.* **2002**, 16, 669.

53. Shirtcliffe, N. J.; McHale, G.; Newton, M. I.; Perry, C. C.; Roach, P. *Mat. Chem. Phys.* **2007**, 103, 112.

54. Rao, A. V.; Hegde, N. D.; Hirashima, H. *J. Colloid Interface Sci.* **2007**, 205, 124.

55. Fujita, M.; Muramatsu, H.; Fujihira, M. *Japanese J App Phys* **2005**, 44, 6726.

56. Shibuichi, S.; Onda, T.; Satoh, N.; Tsujii; K. *J. Phys. Chem.* **1996**, 100, 19512.

57. Shibuichi, S.; Yamamoto, T.; Onda, T.; Tsujii, K. *J. Colloid Interface Sci.* **1998**, 208, 287.

58. http://www.surface-tension.de/, accessed 4-October-2007, methylene iodide listed under IUPAC- name diiodomethane

59. Pierce, E.; Carmona, F. J.; Amirfazli, A. *Colloids and Surfaces A: Physicochemical and Engineering Aspects* **In Press**, DOI: 10.10161/j.colsurfa.2007.09.032.

60. Mohammadi, R.; Wassink, K.; Amirfazli, A. *Langmuir* **2004**, 20, 9657.

61. Starov, V. M.; Kosvintsev, S. R.; Velarde, M. G. *J. Colloid Interface Sci.* **2000**, 227, 185.

62. Starov, V. M. *J. Colloid Interface Sci.* **2004**, 270, 180.

63. Kumar, N.; Varanasi, K.; Tilton, R. D.; Garoff, S. *Langmuir* **2003**, 19, 5366.

64. Varanasi, K. S.; Garoff, S. *Langmuir* **2005**, 21, 9932.

65. Dutschk V.; Sabbatovskiy, K. G.; Stolz, M.; Grundke, K.; Rudoy, V. M. *J. Colloid Interface Sci.* **2003**, 267, 456.

66. Ferrari, M.; Ravera, F.; Rao, S.; Liggieri, L. *App. Phys. Lett.* **2006**, 89, 053104.

67. Hoorfar, M., Neumann, A. W. *J. Adhesion* **2004**, 80, 727.

Chapter 2 - Surfactant solution and pure liquid wetting of fluorinated smooth and textured superhydrophobic surfaces

2.1 Introduction

A superhydrophobic surface (SHS) is generally defined as one with advancing water contact angle above 150° and low contact angle hysteresis (CAH). The surfaces are created by the texturing (at the micron and/or sub micron scale) of a usually low energy material (most commonly a fluorinated surface). Hundreds of papers have been published on the topic of superhydrophobic (ultrahydrophobic) surfaces in the past ten years. Studies have concentrated on fabrication, e.g. [1-7], fundamental studies e.g. [8-11], and industrial uses (e.g. self-cleaning surfaces, low friction surfaces, liquid sensors, etc. e.g. [12-14]). Many studies to date are of limited use for industrial application because they are conducted with ultra-pure, distilled, deionized water as the probe liquid. Industrial applications are unlikely to use such ideal liquid. Non-ideal liquids could affect surface wetting, so the study of superhydrophobicity with other liquids is needed.

If a SHS maintains its behavior for non-aqueous pure liquids it is sometimes called a superlyophobic or superoleophobic surface; in this chapter the term superhydrophobic will refer to all pure liquids and liquid

solutions. Studies of superhydrophobicity with non-aqueous pure liquid and mixtures of these are much less common [e.g. 6,12-18].

Industrial applications may also involve impure liquids; in addition to mixtures of pure liquids, they may use various solutions or contain impurities. The latter systems can be modeled by the addition of surfactants to pure liquids. Only a few studies are available on the wetting of SHS by surfactant solutions [16,19 and to a lesser extent 13]. Our previous study [16], showed that surfactant solutions maintained a higher advancing contact angle on naturally rough alkyl ketene dimer (AKD) compared to pure liquids of similar surface tension. Other studies have reported relatively high contact angles for surfactants on SHS [13,19], but have not provided a comparative study of wetting by pure and impure liquid of similar surface tensions. The previous three studies were conducted using a single SHS each. The present study investigates if previously observed behaviors hold for a variety of SHS and if the wetting repellency can be further increased by varying topography for similar surface chemistries. Below, the previous studies of surfactant solutions on SHS will be outlined, followed by a review of the literature pertaining to wetting of smooth hydrophobic surfaces with surfactant solutions.

Shirtcliffe *et al.* [13] studied a superhydrophobic porous sol-gel with solutions of SDS. They reported a change in advancing contact angle from 140° to about 120°, and a decrease in receding contact angle of 140°

(receding contact angle decreased to zero) at concentrations corresponding to the Critical Micelle Concentration (CMC), but did not present corresponding results with non-aqueous pure liquids for comparison. They suggested that surfactant films stretching across the crevices of the surface could be the cause for significantly decreased receding contact angles.

Ferrari *et al.* [19], studied wetting of a SHS with a 'bumpy' topography. They tested a single concentration of four different surfactant solutions far below CMC and at 2CMC, with no intermediate concentrations, with and without the addition of 20 mM NaCl. They found superhydrophobic behavior for low concentrations. Significantly reduced but non-zero contact angles were reported at 2CMC. Salt was seen to have little effect at low surfactant concentration, and was somewhat detrimental to repellency at 2CMC. They suggested that self-limiting surfactant adsorption (decreased surface tension) explained the results but did not test pure liquids to test this theory. Their suggestion is not supported by the work of Mohammadi *et al.* comparing the wetting results of surfactant solutions and pure liquids of similar surface tension [16].

Smooth hydrophobic surfaces (CF_3 and CH_3 terminated) have both been studied, for ionic and non-ionic surfactants solutions [20-24]. Care must be taken when applying results to rough surfaces since the surfactant behavior might not be the same, but these studies can be used as a starting

point for analysis. All studies ascertained that surfactants promote spreading of drops compared to water beyond that caused by the change in solid-liquid and liquid-vapor surface tension due to surfactant adsorption. Further, predicted and observed spreading was complete in 10-30 seconds. The authors theorize that this spreading is due to observed surfactant adsorption ahead of the contact line on unwetted portions of the solid-vapor interface, and term this the auto-hydrophilic, or autophilic effect. However, no study has been found that compares surfactant and pure liquid wetting on the same surfaces to gauge how this adsorption affects wetting by surfactant solution versus pure liquid of similar surface tension.

Starov [21] studied penetration of surfactant solutions into hydrophobic capillaries. If one extends his data for micron-scale SHS topography, penetration (if any) would be expected in less than 30 seconds.

Varanasi and Garoff [23] observed the receding contact line for cationic and non-ionic surfactants on a CH_3 terminated surface and showed that surfactants at all three interfaces quickly reform at the contact line (within 0.002-0.2s). However, microscopic pinning points held the contact line and decreased the receding angle at locations where the surfactants could not reform sufficiently quickly. The frequency of occurrence of the points was roughly linearly proportional to withdrawal speed, with the proportionality constant dependent on the liquid/solid pairing. Non-ionic surfactant solutions on hydrophobic surfaces showed the greatest

frequency of pinning. This idea of contact line pinning during the recede phase will be discussed in terms of the results presented in this chapter.

Finally, Dutschk *et al.* [24] reported contact angles for anionic SDS, cationic dodecyltrimethylammonium bromide, and nonionic pentaethylene glycol monododecyl ether. They found that drops of surfactant solution spread immediate upon contact with a variety of smooth hydrophobic surfaces, but spreading took 20 seconds or less to complete.

All of the above studies have shown that surfactant adsorption is completed relatively quickly. Considering this, the time scale for surfactant interactions to be complete on SHS is likely under 30 seconds.

Given the demonstrated lack of experimental or theoretical studies of surfactant versus pure liquid wetting on SHS, more investigation is needed to study what effects (if any) liquid type and liquid impurities have on the wetting of topographically different SHS, and to investigate the influences of these different topographies for a given surface chemistry. The comparison of surfactant solution and non-aqueous pure liquid wetting on smooth surfaces is also needed. Therefore, in this paper wetting of various surfactant solution and pure liquids on a smooth control surface (Teflon coated silicon wafer), and three SHS (electrochemically etched Teflon coated aluminum, plasma etched PTFE and Teflon coated AKD) is studied.

2.2 *Theory*

Below the theoretical background for the phenomenon of SHS is presented. These equations were developed for pure liquids, and their thermodynamic application for surfactant solutions is questionable because the impurities could change the interactions of the surface, solid, and surrounding vapor. Nevertheless, in the absence of relevant relations to describe the contact angle on rough surfaces with surfactant solutions, we present the following models as a starting point for analysis.

When a drop of pure liquid rests on a smooth, flat, and homogeneous surface, Young's equation relates the intrinsic contact angle (θ) the drop makes to the interfacial tensions γ_{lv}, γ_{sl} and γ_{sv}, where *l*, *v* and *s* represent liquid, vapor and solid phases, respectively. These interfacial tensions (γ) depend upon solid and liquid chemistry and purity. Young's equation is:

$$\cos\theta = \frac{\gamma_{sv} - \gamma_{sl}}{\gamma_{lv}} \qquad 2\text{-}1$$

The highest contact angle reported on a smooth surface is for a fluorinated surface, and is about 120° [12]. To achieve higher (superhydrophobic) contact angles, a surface must be topographically modified. For non-smooth surfaces, prediction of contact angle is much more difficult. Traditionally, the two equations of Wenzel [25] and Cassie [26] have been used to understand superhydrophobicity. Wenzel's model [25] assumes liquid completely fills the surface pores/crevices whereas Cassie's assumes

liquid sits on top of the surface pores/crevices. With increasing intrinsic contact angle, a transition between the Wenzel and the Cassie state is expected at some limiting intrinsic angle for a given topography [27]. Metastable Cassie states have been suggested for surfaces which should exhibit the Wenzel state [28-30], suggesting energy barriers that must be overcome for this transition to take place.

Wenzel's equation describes the Wenzel contact angle (θ_w) as:

$$\cos\theta_w = r\left(\frac{\gamma_{sv} - \gamma_{sl}}{\gamma_{lv}}\right) = r\cos\theta \qquad 2\text{-}2$$

where the effect of topography is modeled by r, the roughness factor, which is the ratio of actual surface area to projected surface area. By this equation, it is seen that for hydrophobic surfaces ($\theta > 90^o$), roughness increases the apparent contact angle, whereas for hydrophilic surfaces ($\theta < 90^o$) roughness decreases the apparent contact angle.

If the drop instead sits atop the pores/crevices of the surface, leaving vapor in the low regions, the Cassie contact angle (θ_c) can be calculated as:

$$\cos\theta_c = f(\cos\theta + 1) - 1 \qquad 2\text{-}3$$

where the effect of topography is modeled by f, the solid fraction, which is the ratio of the surface area that is wetted by the drop compared to the total surface area of the water interface under the drop.

Both Wenzel's and Cassie's equations describe how the intrinsic equilibrium value of contact angle is modified by topography. The act of advancing a drop across a surface increases the contact angle to a higher metastable state compared to the Wenzel, or Cassie, angle. This is termed the advancing contact angle. Likewise, receding a drop across a surface decreases the contact angle to a lower metastable state, resulting in the receding contact angle. The difference between these two contact angles is termed the contact angle hysteresis (CAH). The Wenzel wetting state is assumed to have a high CAH due to the increased work of adhesion necessary to recede the drop, and the Cassie wetting state to have a low CAH [31].

Several papers [e.g. 28,32-36] have showed that the Wenzel and Cassie models do not always predict observed contact angles. Likewise, many alternatives to/modifications of Wenzel's and Cassie's works have been proposed [8,18,28,29,33,34,37-41]. Researchers such as Extrand [42], and Gao and McCarthy [43], have recently argued that the area averages that Wenzel and Cassie present is somewhat erroneous. They argue that the area around the contact line is of more importance. McHale showed in his response [44] that for a homogeneous topography there is no difference in the two considerations. The focus of this paper is not a detailed analysis of different wetting models but the Wenzel and Cassie models will be used as starting points and other considerations will be discussed as needed.

2.3 *Experimental Procedure*

2.3.1 Fabrication of Surfaces

Four surfaces were fabricated for this study. Representative SEM images of each surface, along with topographical and chemical information are shown in Figure 2-1 and Table 2-1.

Smooth silicon wafer was taken as received, diced, drilled with an abrasive bit, thoroughly rinsed with pure water and acetone, and then coated with a 5:1 v:v mixture of FC 75 and Teflon AF 1600 (DuPont Co.) on a spin coater (Model 6700, Specialty Coating Systems Inc.). The holes are necessary for the sessile drop wetting tests as described in Section 2.3.3. Analysis shows the sample to be chemically fluorinated and SEM images and AFM show the sample to be quite smooth compared to the other three surfaces (see Figure 2-1, Table 2-1). This surface is referred to as the control surface in this paper.

Electrochemically etched aluminum samples (aluminum) were prepared* from mill grade aluminum plates. These plates were cut, drilled and prepared following the process outlined by Hennig *et al.* [31]. Briefly, each sample was placed in a bath of H_2SO_4 and $Al_2(SO_4)_3$, and subjected to 28 mA/cm^2 at approximately 45 ^oC for 2 minutes. Following rinsing with pure water, the samples were dried and fluorinated, either by a fluoro-silane (1H,1H,2H,2H-Perfluoroalkyltriethoxysilane from ABCR-catalog or

* by scientists at Leibniz Institute of Polymer Research the, Dresden, Germany (IPF)

Zonyl®FSP from Sigma-Aldrich), or by Teflon coating as described above. In all cases, the molecule tail projected from the surface is the same (a long fluorinated hydrocarbon chain). XPS analysis shows similar chemistry and tests with several liquids have shown the coatings to yield the same contact angles. XPS analysis is shown in Table 2-1 and SEM and AFM results show that the surfaces have a rough, mountain range like topography, with submicron scale bumps on top of micron scale random ridges. SEM images of surfaces before and after coating show no noticeable change in the topography due to coating. These surfaces were measured to have the topographical characteristics listed in Table 2-1.

Plasma etched poly(tetrafluoroethylene) (PTFE), was prepared* following the procedure outlined by Minko *et al.* [45]. PTFE foils (PTFE Nünchritz GmbH, Nünchritz, Germany), 0.5 mm thick were drilled, then cleaned in a ultrasonic bath of $CHCl_3$ for 10 minutes. A stainless steel cylindrical vacuum chamber (diameter 250 mm, height 250 mm) was used for etching. The base pressure obtained with a turbomolecular pump was $<10^{-6}$ mbar. Oxygen (99.95 %, Messer Griesheim, Germany) was fed into the chamber. The samples were placed on an aluminum holder in the center of the chamber though an automatic load-lock. The holder was capacitively coupled to a 13.56 MHz radio frequency generator (Caesar 136, Dressler, Germany) via an automatic matching network. The metallic chamber was grounded, leading to the electrode configuration being highly

* by scientists at Leibniz Institute of Polymer Research the, Dresden, Germany (IPF)

asymmetric and causing self-bias voltages and ion energies at the RF electrode [46]. Process parameters were: oxygen flow 10 sccm, pressure $2x10^{-2}$ mbar, effective RF power 200 W. The self-bias voltage at the RF generator was approximately 1000 V. After etching, samples were again cleaned for 10 minutes in an ultrasonic bath of $CHCl_3$. These surfaces have a natural fluorination (confirmed by XPS), the resulting topography is of a coniferous forest-like series of vertical cones protruding from the surface as shown in Figure 2-1. Topographical characteristics are in Figure 2-1.

Following the previous study [16], AKD surfaces (AKD) were prepared by melting pellets of AKD (Aquapel 364, Hercules Inc.) in a clean beaker heated to 90° C on a hot plate. The mixture was allowed to cool slowly and occasionally stirred, until the liquid became cloudy, indicating the initiation of nucleation, at approximately 35 °C. The mixture was then poured into a stainless steel mold pressed between aluminum heat sinks to solidify the AKD quickly. After a few minutes to ensure solidification, the molds were opened under a nitrogen atmosphere in an enclosure and left under this atmosphere for 72 hours. The enclosure was refilled every 24 hours and the box was not opened during the 72 hours. During this time, the AKD surface naturally develops a random topography made up of angled, plate-like structures shown in Figure 2-1. After the three days, the samples were removed, coated with Teflon™ in the same way as the silicon wafers and pierced with a beveled syringe needle to create the necessary hole for sessile drop contact angle measurements (Section 2.3.3).

Topographical information for the surface is listed in Table 2-1. SEM images of surfaces before and after coating show no noticeable change in the topography. XPS data shows that the fluorination is incomplete; the chemistry is a mixture of saturated (AKD is naturally composed of saturated hydrocarbons) and fluorinated hydrocarbons.

2.3.2 Liquid Types

Three surfactant solutions were tested. Sodium dodecyl sulfate (Fisher Scientific, New Jersey, USA), hereafter referred to as SDS, was used as an anionic surfactant. Hexadecyltrimethylammonium bromide (Sigma-Aldrich, St Louis, USA), hereafter called HTAB, was used as a cationic surfactant and n-decanoyl-n-methylglucamide (Sigma-Aldrich, St Louis, USA), hereafter denoted as MEGA 10, was used as a non-ionic surfactant. Surfactants were used as received without further purification. Three concentrations below the CMC were chosen for each surfactant solution. Nominally, concentrations were 1, 4 and 8 mM for SDS; 0.1, 0.2 and 1 mM for HTAB and 1, 2 and 9 mM for MEGA 10. Concentrations were chosen to yield similar ranges of surface tension both between surfactant types and between surfactants and pure liquids. The three different surfactants, with different ionic properties, were chosen to examine possible effects of charge interactions on the surface and to relate to various possible types of liquid impurities in industrial applications of SHS.

The pure liquids were deinonized water (hereafter referred to as DI water or water, surface tension measured at ~72.28 mN/m), ethylene glycol, EG, (47 mN/m, 99.8% pure), 1-bromonaphthalene, BN, (44.3 mN/m, 97% pure), and hexadecane, HD, (27 mN/m, 99+% pure). The water was from a Millipore system, resistance 18.2 MΩ/cm, all others were used as received from Sigma-Aldrich, St Louis, USA. For each liquid or solution concentration, at least three different surfaces were tested for wettability by sessile drop contact angle measurement (described below).

2.3.3 Surface Tension and Contact Angle Measurements

Surface tension of the pure liquids and surfactant solutions were measured by means of bubble tensiometry (SITA) and pendant drop analysis (First Ten Angstroms). Reported is the average of measurements on three drops, with thirty measurements taken for each drop. Standard deviation is below 1 mN/m for all but 0.2 mM HTAB (for which standard deviation is 1.5 mN/m. Results are presented versus surface tension and not surfactant concentration to allow for comparison between surfactant solutions and pure liquids.

Wettability was studied by means of contact angle measurement, conducted using Axisymmetric Drop Shape Analysis – Profile (ADSA-P) operating in sessile drop mode [47]. To conduct the sessile drop tests, an experimental apparatus was constructed in-house. For sessile drops, a motorized syringe was mounted below the sample. The syringe was driven

at 0.5 μl/s to give a low rate dynamic advancing contact angle. Every 2 seconds, an image of the drop was taken by a CCD camera, after the advancing stage, the drop was left for a period of 10-30 seconds, to observe any change of the contact angle due to relaxation or surfactant effects, or any change in receding behavior. After this period, the motor was reversed and driven at the same rate to give a low rate dynamic receding angle, imaged at the same frequency.

2.4 Results and Discussion

2.4.1 Pure Liquids

Advancing contact angles for pure liquids on all four surfaces are shown in Figure 2-2, with receding angles for the same in Figure 2-3. Figure 2-2 and Figure 2-3 also show the Wenzel and Cassie predictions of wetting for SHS based on their topographic parameters and the advancing/receding contact angles measured on silicon. The r value used in the graphed prediction was taken for AKD (PTFE shows a similar r value, aluminum shows a lower r value) and the f value used was found by considering the best fit between the calculated Cassie angle for pure water and the observed advancing contact angle for water on AKD. The calculation is similar for PTFE and aluminum, but a smaller f is found for each, and the calculated Cassie contact angles are slightly higher.

The results compare relatively well with what other researchers have seen for pure liquids on smooth hydrophobic surfaces. For smooth surfaces,

Kwok and Neumann [48] reported a smooth transition in contact angle with decreasing pure liquid surface tension. They did not observe the same amount of reduction in contact angle as seen between EG and BN in our results. They did not report receding contact angle, but CAH is nearly constant with decreasing liquid surface tension for Teflon™ coated silicon, which is as expected for a well-coated smooth surface. Overall, the results with Teflon™ coated silicon compare well with those reported [48], with advancing angles matching within 3-4°.

In general, all three SHS show high advancing angles for water and EG, and decreased advancing angles for BN and HD. Receding angles behave likewise, decreasing to zero for BN and HD. The exception is AKD, it should be noted that the receding angle for Teflon™ coated AKD surfaces for all liquids tested (pure and surfactant solutions) was zero degrees (drops were pinned throughout the recede, except for one or two frames). Further analysis of our previous data [16] with the traditional definition of receding angle used support this observation: the receding angle for all liquids (pure and solution) for both surface chemistries (unfluorinated and partially fluorinated) is zero. This does not greatly affect the conclusions made in the previous study [16] regarding wetting states, though it affects CAH and therefore applications where dynamic drop effects are concerned [49]. For all three SHS, transitions in advancing and receding contact angle from higher to lower values correspond to the intrinsic contact angle (control surface advancing contact angle) changing from greater than 90°

to less than 90°. Below, the advancing and receding behaviors are discussed separately in greater detail.

PTFE and aluminum show high advancing contact angles (>105°), for all pure liquids. This cannot be explained using the Wenzel wetting mode, which would result in a lower apparent angle for intrinsic angle <90°, as seen in the calculated Wenzel mode data points on Figure 2-2. The Cassie mode can better explain the results. In Figure 2-2, and in all plots showing a Cassie prediction, the solid-fraction, *f*, was varied to fit the Cassie contact angle to the observed apparent advancing contact angle with water, and the predictions for other liquids/solutions use this same parameter value. The calculated Cassie data match the results for other pure liquids better than those of the Wenzel predictions. Traditionally, it is thought that the Cassie mode should not be stable for intrinsic contact angle below 90° [27], but other researchers have suggested the possibility of 'metastable' Cassie states [28,29]. Therefore, it is suggested that the observed data show a 'metastable' Cassie wetting mode for BN and HD on aluminum and PTFE during the advancing stage. The lower observed contact angles (compared to the Cassie prediction) can be understood by considering partial penetration of liquid into the solid, which would increase *f*, something which Cassie himself accounted for in his original derivation [26]. Later in this section, the wetting results obtained by other researchers for pure liquids on SHS will be reexamined with this hypothesis of 'metastable' Cassie states and partial penetration.

Analyzing the contact angles of Teflon™ coated AKD is more complicated, because as stated in Section 2.3.1, the AKD is incompletely coated with Teflon™, leading to lower intrinsic contact angles. To estimate the effect of incomplete fluorination, results [48] for a paraffin wax surface (composed of mostly saturated hydrocarbons) can be used. For formamide (surface tension 58.2 mN/m) on this surface, intrinsic contact angle was 91°. The surface tensions of EG, BN, and HD are all below 58.2 mN/m, extending the data [48] to the surface tensions of EG, BN, and HD, intrinsic contact angles of 80° or lower would be expected for these liquids on a smooth, saturated hydrocarbon surface like uncoated smooth AKD. The intrinsic contact angles for the semi-fluorinated AKD would be between that measured on Teflon™ coated silicon and the extended data from literature [48]. Conservatively, one could suggest a 10° decrease in intrinsic contact angles for Teflon™ coated AKD compared to Teflon™ coated silicon, i.e., around 90° for EG, 78° for BN and 58° HD.

The advancing contact angles on the Teflon™ coated AKD surface are generally slightly higher than those seen on uncoated (CH_3 terminated) AKD [16], which is expected given that both the coated and uncoated AKD have the same topography and somewhat similar chemistry. The wetting for Teflon™ coated AKD appears to be Cassie mode for water and EG. This is expected based on the modified intrinsic contact angle as discussed above. Normally, the Cassie state would be expected to exhibit low CAH.

Instead, AKD shows a high CAH (recede angle equals zero). This can be explained by chemical heterogeneity on the surface, which would provide pinning points for the contact line, decreasing its recede value. This view is supported by XPS analysis that shows esters and other hydrophilic surface groups present in low quantities on both the unfluorinated and Teflon™ coated AKD surfaces. In concert with this, the somewhat lower intrinsic contact angle on Teflon™ coated AKD (due to incomplete coating) could lead to an easier transition to the Wenzel state during the recede.

For the BN data on Teflon™ coated AKD there are two possible explanations. The finite, hydrophilic contact angle could be a result of the Wenzel mode lowering the apparent contact angle. Alternatively, it can be understood as a partially penetrated Cassie state (as discussed for BN and HD on PTFE and aluminum above) in which the liquid has penetrated the top part of the surface but where there are still air pockets trapped in the very base of the topography. This would obviously be a greater penetration compared to that suggested for aluminum and PTFE. Given the decreased intrinsic contact angle due to incomplete fluorination, the first explanation is more likely. The wetting state for HD appears to be Wenzel, considering intrinsic and apparent contact angles.

The idea of a transition in wetting on Teflon™ coated AKD from Cassie to Wenzel as probe liquid surface tension decreases between EG and BN is well supported in literature. Shirtcliffe *et al.* [13] Rao *et al.* [14] and Fujita

et al. [15] all studied penetration of non-aqueous pure liquids into SHS of various different materials and fabrication techniques. Contact angles were not reported or not reported rigorously, but all three found that for sufficiently low surface tensions (surface tension was unreported for [13], ~30 mN/mm for [14], ~22.3 mN/mm for [15]), liquids penetrated the pores/crevices in the SHS, transitioning from a Cassie to a Wenzel wetting mode. This observed switch to penetration supports the observation of the same switch for Teflon™ coated AKD advancing angles (and PTFE and aluminum receding angles). None of the above three papers reported results for intermediate surface tensions between un-penetrated tests with higher surface tension liquids and the penetrated states observed.

Shibuchi *et al.* [6] observed a similar result to Teflon™ coated AKD for water/dioxane mixtures on purified AKD SHS. They reported a contact angle above 150° for water, decreasing abruptly at 85:15 water/dioxane (no surface tension value was given but the surface tension of dioxane is 33 mN/m at 20 °C [50]). This abrupt drop from above 90° to below 90° was observed to roughly coincide with intrinsic contact angle passing 90°, just as it does for Teflon™ coated AKD and silicon between EG and BN. They did not report receding angle. Shibuichi *et al.*'s results can be interpreted as a switch from the Cassie to the Wenzel mode, as seen with Teflon™ coated AKD. Clearly, the literature supports the observed transition in wetting on Teflon™ coated AKD.

Comparing the three surfaces, the aluminum surface topography results in the least decrease in advancing contact angle for the three topographies and four pure liquids tested. The aluminum has a lower *r* value compared to PTFE and AKD (see Table 2-1), and has a 'bumpy' microtexture, with submicron bumps on top of a mountain range like micron scale structure (see Figure 2-1), whereas PTFE and AKD have higher *r* values, and have mainly vertical, sharp features. The aluminum's dual-scale topography gives possibilities for 'overhanging' or 're-entrant' structures that can explain the higher contact angles compared to the other two surfaces. Herminghaus [29] suggests that these overhanging structures allow a surface with intrinsic contact angles below 90° to form liquid bridges over the pores/crevices of a surface, more easily leading to a 'meta-stable' Cassie state. This concept is shown schematically in Figure 2-4.

The observed high apparent contact angles for aluminum and PTFE when intrinsic angles are below 90° are also seen by other experimenters. Shibuichi *et al.* [17] studied electrochemically etched fluorinated aluminum. They reported high contact angles, 166° with water. With hexadecane, they found angles of 75.5° and 135.5° on smooth and etched samples, respectively, which compare well with hexadecane results on Teflon™ coated silicon and aluminum/PTFE samples in this study respectively. They did not present receding values. They suggested the observed high apparent contact angles for intrinsic contact angles below 90° could be explained by differences in chemical structure on smooth and

rough surfaces. This explanation is questionable; they measured a contact angle of 119° on their smooth fluorinated surface. This is very close to the theoretically maximum attainable intrinsic contact angle [12]. It is difficult to imagine how a rough surface could show a packing of fluorinated tail groups that is closer than the closest packed hexagonal structure reported in literature [12]. Shibuichi *et al.*'s data can, however, be explained as a 'metastable' Cassie based wetting mode aided by the topography [29], along with partial penetration of liquid into the surface, as suggested in our analysis for aluminum and PTFE SHS.

Chen *et al.*'s [18] results also support the 'metastable' Cassie state hypothesis suggested for aluminum and PTFE. For packed spherical particles of PTFE they reported advancing/receding angles of 177°/177° with water, 140°/138° with methylene iodide (γ_{lv} = ~50.8 mN/m at 20 °C [50]) and 140°/125° with hexadecane. Their results with hexadecane reinforce the idea that re-entrant structures (formed here by the packing of the PTFE spheres) can result in 'meta-stable' Cassie states and high contact angles for liquids with intrinsic contact angle below 90°.

Now the receding behavior of aluminum and PTFE surfaces will be considered in more detail. For EG on aluminum, and water on PTFE and aluminum, one sees high receding contact angles, suggesting the Cassie receding state, which is supported by consideration of the intrinsic contact angle. For other liquids, it is generally seen that when the intrinsic contact

angle (advancing contact angle on the control surface) is below 90°, any topographic modification results in an apparent receding contact angle of zero degrees. This can be understood from the Wenzel wetting mode, since the high roughness of the surfaces decreases apparent contact angles below 90°. Based upon these observations, we propose that there is a transition to the Wenzel mode on the recede of BN and HD for aluminum and PTFE surfaces. The transition from a 'metastable' Cassie state on the advance to a Wenzel state on the recede could be due to microscopic contact line pinning by chemical heterogeneities or topography, or could be an effect of the constrained wetting seen in re-entrant structures.

Figure 2-2 and Figure 2-3 show that the Wenzel prediction of equilibrium contact angle for HD is zero, while it is low but not zero for BN. To have a better match between observations and the predictions of the Wenzel equation, r would have to be ~10. The discrepancy between measured and predicted receding contact angle for BN and HD can be accounted for by considering that 1) the r values are likely higher than measured due to the tip radius of the AFM. 2) chemically heterogeneous patches can lead to pinning and further decrease the receding contact angle. 3) receding the drop will lead to a receding contact angle lower than the equilibrium Wenzel predictions (due, in part, to (2)). The second and third considerations are likely more important. The AFM tip size issue is unlikely to result in an underestimation of the roughness factors of the SHS by 4-5 times.

The large standard deviation of the receding angle of EG on PTFE is representative of one test showing a high receding value, and two where the contact line was pinned resulting in a receding contact angle of zero degrees. Given that this data point is the average of three tests, no concrete conclusions can be drawn regarding the cause of this result without further tests of EG on PTFE with fine control of the surface chemistry.

Comparing to literature, Chen *et al.* [18] reported a receding angle for hexadecane above 90° on their SHS, for an intrinsic angle that should be below 90°. This suggests that the topography of Teflon™ coated aluminum could be even further improved, but it is certainly the best of those tested here for repellency of non-aqueous pure liquids. Otherwise, most researchers have either not reported receding contact angles, or found them to be low for the collapsed Wenzel state on SHS, as with our results. In the next section, the wetting results for surfactant solutions are presented.

2.4.2 Surfactant Solutions

Surfactant wetting results are presented in Figure 2-5 through Figure 2-9. Advancing and receding contact angles are shown for all three surfactant solutions with the pure liquid values plotted for comparison purposes for each surface (Control in Figure 2-5, AKD in Figure 2-7, PTFE in Figure 2-8, and aluminum in Figure 2-9). As stated in Section 2.3.3, drops were

monitored for at least 10-30 seconds between advancing and receding stages, in some cases they were monitored for 5 minutes. The dwell time was therefore beyond the expected time for spreading of surfactant solutions on smooth surfaces [20-24] which could lead to penetration into the pores and crevices of SHS; little to no spreading of the drop was seen in this time frame (1-2° maximum, which is within the error bars on the data points).

Examining the accumulated results, one can see that wetting by surfactant solutions seems largely independent of surfactant polarity. Also, there are differences in the way surfactants and pure liquids of similar surface tension wet SHS *and* a smooth hydrophobic surface. The interesting results seen on Teflon™ coated silicon are discussed first.

Figure 2-5 shows an interesting result, finding that surfactant solution contact angles match pure liquid results well for surface tensions above ~45 mN/m, but are higher for lower surface tensions Note that below ~45 mN/m the intrinsic contact angle of pure liquids is measured to be below 90°. Kumar *et al.* [22] and others [20,21,23] suggested that surfactant solutions should show decreased contact angles beyond that expected due to the decrease in solid-liquid and liquid-vapor surface tensions alone. They term this effect autophilicity but did not consider how contact angles of solutions would compare to those of pure liquids with similar surface tension. Clearly however, the autophilic effect is not seen to decrease the

contact angle of surfactant solutions on hydrophobic Teflon™ coated silicon when compared to pure liquids of similar surface tension. This could be due to differences in the way that surfactants change the solid-liquid surface tension compared to the value the solid-liquid surface tension takes for pure liquids. Plotted in Figure 2-6 are the surfactant results from Figure 2-5, as well as contact angle data for SDS [24] and pure liquids [48] for Teflon™ coated silicon. The pure liquid results from Figure 2-5 have been removed for graphical clarity. Again, surfactant solution contact angles are seen to be equal to or higher than pure liquid results. We do not have a complete explanation for these observations at this time. This result suggests the subject as it appears in the literature is not completely understood. Thus, further theoretical and experimental study is needed to investigate the importance of the autophilic effect and see how surfactant wetting compares to pure liquid wetting on smooth hydrophobic surfaces.

Considering the results seen on smooth Teflon™ coated silicon, several possible mechanisms exist to explain the observed difference in contact angles between surfactant solutions and pure liquids of similar surface tension on SHS. These mechanisms will be outlined below, and then the observed results will be discussed with regards to these mechanisms to determine which one(s) best explain the observed behavior.

The higher contact angles seen on SHS for surfactants versus pure liquids could simply be the result of intrinsic contact angle. The advancing contact angle on silicon is above 90° for all solutions except the maximum concentration of MEGA 10, which shows a contact angle of 86.1° (see Figure 2-5). This could lead to a more stable Cassie wetting state for SHS wetted by surfactant solutions compared to those wetted by pure liquids of a similar surface tension, but lower intrinsic contact angle.

The surfactants themselves could also be inhibiting the penetration of liquid into the pores/crevices of the surface. As suggested before [13,16], surfactants could be forming a film at the liquid-vapor interface that exists underneath the drop at the pores/crevices in the surface. A surfactant film could inhibit penetration of liquid into these crevices, maintaining a Cassie wetting state for lower surface tensions.

Regarding the receding angle of surfactant solutions on SHS, Shirtcliffe *et al.* [13] hypothesize that a surfactant film could stretch between features on the receding. They suggested that this elastic stretching could pin the contact line and decrease receding contact angle. Varanasi and Garoff's observations [23] of contact line pinning due to surfactant re-self-assembly on smooth hydrophobic surface could also affect the receding angle on SHS since microscopic pinning points would decrease the local contact angle at a pore/crevice and could conceivably trigger a transition

to the Wenzel wetting state. Finally, the possibility of constrained wetting could inhibit the leakage of surfactant solutions into crevices. Surfactant solutions have been shown to resist passing sharp corners in constrained wetting situations as demonstrated in the application of inverted frusta for extremely low surface tension measurements [51].

Considering the above mechanisms to describe the wetting of surfactant solutions on SHS, the similarities and differences in wetting behavior of these solutions compared to pure liquids are discussed next.

For advancing contact angle, one can see that the previously observed [16] higher values for surfactants versus pure liquids are repeated for all three SHS. This is similar to the results of Ferrari *et al.* [19] and Shirtcliffe *et al.* [13], both of whom showed SHS maintain high contact angles for surfactant solutions of high concentration (both studied fluorinated surfaces). Altogether, this suggests that dependant on the topography, the surfactants must somehow inhibit the penetration of liquid into the crevices of the SHS (since as discussed in the Section 2.4.1, penetration of liquid into the surface leads to extremely low contact angles).

The fact that all measured advancing contact angles for SHS are above 90° suggests the surfactant solutions are wetting the surface in the Cassie mode. This is supported by observing the Cassie and Wenzel calculations on Figure 2-7 through Figure 2-9, which show that the Cassie predictions

match the observed behavior well for aluminum and PTFE (using the solid fraction, *f*, as a fitting parameter just for the advancing contact angle of water on each surface). The Wenzel predictions do not match the data, and provide several predictions of contact angle greater than 180° (physically impossible, and denoted on the graph as a contact angle of 180°). The Cassie predictions fail at the highest concentration of MEGA 10 for PTFE and generally overestimate the contact angle at higher surfactant concentrations on AKD. This suggests a Cassie mode wetting with partial penetration of the surfactant solution into the AKD and PTFE surfaces as surfactant concentration is increased. This was seen on PTFE and aluminum surface with BN and HD, which suggests that surfactant solutions and pure liquids can show similar wetting states but to different extents and at different surface tensions.

As discussed above, the increased intrinsic contact angle, taken from the advancing angle of surfactant solutions on silicon, does lead to higher contact angles on SHS. Even considering this increase in intrinsic contact angle, surfactants must be further preventing penetration of liquid into the crevices of the surface. Consider intrinsic contact angle as measured by advancing contact angle on Teflon™ coated silicon. On Teflon™ coated silicon the advancing angles for EG and BN are 102.9° and 88.4°. In this range of intrinsic contact angles, there are five contact angle data points for surfactant solutions (the three concentrations of MEGA 10 and the maximum concentrations of HTAB and SDS). These solutions span a range

of advancing contact angle on Teflon™ coated silicon from 103.8° to 86.1°. Plotting the contact angle on the SHS versus intrinsic contact angle in Figure 2-10 through Figure 2-12, one can see that pure liquids present a range of apparent advancing contact angle (advancing angle on SHS) that are generally significantly lower than the range of apparent advancing contact angle for surfactants solutions *within the same intrinsic contact angle range.* On the figures, the Cassie prediction has been plotted for comparison, calculated for intrinsic contact angle from 85° to 105° in steps of one degree.

The increase in surfactant solution wetting compared to pure liquid wetting is most apparent in Figure 2-10. Here two distinct regions have been drawn delineating the apparent contact angle range for pure liquids and the higher intrinsic contact angle range for surfactant solutions. The difference can also be seen in Figure 2-11. While solutions and pure liquids show similar wetting for control surface advancing contact angle greater than 90°, for lower intrinsic contact angles the pure liquid results drop lower and faster than the surfactant solution results. On Figure 2-12 the results are quite close to each other, and standard deviations of the data point overlap. The aluminum gives very high contact angles with pure liquids compared to PTFE and AKD, and this was understood to signify an unpenetrated Cassie state for EG and BN on aluminum. While the surfactant solutions do show even higher advancing contact angles, if pure liquids are already not penetrating the SHS, surfactant solutions could not

be expected to further inhibit penetration. If the pure liquids are showing some partial penetration into the aluminum SHS, it is possible that the surfactant solutions would inhibit this, explaining the slightly higher values.

With the possible exception of aluminum, the increases seen cannot be explained by the higher intrinsic contact angle for surfactant solutions compared to pure liquids of similar surface tension. The data in Figure 2-10 through Figure 2-12 accounts for the increased intrinsic contact angle (i.e. the data are effectively normalized for intrinsic contact angle). We therefore propose that in addition to the effect of increased intrinsic contact angle, the surfactants are forming a film over the crevices of the surface at the liquid/air interfaces below the drop as suggested in previous literature [13,16]. The surfactant solution wetting results generally match the Cassie predictions better than pure liquids do for all three surfaces, especially at lower intrinsic contact angles, further supporting the idea that surfactant films are maintaining the drop in the Cassie state and leading to an increased contact angle compared to pure liquids of similar intrinsic contact angle. Below, the receding behavior of surfactant solutions on the SHS is investigated.

The surfactant solution receding contact angles on aluminum show the same trend as pure liquids, pinning to zero degrees for surface tensions below ~45 mN/m. This behavior is similar to the receding contact angle

data in [13] where for high surfactant concentrations receding angle was reduced to zero. Contact angle measurements on Teflon™ coated AKD again show zero contact angle. Together, these results suggest that the effect of surfactants in increasing advancing contact angles is not necessarily carried over to receding angles.

PTFE surfaces show non-zero receding contact angles, this observation suggests a maintained Cassie state in the receding phase. This is similar to the data presented in [19] where receding contact angle remained above 140° for very high SDS concentrations (i.e. 2cmc). This suggests that topography can play an important role in the receding behavior of surfactant solutions. The PTFE surfaces show receding contact angles of 120.2° and 114.7° with maximum surfactant concentration of SDS and intermediate concentration of MEGA 10, respectively. The receding contact angles on Teflon™ coated silicon for these solutions are 86.1° and 90.8°, respectively, and pure liquids of similar and even higher surface tension/intrinsic contact angle show receding contact angles of zero on PTFE. The maximum SDS concentration data suggests that surfactant films can prevent penetration on the recede for control surface receding contact angle less than 90° (unseen for receding contact angles of pure liquids, but similar to the advancing case seen on all three surfaces). The maximum concentrations of HTAB and MEGA 10 show the lowest control surface advancing and receding contact angles for surfactant solutions, and give a receding angle of zero on PTFE. This suggests there is a critical

control surface contact angle below which surfactants cannot aid in maintaining the Cassie state during the recede. Given that the maximum concentration of HTAB has a larger surface tension but lower intrinsic contact angle than the maximum concentration of SDS, this suggests that there might be an effect of surfactant polarity (possibly manifested through intrinsic contact angle) on the receding behavior of surfactant solutions on SHS.

Simple consideration of the intrinsic contact angle cannot entirely explain how surfactants affect the receding behavior on SHS, as seen on PTFE compared to aluminum. Pinning of the contact line due to surfactant film stretching [13] and/or surfactant re-self-assembly [23] can explain the behaviors on aluminum and PTFE. The dual-scale topography of the aluminum could give a greater number of pinning points for the surfactants whereas the sharper topography of the PTFE could provide fewer pinning points, leading to lower and higher receding contact angles, respectively. Constrained wetting on the PTFE could also inhibit leakage of solution into crevices. Finally, XPS data shows PTFE and aluminum have low levels of surface impurities. These impurities could pin the contact line on the recede, but without greater study no conclusions can be drawn on the relative impacts for each surface. Given the incomplete understanding, the receding behavior of high concentration, sub-CMC surfactant solutions on SHS is a topic that warrants further study.

2.5 *Summary, Applications, and Conclusions*

The wetting of four pure liquids of various surface tensions (~27-73 mN/m) and nine surfactant solutions of various polarities was studied on fluorinated surfaces with four different topographies. Surfactant solutions gave equal or higher contact angle compared to pure liquids of similar surface tension on all surfaces.

For pure liquids on all superhydrophobic surfaces (SHS), advancing contact angles remained high for intrinsic contact angles above 90°. Below this, results depend strongly on topography. The plate like topography of the AKD (Ra = 1.248) shows an abrupt decrease in advancing angle for pure liquids with intrinsic angle below 90°, in keeping with a change from Cassie to Wenzel wetting. The lower roughness (Ra = 0.4 μm) dual-scale topography of the aluminum is seen to give higher advancing contact angles than the higher roughness (Ra = 1.328 μm) single-scale sharp topography of the PTFE samples. For both, contact angle is above 120° for intrinsic contact angle below 90°. This is explained as 'metastable' Cassie states, which is supported by the literature.

Pure liquid receding angle is also topography dependant. For similar surface chemistries receding contact angles with EG range from zero on PTFE to a value close to the advancing contact angle on aluminum. In general, receding contact angle on SHS is high for intrinsic contact angles greater than 90° and zero otherwise (showing the Cassie and Wenzel

states, respectively, during the recede) Receding angle is zero for AKD for all surface coatings/liquids tested, a correction to previous work [16]. It is understood as the result of topography and/or chemistry aided pinning of the contact line.

For industrial applications involving non-aqueous pure liquid repellency, the aluminum surface (or a similar topography) would be the best choice of the three SHS presented, maintaining high advancing contact angles for all pure liquids tested, and high receding contact angles for pure liquids with intrinsic contact angle >90°. With water, the PTFE surface yields the lowest CAH of the surfaces tested. For industrial applications, the sharp forest-like topography of the PTFE surface might allow greater drop mobility for water compared to the bumpy, dual-scale topography of the aluminum.

On smooth hydrophobic surfaces, surfactant solutions (used as an analog for impure liquids) do not decrease the contact angles compared to pure liquids of similar surface tension. Further, for pure liquid intrinsic contact angles less than 90°, surfactant solutions show intrinsic contact angles greater than those for pure liquids. This type of comparative test on a smooth hydrophobic surface is unreported to date, and the somewhat surprising results here question how the autophilic effect [20-23] affects wetting by surfactant solutions versus pure liquids.

Surfactant solution wetting on SHS is more complicated. As before, [16], solutions show equal or higher advancing contact angles than pure liquids of similar surface tension (as seen in Figure 2-7 through Figure 2-9). The increased intrinsic contact angle cannot alone explain this result (as seen in Figure 2-10, and to a lesser extent Figure 2-11 and Figure 2-12); we therefore propose that surfactant films are inhibiting penetration of solution into SHS. Aluminum shows the highest advancing contact angle with surfactant solutions, but follows the receding behavior of pure liquids, decreasing to zero for the same surface tensions (below ~45 mN/m). This is explained as a result of microscopic pinning of the contact line by surfactant film stretching and re-self-assembly. PTFE shows advancing contact angles near those on aluminum, and hydrophobic receding contact angles for some surfactant solutions with surface tensions below 45 mN/m. This suggests that with a sharper topography, 'metastable' Cassie states can exist for receding drops of surfactant solution. This result bears further investigation to determine if it is repeated and what its exact cause is.

To try to make a SHS repellent for both pure and impure liquids, one could construct a dual-scale surface of sharp features and test if this topography gave repellency for all liquid/solutions. A combination of sharp and bumpy features might also combine the repellent behaviors seen in the aluminum and PTFE samples. Failing this, when considering a SHS for industrial applications trade offs may be necessary. It would be important to

consider the expected level and type of liquid(s)/impurities. This information could be related to an equivalent type and concentration of surfactant. Considering this information and the desired wetting performance [49] one could choose an appropriate topography for a surface. For example, if high advancing angle were more important at high impurity concentration, the generally bumpy and dual-scale topography of the aluminum samples may be a better choice. If low CAH (related to drop friction) or higher receding angles were more important, the spiky structure of the PTFE samples would be advisable. If the surface is to be used as a sensor [13], topography like the AKD sample would be better, giving a gradual decline that seems simply dependant on impurity concentration.

Table 2-1: AFM, and XPS results for AKD (Teflon™ coated), plasma etched PTFE (naturally fluorinated), electrochemically etched aluminum SHS (Teflon™ coated), and smooth Teflon™ coated silicon control sample. Value in parenthesis denotes standard deviation. * For silicon, measurements are in nanometers, not microns.

	AKD	PTFE	Aluminum	Silicon
Ra (microns*)	1.248 (0.17)	1.328 (0.41)	0.40 (0.19)	48.35 (25.48)
Rq (microns*)	1.53 (0.15)	1.65 (0.78)	0.50 (0.21)	57.17 (28.70)
Rmax	7.82 (0.18)	8.741 (0.35)	3.80 (0.37)	275.69 (72.6)
Wenzel Roughness Factor, *r*	2.85 (0.27)	2.78 (0.15)	1.77 (0.15)	Not Available
Fractal Dimension (by cube counting)	2.23 (0.06)	2.29 (0.07)	2.38 (0.09)	Not Available
[F]:[C]	~0.3	~1.2	~1	~1.45

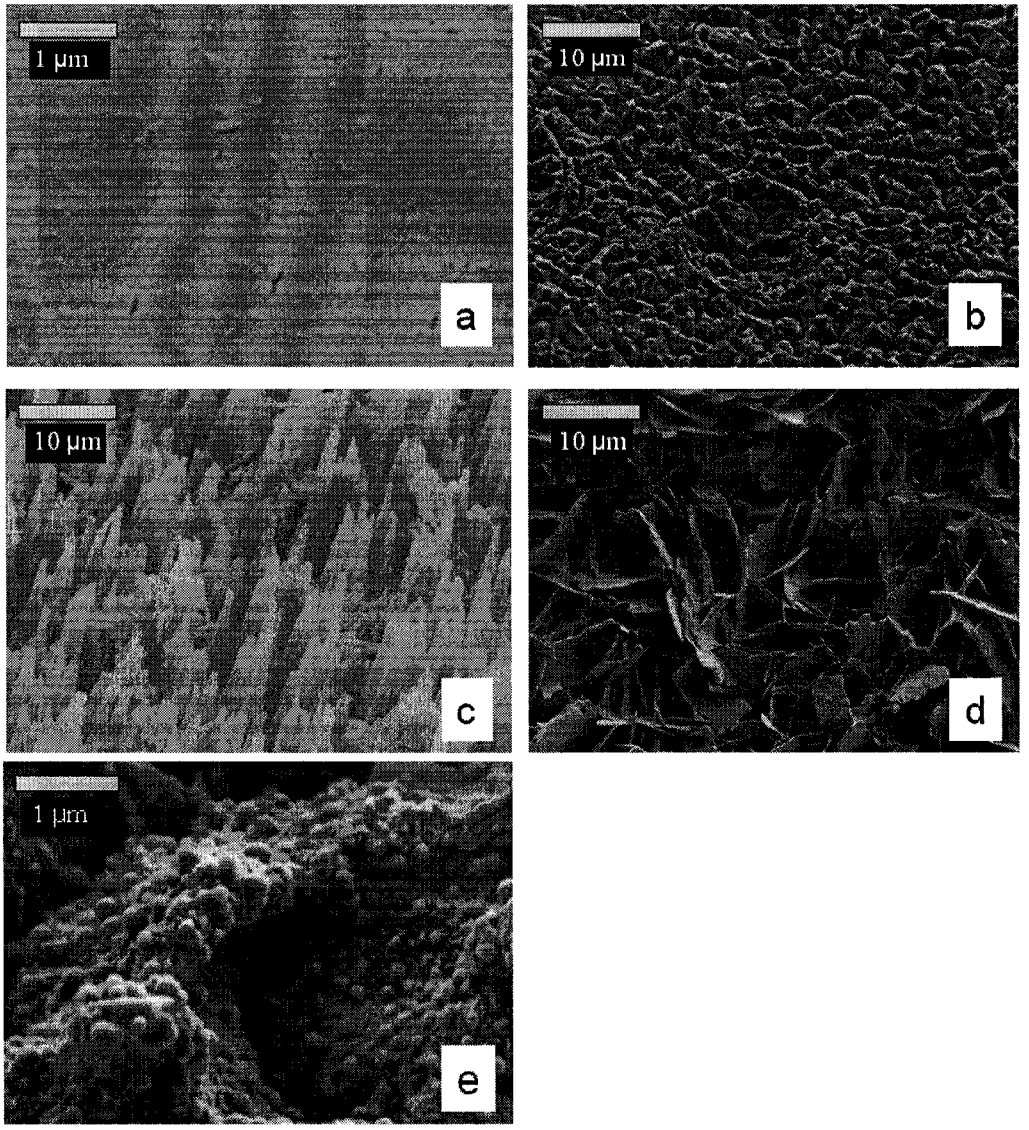

Figure 2-1: SEM images of: (a) Teflon™ coated silicon, (b) fluorinated electrochemically etched aluminum, (c) plasma etched PTFE, and (d) Teflon™ coated AKD. Scale bar for (a) is approximately 1 micron, scale bars for (b),(c),(d) are approximately 10 microns. (e) SEM image of aluminum at higher magnification, showing fine features on top of larger features seen in (b), signifying dual-scale nature of the topography; scale bar is approximately 1 micron.

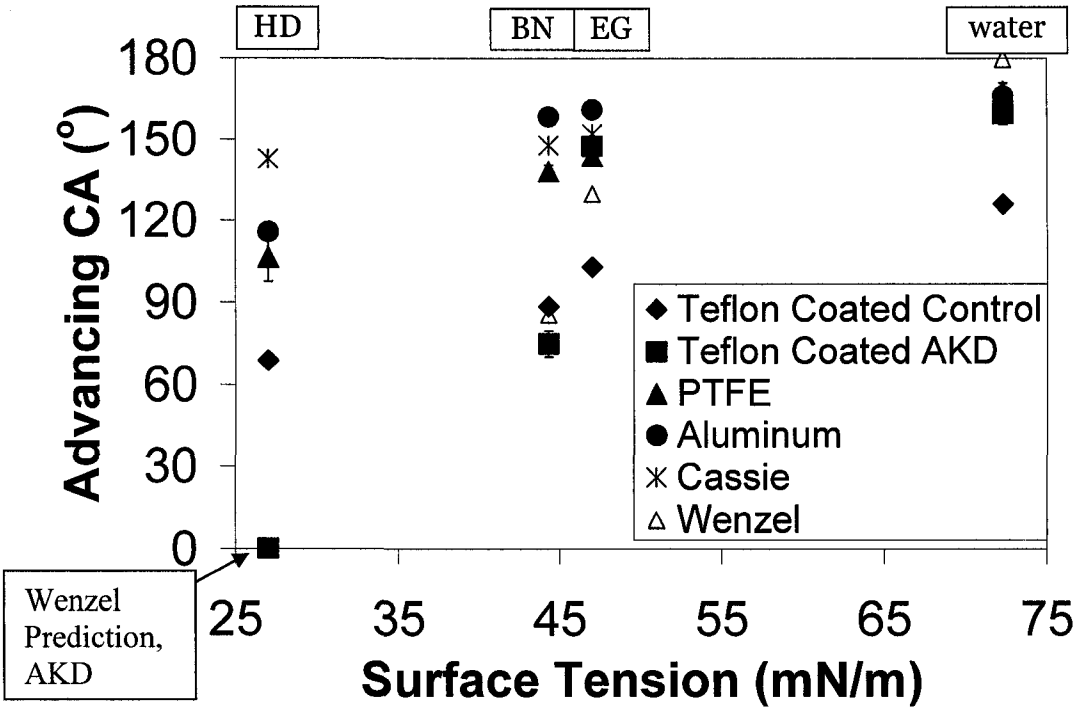

Figure 2-2: Advancing contact angle (CA) for water, ethylene glycol, 1-bromonaphthalene, and hexadecane on three topographically modified fluorinated surfaces and smooth fluorinated control surface. Pure liquids are labeled above the graph. Standard deviation was calculated for each data point, in several cases the value is so low that the error bars are within the symbol itself. The calculated Cassie (f=0.15) and Wenzel (r=2.85) predictions are shown using the intrinsic advancing contact angle data from Teflon™ coated silicon. Wenzel predictions above 180° (physically impossible) are shown equal to 180°. Cassie and Wenzel wetting equations describe equilibrium contact angle (between advancing and receding).

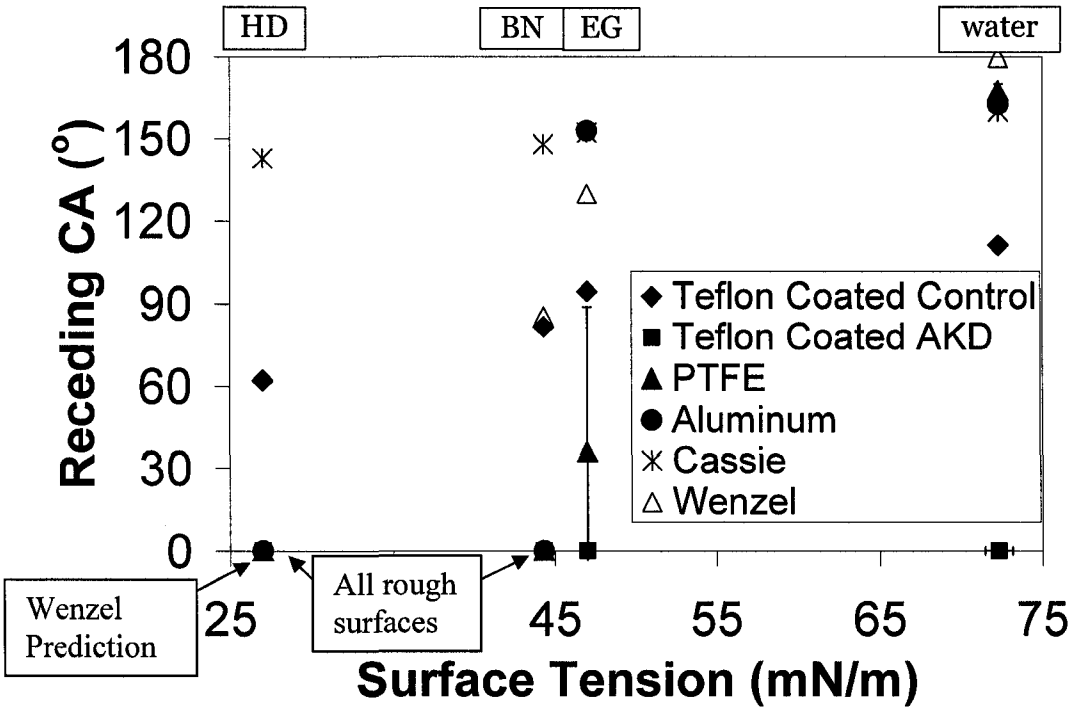

Figure 2-3: Receding contact angle (CA) for water, ethylene glycol, 1-bromonaphthalene, and hexadecane on three topographically modified fluorinated surfaces and smooth fluorinated control surface. Pure liquids are labeled above the graph. Standard deviation was calculated for each data point, in several cases the value is so low that the error bars are within the symbol itself. The calculated Cassie (f=0.15) and Wenzel (r=2.85) predictions are shown using the intrinsic advancing contact angle data from Teflon™ coated silicon. Wenzel predictions above 180° (physically impossible) are shown equal to 180°. Cassie and Wenzel wetting equations describe equilibrium contact angle (between advancing and receding).

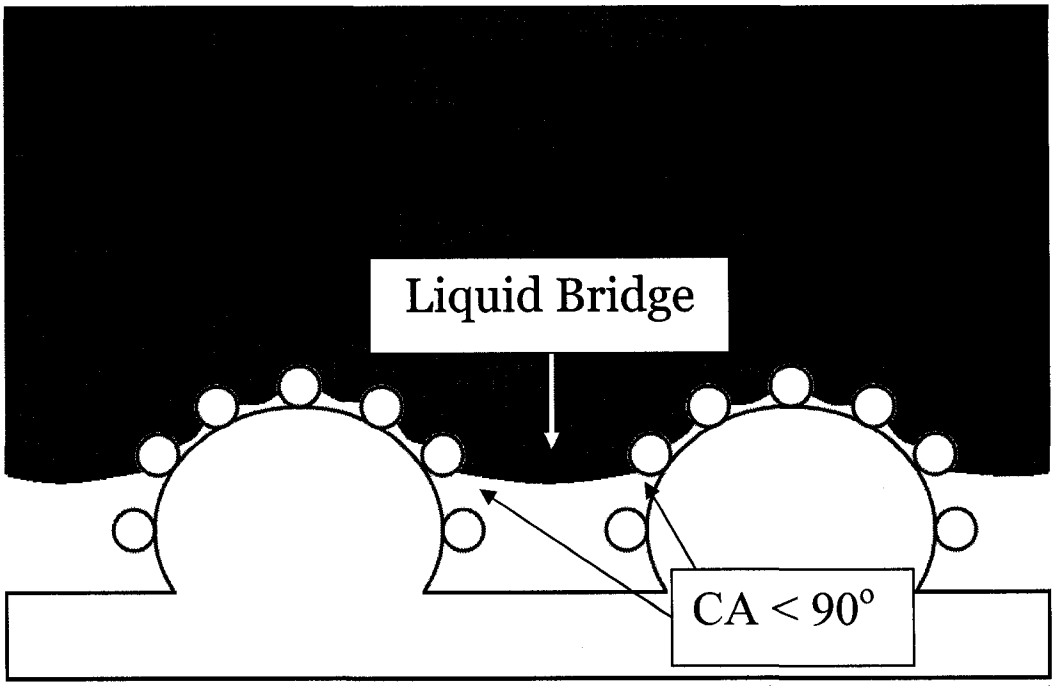

Figure 2-4: Schematic of topography resulting in overhanging (re-entrant) liquid bridging for local microscopic contact angle.

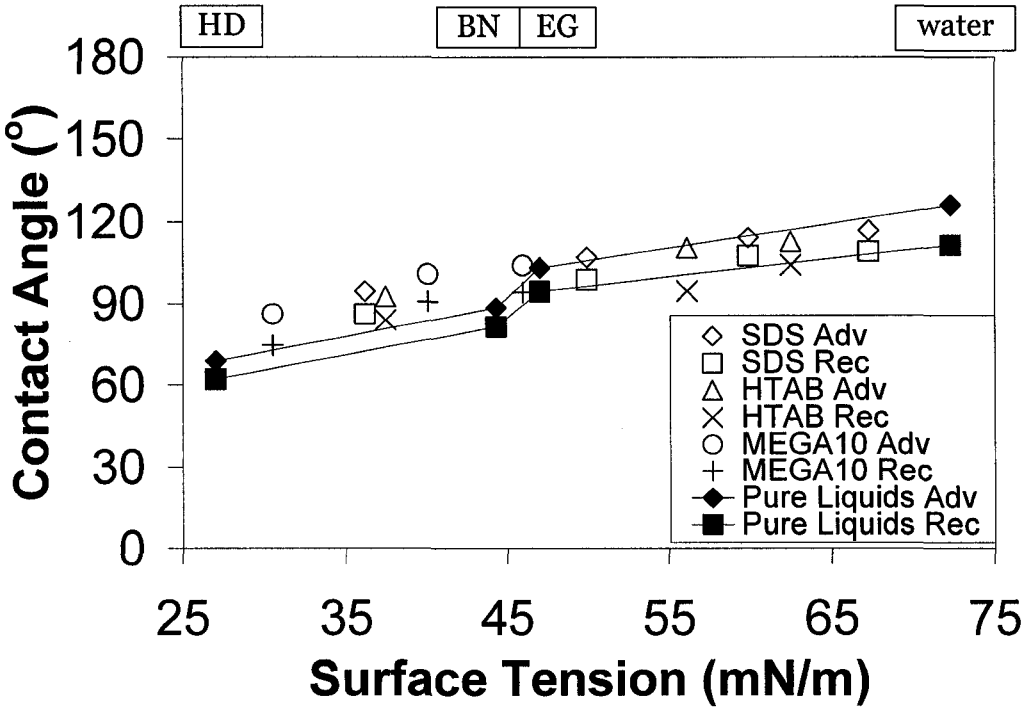

Figure 2-5: Surfactant solution and pure liquid contact angles for Teflon™ coated silicon control surface. Pure liquids are labeled above the graph. Standard deviation was calculated for each data point, in each case the value is so low that the error bars are within the symbol itself. Lines are to guide the eye.

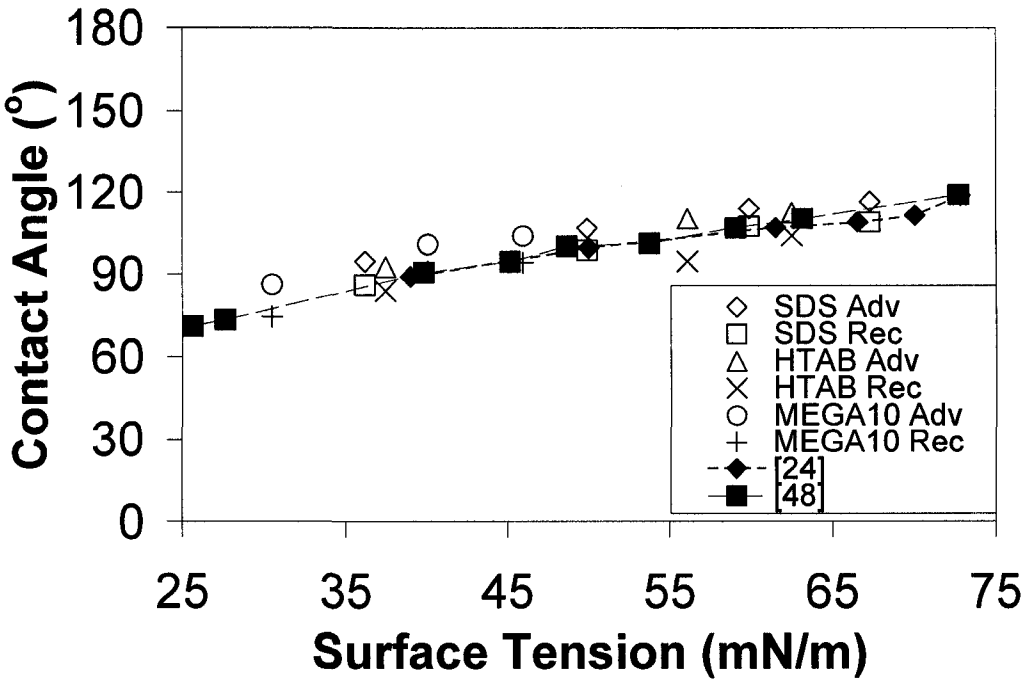

Figure 2-6: Advancing and receding surfactant solution contact angles for Teflon™ coated silicon control surface. Standard deviation was calculated for each data point, in each case the value is so low that the error bars are within the symbol itself. Also plotted are advancing contact angles for SDS solutions [24] and pure liquids [48] on Teflon™ coated silicon. Lines are to guide the eye.

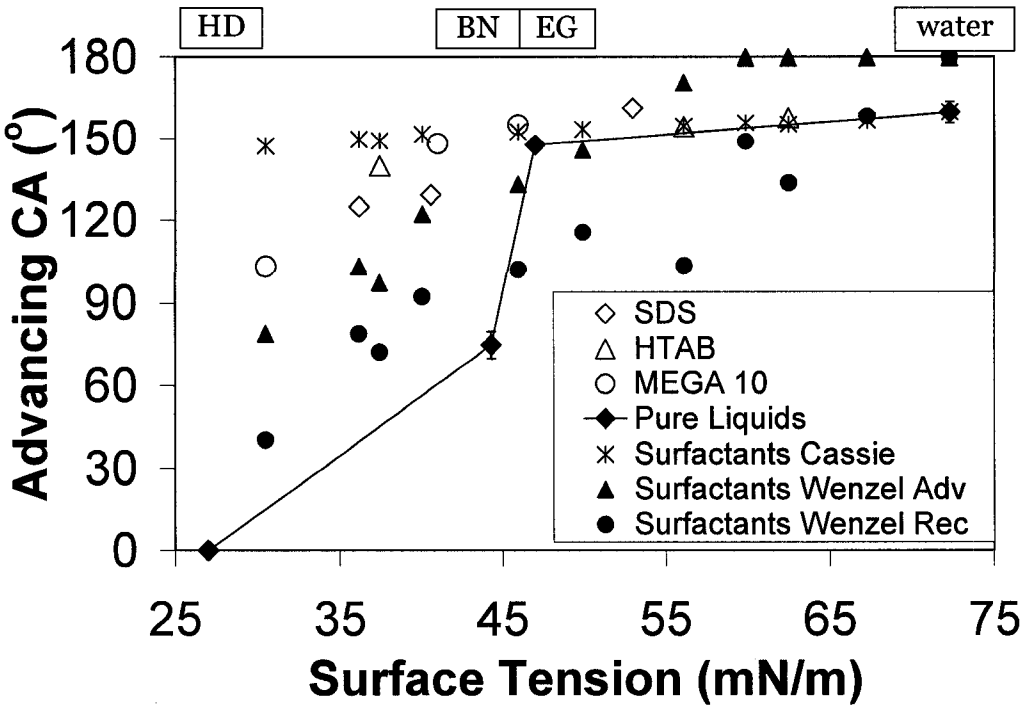

Figure 2-7: Surfactant solution and pure liquid advancing contact angles (CA) for partially fluorinated Teflon™ coated naturally rough AKD. Pure liquids are labeled above the graph. Standard deviation was calculated for each data point, in several cases the value is so low that the error bars are within the symbol itself. Lines are to guide the eye. The calculated Cassie (f=0.15) and Wenzel (r=2.85) predictions are shown using contact angle values on Teflon™ coated silicon. Wenzel predictions above 180° (physically impossible) are shown equal to 180°. Calculated Cassie angle based on receding angle is approximately equal to advancing value and is not shown. Two calculations for Wenzel angle (based on advancing and receding control surface contact angles) are shown and the true value is between them. Strictly speaking, Cassie and Wenzel wetting equations describe equilibrium contact angle (between advancing and receding).

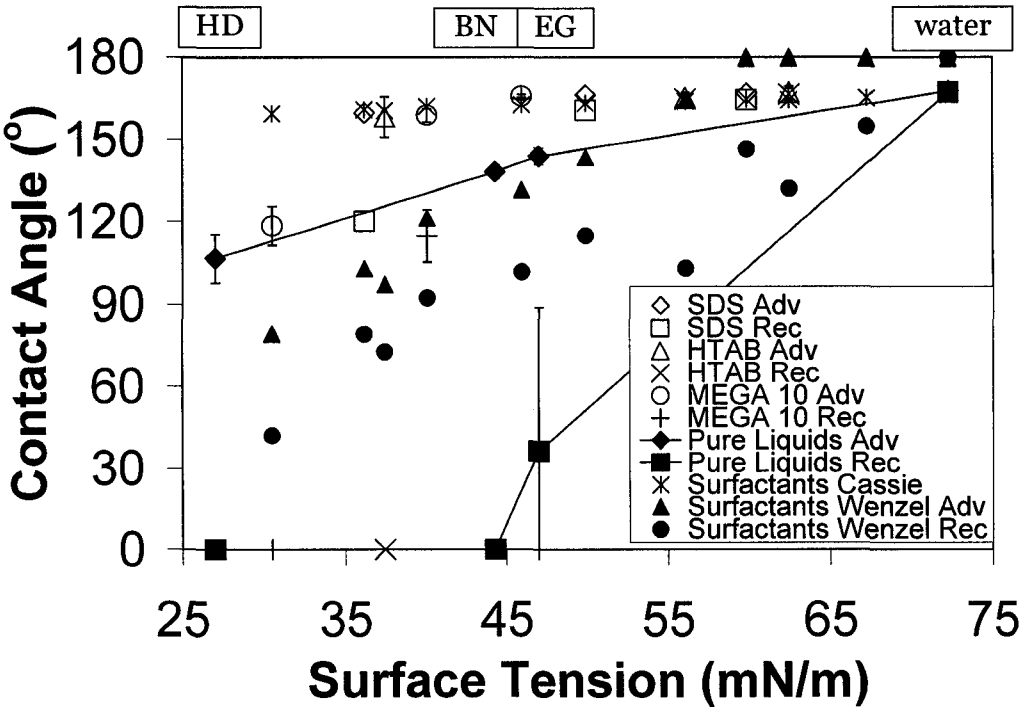

Figure 2-8: Surfactant solution and pure liquid contact angles for plasma etched PTFE. Pure liquids are labeled above the graph. Standard deviation was calculated for each data point, in several cases the value is so low that the error bars are within the symbol itself. Lines are to guide the eye. The calculated Cassie (f=0.06) and Wenzel (r=2.78) predictions are shown using contact angle values on Teflon™ coated silicon. Wenzel predictions above 180° (physically impossible) are shown equal to 180°. Calculated Cassie angle based on receding angle is approximately equal to advancing value and is not shown. Two calculations for Wenzel angle (based on advancing and receding control surface contact angles) are shown and the true value is between them. Strictly speaking, Cassie and Wenzel wetting equations describe equilibrium contact angle (between advancing and receding). The large error on the ethylene glycol receding data point is indicative of one test with a high receding contact angle, and two with zero.

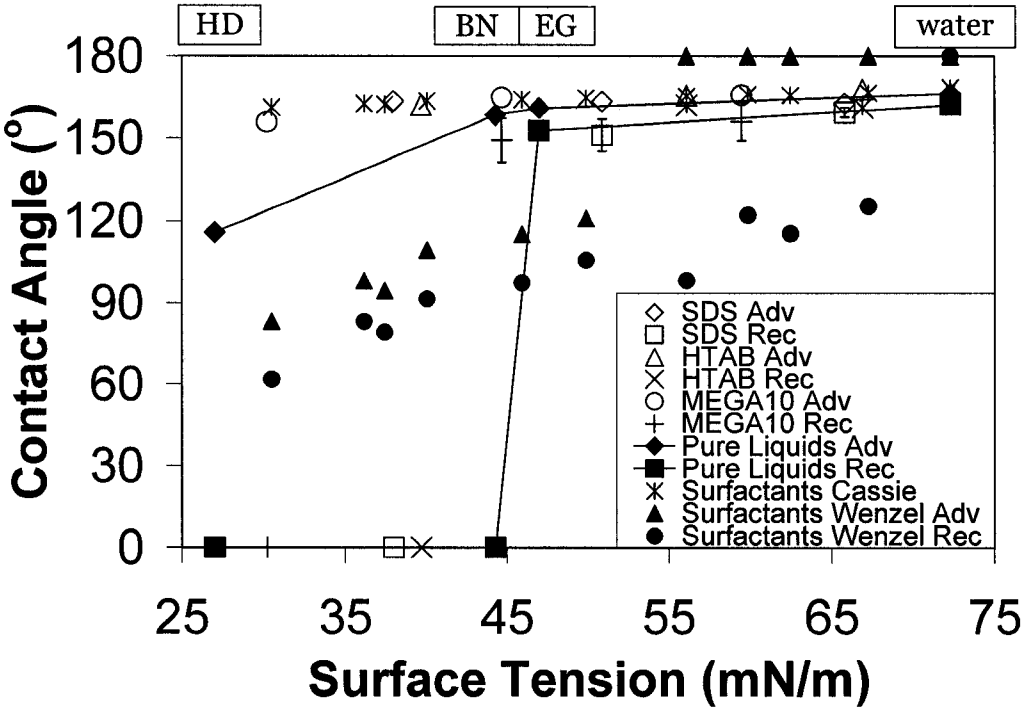

Figure 2-9: Surfactant solution and pure liquid contact angles for fluorinated electrochemically etched aluminum. Pure liquids are labeled above the graph. Standard deviation was calculated for each data point, in several cases the value is so low that the error bars are within the symbol itself. Lines are to guide the eye. The calculated Cassie (f=0.05) and Wenzel (r=1.77) predictions are shown using contact angle values on Teflon™ coated silicon. Wenzel predictions above 180° (physically impossible) are shown equal to 180°. Calculated Cassie angle based on receding angle is approximately equal to advancing value and is not shown. Two calculations for Wenzel angle (based on advancing and receding control surface contact angles) are shown and the true value is between them. Strictly speaking, Cassie and Wenzel wetting equations describe equilibrium contact angle (between advancing and receding).

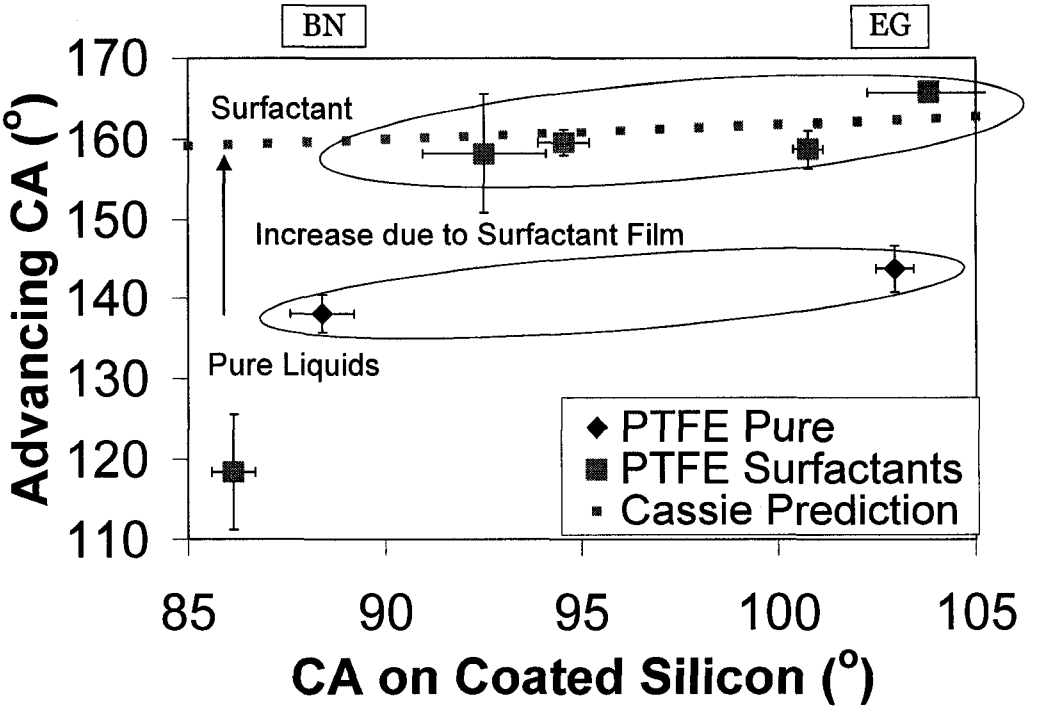

Figure 2-10: Advancing contact angle (CA) of PTFE versus advancing contact angle of Teflon™ coated silicon for pure liquids ethylene glycol and 1-bromonaphthalene (labeled above the graph) and surfactant solutions of similar intrinsic contact angle. Surfactant solutions show generally higher contact angle on PTFE. For the Cassie prediction, f is 0.06, and intrinsic contact angle is taken from the x-axis.

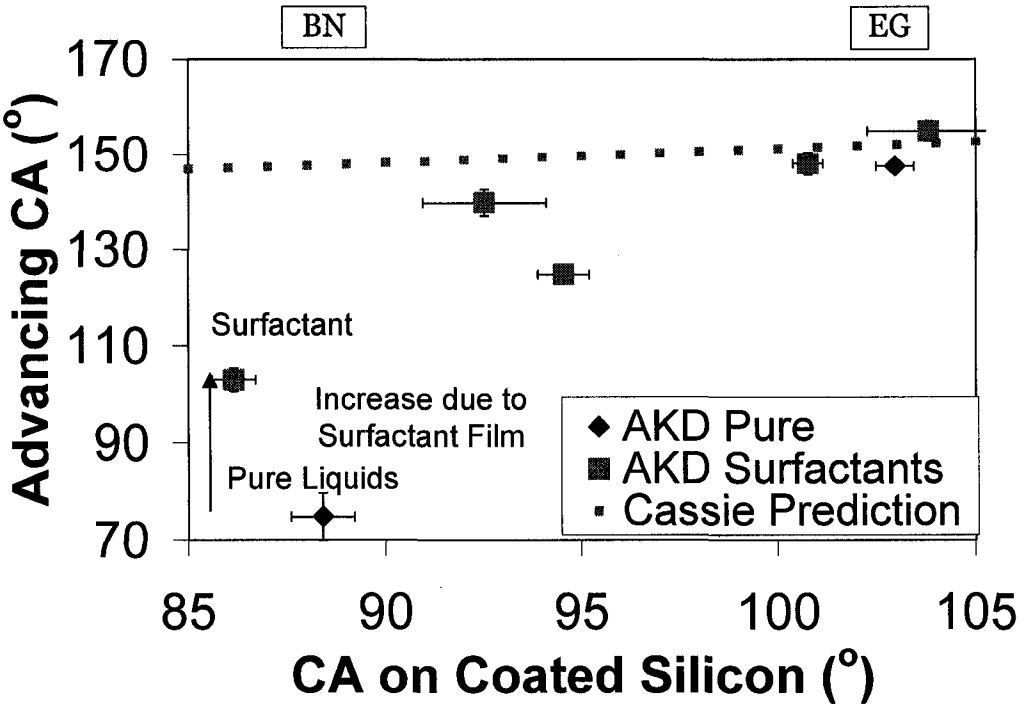

Figure 2-11: Advancing contact angle (CA) of Teflon™ coated AKD versus advancing contact angle of Teflon™ coated silicon for pure liquids ethylene glycol and 1-bromonaphthalene (labeled above the graph) and surfactant solutions of similar intrinsic contact angle. Surfactant solutions show generally higher contact angle on Teflon™ coated AKD. For the Cassie prediction, f is 0.15, and intrinsic contact angle is taken from the x-axis.

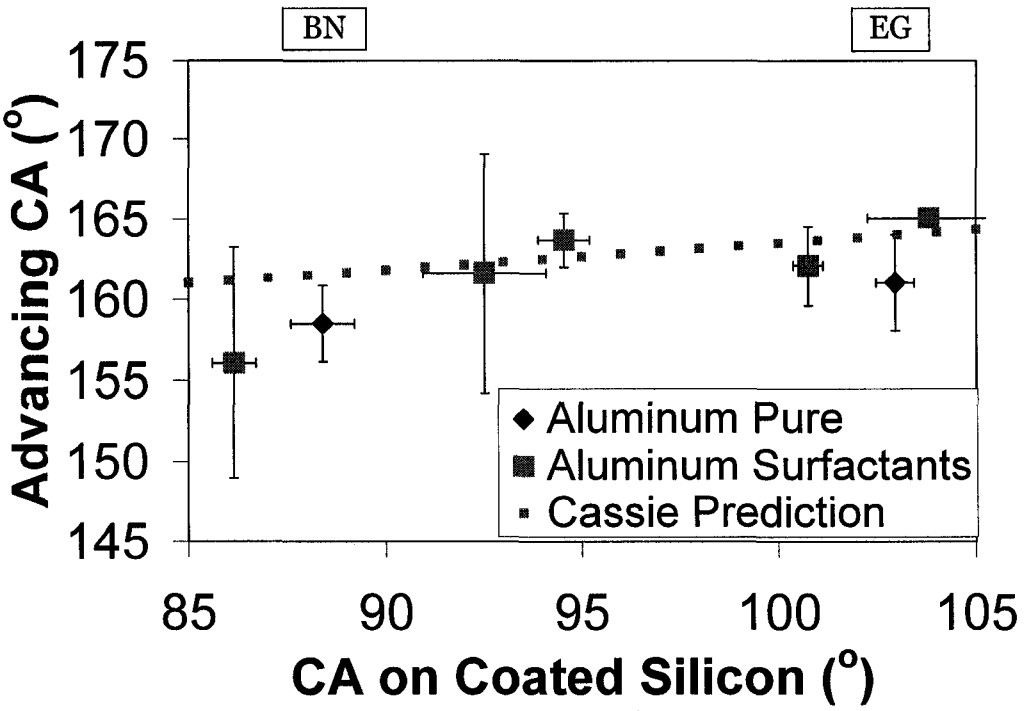

Figure 2-12: Advancing contact angle (CA) of Teflon™ coated aluminum versus advancing contact angle of Teflon™ coated silicon for pure liquids ethylene glycol and 1-bromonaphthalene (labeled above the graph) and surfactant solutions of similar intrinsic contact angle. Surfactant solutions show generally higher apparent contact angle, though standard deviations overlap. For the Cassie prediction, f is 0.05, and intrinsic contact angle is taken from the x-axis. The aluminum surfaces were tested in Dresden, Germany, and used different surfactant solutions with different surface tensions, in Figure 2-12 the apparent contact angles are linear interpolations or extrapolations from the closest measured data on aluminum to match the measured surface tensions of surfactant solutions used on aluminum to those used on Teflon™ coated silicon.

References

1. Hozumi, A.; Takai, O. *Thin Solid Films* **1997**, 203, 222.
2. Hozumi, A.; Takai, O. *Thin Solid Films* **1998**, 334, 54.
3. Feng, L.; Li, S.; Li, H.; Zhai, J.; Song, Y.; Jiang, L.; Zhu, D. *Angew. Chem., Int. Ed.* **2002**, 41, 1221.
4. Nakajima, A.; Fujishima, A.; Hashimoto, K.; Watanabe, T. *Adv. Mater.* **1999**, 11, 1365.
5. Tadanaga, K.; Katata, N.; Minami, T. *J. Am. Ceram. Soc.* **1997**, 80, 3213.
6. Shibuichi, S.; Onda, T.; Satoh, N.; Tsujii; K. *J. Phys. Chem.* **1996**, 100, 19512.
7. Erbil, H. Y.; Demirel, A. L.; Avci, Y.; Mert, O. *Science* **2003**, 299, 1377.
8. Extrand C.W. *Langmuir* **2004**, 20, 5013.
9. Extrand C.W. *Langmuir* **2005**, 21, 10370.
10. Extrand C.W. *Langmuir* **2006**, 22, 1711.
11. Li, W.; Amirfazli, A. *Adv. Colloid Interface Sci.* **2007**, 132, 51, 2007.
12. Nakajima, A.; Hashimoto, K.; Watanabe, T. *Chemical Monthly* **2001**, 132, 31.
13. Shirtcliffe, N. J.; McHale, G.; Newton, M. I.; Perry, C. C.; Roach, P. *Mat. Chem. Phys.* **2007**, 103, 112.
14. Rao, A. V.; Hegde, N. D.; Hirashima, H. *J. Colloid Interface Sci.* **2007**, 205, 124.
15. Fujita, M.; Muramatsu, H.; Fujihira, M. *Japanese J. App. Phys.* **2005**, 44, 6726.

16. Mohammadi, R.; Wassink, K.; Amirfazli, A. *Langmuir* **2004**, 20, 9657.

17. Shibuichi, S.; Yamamoto, T.; Onda, T.; Tsujii, K. *J. Colloid Interface Sci.* **1998**, 208, 287.

18. Chen, W.; Fadeev, Y.; Hsieh, M. C.; Öner, D.; Youngblood, J.; McCarthy, T. J. *Langmuir* **1999**, 15, 3395.

19. Ferrari, M.; Ravera, F.; Rao, S.; Liggieri, L. *App. Phys. Lett.* **2006**, 89, 053104.

20. Starov, V. M.; Kosvintsev, S. R.; Velarde, M. G. *J. Colloid Interface Sci.* **2000**, 227, 185.

21. Starov, V. M. *J. Colloid Interface Sci.* **2004**, 270, 180.

22. Kumar, N.; Varanasi, K.; Tilton, R. D.; Garoff, S. *Langmuir* **2003**, 19, 5366.

23. Varanasi, K. S.; Garoff, S. *Langmuir* **2005**, 21, 9932.

24. Dutschk V.; Sabbatovskiy, K. G.; Stolz, M.; Grundke, K.; Rudoy, V. M. *J. Colloid Interface Sci.* **2003**, 267, 456.

25. Wenzel, R. N. *J. Ind. Eng. Chem.* **1936**, 28, 988.

26. Cassie, A. B. D.; Baxter, S. *Trans. Faraday Soc.* **1944**, 40, 546.

27. Quéré, D.; Lafuma, A.; Bico, J. *Nanotechnology* **2003**, 14, 1109.

28. Jeong, H. E.; Lee, S. H.; Kim, J. K.; Suh, K. Y.; *Langmuir* **2006**, 22, 1640.

29. Herminghaus, S. *Euro. Phys. Lett.* **2000**, 52, 165.

30. Barbieri, L.; Wagner, E.; Hoffmann, P. *Langmuir* **2007**, 23, 1723.

31. Hennig, A.; Grundke, K.; Frenzel, R.; Stamm, M. *Tenside Surf. Det.* **2002**, 29, 243.

32. Shirtcliffe, N. J.; Aqil, A.; Evans, C.; McHale, G.; Newton, M. I.; Perry, C. C.; Roach, P. *J. Micromech. Microeng.* **2004**, 14, 1384.

33. Wagner, P.; Fürstner, R.; Barthlott, W.; Neinhuis, C. *J. Exp. Bot.* **2003**, 54 1295.

34. Yoshimitsu, Z.; Nakajima, A.; Watanabe, T.; Hashimoto, K. *Langmuir* **2002**, 18, 5818.

35. Shiu, J. Y.; Kuo, C. W.; Chen, P.; Mou, C. Y.; *Chem. Matter.* **2004**, 16, 561.

36. Jung, D. H.; Park, I. J.; Choi, Y. K.; Lee, S. B.; Park, H. S.; Ruhe, J. *Langmuir* **2002**, 18, 6133.

37. Drelich J.; Miller, J. D. *Langmuir* **1993**, 9, 619.

38. Li W.; Amirfazli A. *J. Colloid Surface Sci.* **2005**, 292, 195.

39. Nakajima, A.; Hashimoto, K.; Watanabe, T. *Chem. Monthly* **2001**, 132, 31.

40. Roura, P.; Fort, J. *Langmuir* **2002**, 18, 566.

41. Extrand, C. W. *Langmuir* **2002**, 18, 7991.

42. Extrand, C.W. *Langmuir* **2003**, 19, 3793.

43. Gao, L.; McCarthy, T. J. *Langmuir* **2007**, 23, 3762.

44. McHale, G. *Langmuir* **2007**, 23, 8200.

45. Minko, S.; Müller, M.; Motornov, M.; Nitschke, M.; Grundke, K.; Stamm, M. *J. Am. Chem. Soc.* **2003**, 125, 3896.

46. Köhler, K.; Coburn, J. W.; Horne, D. E.; Kay, E. *J. Appl. Phys.* **1985**, 57, 59.

47. Hoorfar, M., Neumann, A. W. *J. Adhesion* **2004**, 80, 727.

48. Kwok, D. Y.; Neumann, A. W. *Adv. Colloid Interface Sci.* **1999**, 81, 167.

49. Pierce, E.; Carmona, F. J.; Amirfazli, A. *Colloids and Surfaces A: Physicochemical and Engineering Aspects* **In Press**, DOI: 10.10161/j.colsurfa.2007.09.032.

50. http://www.surface-tension.de/, accessed 4-October-2007, methylene iodide listed under IUPAC- name diiodomethane

51. Yu, L. M. Y.; Lu, J. J.; Chan, Y. W.; Ng, A.; Zhang, L.; Hoorfar, M.; Policova, Z.; Grundke, K.; Neumann, A. W. *J. Appl. Physiol.* **2004**, 97, 704.

Chapter 3 – Effects of topography and chemistry on wetting of surfaces by pure liquids and surfactants

3.1 Introduction

Superhydrophobic surfaces (SHS) have attracted a great deal of interest over the last ten years or so. Industrial applications are diverse, including, for example, anti-fouling and self-cleaning [1-5], microfluidics [6-11], and decreased friction [12-16]. Academic study is aimed toward better understanding the physics and thermodynamics of liquid interaction with topographically and chemically modified surfaces e.g. [17-20].

Considering industrial interest, most studies to date are of limited use because they have mainly probed SHS with ultra-pure, distilled, deionized water. Industrial applications are unlikely to use such a pristine liquid. Some studies exist which examine non-aqueous pure liquid wetting on SHS [21-27], but they are generally not focused on the specific study of non-aqueous liquids. Impure systems can be modeled by the addition of surfactants to pure water. Studies of surfactant solutions on SHS are less common [21,22,28, Chapter 2].

SHS are understood to be the result of topographically enhanced liquid repellency of a generally low interfacial tension surface. Young's equation relates the intrinsic contact angle (θ) a drop of pure liquid makes on a smooth, flat, and homogeneous surface to the interfacial tensions γ_{lv}, γ_{sl}

and γ_{sv}, where l, v and s represent liquid, vapor and solid phases, respectively. Young's equation is:

$$\cos\theta = \frac{\gamma_{sv} - \gamma_{sl}}{\gamma_{lv}} \qquad 3\text{-}1$$

Young's equation, and the equations based upon it were all derived for pure liquids, and may not be applicable to impure liquids. In the absence of relevant relations to describe the contact angle on smooth and rough surfaces with surfactant solutions, Equation 3-1 and the following equations will be used as a starting point for analysis.

For non-smooth surfaces, prediction of contact angle is much more difficult. Traditionally, the two equations of Wenzel [29] and Cassie [30] have been used to understand superhydrophobicity. Wenzel's model [29] assumes liquid completely fills the surface pores/crevices. Wenzel's equation describes the Wenzel contact angle (θ_w) as:

$$\cos\theta_w = r\left(\frac{\gamma_{sv} - \gamma_{sl}}{\gamma_{lv}}\right) = r\cos\theta \qquad 3\text{-}2$$

where the effect of topography is modeled by r, the roughness factor, which is the ratio of actual surface area to projected surface area. Thus, for hydrophobic surfaces ($\theta>90^o$), roughness should increase the apparent contact angle compared to the intrinsic contact angle, whereas for hydrophilic surfaces ($\theta<90^o$) roughness should decrease the apparent contact angle compared to the intrinsic contact angle.

If the drop instead sits atop the pores/crevices of the surface, leaving vapor in the low regions, the Cassie equation can be written for the Cassie contact angle (θ_c) as:

$$\cos\theta_c = f(\cos\theta + 1) - 1 \qquad 3\text{-}3$$

where the effect of topography is modeled by f, the solid fraction, which is the ratio of the surface area that is wetted by the drop compared to the total surface area of the liquid interface under the drop.

The above equations were derived to describe the equilibrium contact angle. If a drop is advanced/receded across a surface (for example by adding to or removing from the volume of a drop), the added energy of the act gives rise to higher/lower contact angles, called the advancing/receding contact angle, respectively. The difference between these contact angles is called the contact angle hysteresis (CAH), and affects wetting and drop motion on a surface in sometimes complex ways [31]. The Wenzel wetting state is understood to have a high CAH due to the increased work of adhesion necessary to recede the drop, and the Cassie wetting state to have a low CAH [32].

The interaction of aqueous solutions of surfactants on SHS [21,22,28, Chapter 2] and smooth surfaces [22,33-37, Chapter 2] is incompletely understood. Especially lacking are studies that test both non-aqueous pure liquids and surfactant solutions on the same surface for comparative

purposes [21, Chapter 2]. Also, the vast majority of studies of SHS are conducted with fluorinated (CF_2 and CF_3 terminated) surface chemistries. This chemistry is generally recognized to be the most hydrophobic coating possible, followed by a saturated (CH_2 and CH_3 terminated) hydrocarbon chemistry [38,39].

In Chapter 2, surfaces were tested with a fluorinated chemistry. Reported in this chapter are the wetting results for four pure liquids of various surface tensions (~27-73 mN/m) and nine surfactant solutions of various polarities on saturated hydrocarbon coated surfaces with three different topographies the same as those in Chapter 2. The results will be compared to those in Chapter 2. A comparison of wetting for surfaces of the same topography but different chemistries should elucidate what effect chemistry has on wetting, and possibly also how the transition from the Cassie non-penetrated wetting state (desirable for SHS) to the Wenzel penetrated wetting state (undesirable for SHS) occurs. Previous studies of surfactant solution wetting on SHS [21,22,28, Chapter 2] are reviewed below as background for the present study.

Previously [21], testing was performed on a SHS produced by the natural formation of a rough microstructure on alkyl ketene dimmer (AKD), a wax that presents a saturated hydrocarbon surface. An abrupt reduction in advancing contact angle was seen for pure liquids with a surface tension below ~45 mN/m [21], similar to what others have seen [23] for pure

liquids. The surfactant solution contact angle data in [21] for similar surface tensions as pure liquids did not show a similar behavior, and instead maintained high advancing contact angles (above 90° in nearly all cases). After re-evaluation of the original images in [21] using the traditional definition of receding contact angle (uninterrupted movement of the contact line during the recede with a constant contact angle) it is now found that receding contact angle was zero for all systems tested. As such, the data in [21] should be viewed with caution, but this does not greatly affect the conclusions made regarding wetting states, though it affects CAH and therefore applications where dynamic drop effects are concerned [31].

The surfactant solution results in [21] compare well with that of Ferrari *et al.* [28] and Shirtcliffe *et al.* [22], who studied surfactant solutions on different SHS, without comparative tests with pure liquids. They both found that advancing contact angles remain high with decreasing surface tension. Ferrari *et al.* found that receding contact angle also remained high, while Shirtcliffe *et al.* found that it decreased with decreasing surface tension to zero degrees, so clearly SHS can behave very differently during the receding stage with surfactant solutions. The finding in Chapter 2 confirms the varied behavior of receding contact angle, where three types of fluorinated SHS were probed with pure liquids and surfactant solutions. Each of the three SHS tested in Chapter 2 showed different receding contact angle behavior. The receding contact angle is important because it

affects drop mobility [31]. The results in Chapter 2 also agree well with the finding [21] that advancing contact angles are higher with surfactant solutions than with pure liquids of similar surface tension.

3.2 Experimental Procedure

3.2.1 Fabrication of Surfaces

Two surfaces were fabricated for this study. Representative SEM images of each surface, along with topographical and chemical information are shown in Figure 3-1 and Table 3-1.

Smooth silicon wafer was taken as received, diced, drilled with an abrasive bit, and thoroughly rinsed with pure water and acetone. The holes are necessary for the sessile drop wetting tests as described in Section 3.2.3. The surfaces were then coated with octadecyltrichlorosilane (OTS) in the following manner. Into a 500 or 1000 ml beaker, OTS (Sigma Aldrich), was added to 100 ml of extra dry toluene (Sigma Aldrich, <30 ppm water) to form a 12 mM solution. The beaker was then covered and swirled to mix the liquids. The silicon samples were rinsed in ethanol to drive off any trace amounts of water and dried in a nitrogen stream, and immediately added to the solution. The samples were left for 3-3.5 hrs and after removal were rinsed with water and then ethanol (this cycle of rinsing repeated three times), and dried with nitrogen. Water contact angle was measured on the samples to ensure a good coating. Samples that did not result in an advancing/receding angle of approximately 105°/95° were not

used. To avoid degradation of the monolayer, all samples were used the same day they were produced. XPS analysis shows the sample to be covered with a saturated hydrocarbon chemistry and SEM images and AFM show the sample to be quite smooth compared to the other two surfaces (see Figure 3-1, Table 3-1). This surface is referred to as the control surface in this chapter.

Electrochemically etched aluminum samples (aluminum) were prepared from mill grade aluminum plates. These plates were cut, drilled and prepared* following the process outlined by Hennig *et al.* [32]. Briefly, each sample was placed in a bath of H_2SO_4 and $Al_2(SO_4)_3$, and subjected to 28 mA/cm^2 at approximately 45 ^oC for 2 minutes. Following rinsing with pure water, the samples were dried and coated with OTS as described for silicon above with one exception; the samples were only left in solution for one and a half hours. Water contact angle was again measured, samples which did not show high advancing and receding angles (above ~160^o) were not used. Samples were again used the same day they were produced. XPS analysis is shown in Table 3-1 and SEM and AFM results show that the surfaces have a rough, mountain range like topography, with submicron scale bumps on top of micron scale random ridges. SEM images of surfaces before and after coating show no noticeable change in the topography due to coating. These surfaces were measured using AFM to have the topographical characteristics listed in Table 3-1. SEM images of

* by scientists at Leibniz Institute of Polymer Research the, Dresden, Germany (IPF)

fluorinated aluminum showed a dual-scale topography (see Figure 2-1). A similar image of the OTS coated aluminum could not be obtained due to limited access to the high quality SEM machine used for the first image. Trace profiles through the AFM data of the OTS coated aluminum show it to have a similar dual-scale topography (see Figure 3-1). This is not surprising given that the OTS coating is very thin and would not be expected to cover the smaller scale of topography on the aluminum.

Wetting data for AKD was taken from a previous study conducted in our lab [21], with corrected receding contact angle values. However, a number of AKD samples were produced in the same manner as before [21] to obtain topographical and chemical information. Figure 3-1 shows a representative SEM images of the produced AKD surface. Table 3-1 provides the XPS data that indicates saturated hydrocarbons make up most of the surface, with some oxygen bonds indicating hydrophilic heterogeneities. AKD is naturally made up of mostly saturated hydrocarbons (its chemical formula is $C_{36}H_{68}O_2$). Roughness data for AKD can also be found in Table 3-1.

3.2.2 Liquid Types

Three surfactant solutions were tested. Sodium dodecyl sulfate (Fisher Scientific, New Jersey, USA), hereafter referred to as SDS, was used as an anionic surfactant. Hexadecyltrimethylammonium bromide (Sigma-Aldrich, St Louis, USA), hereafter called HTAB, was used as a cationic

surfactant and n-decanoyl-n-methylglucamide (Sigma-Aldrich, St Louis, USA), hereafter denoted as MEGA 10, was used as a non-ionic surfactant. Surfactants were used as received without further purification. Three concentrations below the CMC were mixed for each surfactant solution. Nominally concentrations were 1, 4 and 8 mM for SDS; 0.1, 0.2 and 1 mM for HTAB and 1, 2 and 9 mM for MEGA 10. Concentrations were chosen to yield similar ranges of surface tension both between surfactant types and between surfactant solutions and pure liquids. The three different surfactants, with different ionic properties, were chosen to examine possible effects of charge interactions on the surface and to relate to possible types of liquid impurities in industrial applications of SHS.

The pure liquids were DI water (hereafter referred to as water, surface tension measured at ~72.28 mN/m), ethylene glycol, EG, (47 mM/m, 99.8% pure), 1-bromonaphthalene, BN, (44.3 mN/m, 97% pure), and hexadecane, HD, (27 mN/m, 99+% pure). The water was from a Millipore system, resistance 18.2 MΩ/cm, all others were used as received from Sigma-Aldrich, St Louis, USA. For each liquid or solution concentration, at least three different surfaces were tested for wettability by sessile drop contact angle measurement (described below).

3.2.3 Surface Tension and Contact Angle Measurements

Surface tension of the pure liquids and surfactant solutions were measured by means of bubble tensiometry (SITA) and pendant drop analysis (First

Ten Angstroms). Reported is the average of measurements from at least three drops, with thirty measurements generally taken for each drop. Standard deviation is generally below 1 mN/m (0.2 mM HTAB had a standard deviation or 1.5 mN/m). Results are presented versus surface tension and not surfactant concentration to allow for comparison between surfactants and pure liquids.

Wettability was studied by means of contact angle measurement, conducted using Axisymmetric Drop Shape Analysis – Profile (ADSA-P) operating in sessile drop mode [40]. To conduct the sessile drop tests an experimental apparatus, constructed in-house, was used. For sessile drops, a motorized syringe was mounted below the sample. The syringe was driven at ~0.5 μl/s to give a low rate dynamic advancing contact angle. Every 2 seconds, an image of the drop was taken by a CCD camera, after the advancing stage, the drop was left for a period of 10-30 seconds, to observe any change of the contact angle due to relaxation or surfactant effects, or any change in receding behavior. After this period, the motor was reversed and driven at the same rate to give a low rate dynamic receding angle, imaged at the same frequency.

3.3 Results and Discussion

3.3.1 Pure Liquids

Figure 3-2 shows advancing contact angles for pure liquids on all three surfaces, with receding angles in Figure 3-3. Shown on Figure 3-2 and

Figure 3-3 are the Wenzel and Cassie predictions of wetting for SHS based on their topographic parameters and the contact angles measured on coated silicon. The solid fraction, f, values were found as a fitting parameter between the advancing water contact angle on OTS coated silicon and the advancing water contact angle on each saturated hydrocarbon SHS. This calculated f value was also used to find the Cassie prediction for other liquids/solutions.

The f value for OTS coated aluminum is the same as for fluorinated aluminum in Chapter 2, which supports the observation of no change in topography due to coatings applied to the etched aluminum. For the uncoated AKD, f equals 0.1. For Teflon™ coated AKD in Chapter 2, f was 0.15. This difference can be understood by considering that the Teflon™ coated AKD was incompletely fluorinated, leading to a lower intrinsic contact angle on Teflon™ coated AKD. Therefore the f value was likely overestimated in Chapter 2 (less vapor phase contact was required to yield a SHS prediction based on the overestimated intrinsic contact angle. The f value of 0.1 for Teflon (coated or not) is likely a more accurate estimate for both uncoated and coated AKD, but the value of f = 0.15 is internally consistent for Chapter 2.

On smooth OTS coated silicon, one observes a similar amount of reduction in contact angle between the surface tensions on EG and BN as was seen on Teflon™ coated silicon in Chapter 2. This reduction is greater than that

between water and EG, or BN ad HD (considering the relative changes in surface tension). Otherwise the results compare well with what other researchers have reported for similar smooth, saturated hydrocarbon chemistry surfaces [23,41].

On both AKD and OTS coated aluminum, one can observe an abrupt change from high advancing contact angle to low advancing contact angle between the surface tensions of EG and BN. This was also seen in the results presented in Chapter 2, where intrinsic contact angle for probe liquids is above 90° for EG and well below 90° for BN.

The results on saturated hydrocarbon SHS can be interpreted with a similar logic to those for fluorinated SHS in Chapter 2. For saturated hydrocarbon surfaces, the high advancing contact angle of EG occurs at intrinsic contact angle of 85°. Therefore, the high advancing contact angles on SHS cannot be described by the Wenzel wetting state which would decrease contact angle for intrinsic contact angle above 90°. It can be seen that the Cassie prediction matches the observed advancing contact angles on SHS much better than the Wenzel prediction for water and EG. 'Metastable' Cassie states have been observed by other researchers [42,43], and were seen in the results presented in Chapter 2. This explanation is proposed to describe the data here as well. Three other studies [23,26,27] have also shown high advancing contact angles on SHS for intrinsic contact angle slightly or far below 90°. The results have been observed

specifically for fluorinated electrochemically etched aluminum [26] and uncoated AKD [23], supporting the hypothesis that we are observing 'metastable' Cassie states on OTS coated aluminum and uncoated AKD.

For BN and HD, intrinsic contact angle data and apparent contact angles on the SHS suggest the Wenzel wetting state, with hydrophilic behavior being amplified by topography. For fluorinated aluminum, the 'metastable' Cassie state was observed for BN and HD; further, for HD, the intrinsic contact angle was ~70° while the advancing contact angle on fluorinated aluminum was ~120°. For saturated hydrocarbon chemistry, BN has a intrinsic contact angle of ~65°, (close to 70°). However, the advancing contact angle of BN on OTS coated aluminum is ~67°. Altogether, this shows that while topography can play an important role in wetting, chemistry effects could overshadow the effect of topography when sufficiently low intrinsic contact angles are seen.

Receding contact angle is seen to be high only for water on SHS aluminum; otherwise the receding contact angle is zero degrees. Receding contact angle decreasing to zero on aluminum corresponds to intrinsic contact angle (contact angle on OTS coated silicon) being less than 90°. This is the same as was seen with fluorinated SHS in Chapter 2, and suggests the Wenzel wetting state during the receding phase for all pure liquid/saturated hydrocarbon SHS combinations except for water on OTS coated aluminum. In Chapter 2, the zero receding angle of Teflon™ coated

AKD for all liquids was explained as a result of hydrophilic heterogeneities and/or decreased intrinsic contact angle due to the incomplete fluorination of the surface. Minute hydrophilic heterogeneities are observed with XPS data on both coated and uncoated AKD. While low intrinsic contact angle can explain the Wenzel state zero receding contact angle on AKD for EG, BN, and HD, it is proposed that contact line pinning leads to a zero receding angle for water on uncoated AKD. This pinning can be based both on chemical heterogeneities and a topography that provides a more continuous contact line, enhancing contact line pinning.

Results with pure liquids compare very well with those seen in literature for SHS. Shirtcliffe *et al.* [22], Rao *et al.* [24] and Fujita *et al.* [25] all showed penetration of pure liquids into the crevises/pores of SHS (i.e. the Wenzel wetting state) for sufficiently low probe liquid surface tensions. Surface tension was not reported in [22] for the water/ethanol mixture used in this study, but in [24] it was ~30 mN/mm, and ~22.3 mN/mm in [25]. None of the studies reported contact angles for intermediate values of surface tension. Regardless, the penetration of BN and HD into the pores/crevices of the aluminum and AKD is supported by literature.

The data here shows that the 'bumpy', dual-scale topography of the aluminum surface is seen to give higher contact angles than AKD, as was seen in Chapter 2, even with a new surface chemistry. This suggests that the dual-scale topography of the aluminum is the best of those tested for

liquid repellency, and would be desirable in an industrial application where repellency is required.

In comparing the results of Chapter 2 to those presented here it is seen that for a given topography (aluminum) saturated hydrocarbon chemistry (Figure 3-2) results in similar behavior to fluorinated chemistry (Figure 2-2) in terms of general wetting trends with decreasing surface tension. However, for a given surface tension the contact angles are generally lower for saturated hydrocarbon chemistry and contact angles drop to lower values more abruptly, at higher surface tensions. This is understandable, given that saturated hydrocarbon chemistry results in lower intrinsic contact angles compared to fluorination, which would in turn lead to lower contact angles on SHS. This decreased repellency could be used to tune the wetting of a SHS for different liquids as suggested by others [22,24].

3.3.2 Surfactant Solutions

Surfactant solution wetting results are presented in Figure 3-4 through Figure 3-7. Advancing and receding contact angles are shown for all three surfactant solutions with the pure liquid values plotted for comparison purposes for each surface (Control in Figure 3-4, AKD in Figure 3-6, and aluminum in Figure 3-7).

An interesting finding is that Chapter 2, surfactant solutions showed higher advancing contact angles than pure liquids on smooth OTS coated

silicon. In Chapter 2, higher contact angles were seen when pure liquid intrinsic contact angle was less than 90°. For saturated hydrocarbon surface, higher contact angles are seen when pure liquid intrinsic contact angles are less than 85°, and not seen for surfactant solutions with surface tension similar to that of EG, which has an intrinsic contact angle less than 90°, but greater than 85°. This suggests that the difference in contact angles between solutions and pure liquids is not due to intrinsic contact angle passing 90°, but instead to liquid type/surface tension. In both Chapter 2 and here, the higher contact angles are seen for surface tension less than ~45 mN/m. Figure 3-5 shows the surfactant solution wetting results on OTS coated silicon compared to literature results for SDS [37] and pure liquids [41] on Parafilm™, a smooth saturated hydrocarbon surface. The literature results for pure liquids and surfactant solutions match the results generated here well, and show that surfactant solution contact angles on smooth hydrophobic surfaces are the same or higher than contact angles with pure liquids of similar surface tension. Altogether, these results suggest more theoretical modeling of surfactant interactions on smooth hydrophobic surfaces is needed to see how the 'autophilic effect' [33] and surfactant adsorption on solid-liquid and liquid-vapor interfaces affect wetting by surfactant solutions compared to pure liquids.

Surfactant solutions (independent of polarity) showed higher contact angles than pure liquids of similar surface tension on OTS coated

aluminum. This is similar to reported data in Chapter 2 for fluorinated SHS of aluminum, AKD, and PTFE and for uncoated AKD [21] (re-reported in Figure 3-6). The data shown in Figure 3-6 and Figure 3-7 also compares well with literature results for fluorinated SHS [22,28]. As stated in Section 3.2.3, drops were monitored for at least 10-30 seconds between advancing and receding stages, in some cases they were monitored for 5 minutes. The dwell time was therefore beyond the expected time for spreading of surfactant solutions on smooth surfaces [33-37], which could lead to penetration/spreading of surfactant solutions into/across a SHS. Little to no spreading of the drop was seen in this time frame (1-2° maximum, which is within the error bars of the measurements shown).

In Chapter 2, four possible mechanisms to describe the wetting of surfactant solutions on SHS were suggested. First, the higher intrinsic contact angle for surfactant solutions should lead to higher apparent contact angles and more stable Cassie wetting states on SHS. Second, the surfactants could also be inhibiting the penetration of liquid into the surface by forming a film over the pores/crevices, as suggested by others [21,22]. This surfactant film could stretch between features during the receding phase, pinning the contact line and decrease receding contact angle [22]. Third, contact line pinning during the receding phased has been observed [36] due to surfactant re-self-assembly on smooth hydrophobic surfaces. This could affect the receding angle on SHS since microscopic pinning points would decrease the local contact angle at a

pore/crevice, decreasing apparent contact angle and possibly triggering a transition to the Wenzel wetting state. Fourth, constrained wetting could inhibit the leakage of surfactant solutions into crevices. Surfactant solutions have been shown to resist passing sharp corners in constrained wetting situations as demonstrated in the application of inverted frusta for extremely low surface tension measurements [44]. The wetting results of surfactant solutions on saturated hydrocarbon SHS will now be examined considering these four possible mechanisms individually and in combinations.

The high advancing contact angles on aluminum and AKD, and the inability of the predictions using Wenzel's equation (Equation 3-2) to describe observations, suggest that surfactant solutions wet the SHS in the Cassie state. This is especially apparent at lower surfactant concentrations (surface tension above ~45 mN/m). At higher concentrations of surfactants (surface tension below ~45 mN/m) the Cassie prediction overestimates the observed data. This can be explained by partial penetration of the solution into the pores/crevices of the surface topography, leading to an increased f value and a decreased Cassie contact angle. Partial penetration of surfactant solutions was suggested for Teflon™ coated AKD and PTFE in Chapter 2.

The difference in contact angles for pure liquids and surfactant solutions can be analyzed by considering apparent contact angle versus intrinsic

contact angle. The intrinsic contact angles of EG and BN on OTS coated silicon are 84.5° and 65.2°, respectively. The three concentrations of MEGA 10 and the maximum concentrations of SDS and HTAB show a similar range of intrinsic contact angles. Plotting apparent contact angle on the SHS versus intrinsic contact angle (contact angle on the smooth OTS coated silicon), one can generate Figure 3-8 for aluminum and Figure 3-9 for AKD surfaces. While the data sets for surfactant solutions and pure liquids are similar for higher surface tensions (near that of EG), surfactant solutions result in higher contact angles compared to BN as surface tension decreases to that of BN. This cannot be explained by the first mechanism since the data in these graphs account for the increased intrinsic contact angle (i.e. the data are effectively normalized for intrinsic contact angle).

Further to the above arguments, at surface tensions below ~45 mN/m, intrinsic contact angle with surfactants is below 90°. The wetting state on SHS should therefore be Wenzel, with roughness increasing the hydrophilicity of the surface. Instead, high contact angles are seen. These high contact angles can be explained by considering that surfactant films over the pores of the surface could be inhibiting the penetration of surfactant solution into the pores/crevices of the surface (mechanism 2) as argued in Chapter 2. Mechanism 2 can act in concert with mechanism 1, the surfactant films can inhibit penetration allowing the higher intrinsic

contact angles to result in higher apparent contact angles due to Cassie state non-penetrated wetting.

The AKD SHS yields zero receding contact angle for all liquids, for reasons discussed elsewhere in this paper. The aluminum SHS shows very high receding contact angles for water, as well as minimum concentrations of HTAB and SDS, and the intermediate concentration of SDS. Other than with these probe liquids, aluminum shows zero receding contact angle. Further to this, observation of the individual wetting tests show that the receding phase of surfactant solutions for OTS coated aluminum was somewhat intermittent and not as smooth as it was on fluorinated SHS, with occasions of contact line pinning to much lower values (sometimes zero degrees) for OTS coated aluminum. This observed behavior for the receding phase of saturated hydrocarbon chemistry SHS can be understood as a result of the lower intrinsic contact angle. For a lower intrinsic contact angle, slight pinning of the receding contact line could lead to an even lower local (microscopic) contact angle, and trigger a transition to the Wenzel wetting state after a short period of higher receding contact angle (due to a 'metastable' Cassie state).

The zero receding angle of aluminum for lower surface tensions solutions can easily be explained by consideration of the lower intrinsic contact angle resulting in the Wenzel state during the recede as was seen in Chapter 2. In Figure 3-7 the high receding contact angles for water and the

lowest concentrations of SDS and HTAB, as well as the intermediate concentration of SDS, can be understood simply as a result of the high intrinsic contact angle. For these surfactant solutions the intrinsic contact angle is above 90°, and we propose that the Cassie wetting state on the recede for these surfactant solutions is observed.

It is interesting to note that the intermediate concentration of HTAB shows a higher surface tension and a similar intrinsic contact angle to the intermediate concentration of SDS, yet shows a zero receding contact angle on OTS coated aluminum. Based on the apparent contact angle for the intermediate concentration of HTAB, it seems that there is a Wenzel wetting state during the recede. The Wenzel state could be caused by increased contact line pinning as a result of surfactant film stretching (mechanism 2) and re-self-assembly (mechanism 3) during the recede of surfactant solutions on SHS. It is curious that the zero receding contact angle occurs for a solution of HTAB, while not occurring for solutions of SDS. This may suggest there may be slight effects of surfactant polarity in the receding behavior or SHS, but bears more investigation.

Further information can be gleaned from the receding contact angle data of surfactant solutions on OTS coated aluminum by considering the same data for fluorinated aluminum from Chapter 2. The range of intrinsic contact angle for the low concentration surfactant solutions (surface tension above ~45 mN/m) on OTS coated silicon is 96.5° – 91.5°. The

range of intrinsic contact angles for high concentration surfactant solutions (surface tension below ~45 mN/m) on Teflon™ coated silicon is slightly higher (103.8° – 94.5°). However, the fluorinated aluminum shows zero receding contact angle with high concentration surfactant solutions while the OTS coated aluminum shows (generally) high receding contact angles. In Chapter 2 it was suggested that the contact line of surfactant solutions on fluorinated aluminum was being pinned by surfactant film stretching (mechanism 1) and re-self-assembly (mechanism 2) during the recede. For OTS coated aluminum, the surfactant solutions are of a lower concentration, so both mechanisms for decreasing receding contact angles would be weaker [22,36], explaining the difference in observed behavior. So, by making use of the similarity in intrinsic contact angle for surfactant solutions on different surface chemistries, one can distinguish effects of surfactant concentration on the wetting of SHS.

The results of PTFE in Chapter 2 are somewhat similar to those of OTS coated aluminum (i.e. both show high receding contact angles for some surfactant solutions, but zero for others of similar intrinsic contact angle). Given that the PTFE has a different topography and surface chemistry to the OTS coated aluminum, no conclusions can be drawn from this. It is worthy of note, however, that it was again a solution of HTAB that showed zero receding contact angle on PTFE for intrinsic contact angle above 90°, while solutions of SDS and MEGA 10 did not. This lends some credence to the hypothesis put forth above that surfactant polarity might affect the

receding contact angle, but a concentrated study of this topic would be required for firm conclusions to be drawn.

Overall, the less rough, dual-scale topography of the aluminum (Ra = 0.4 μm) is seen to result in higher advancing and receding contact angles with surfactant solutions compared to the more rough, sharper topography of the AKD (Ra = 1.248 μm). In comparing the results of Chapter 2 to those presented here, it is seen that for a given topography (aluminum) saturated hydrocarbon chemistry results in similar behavior to fluorinated chemistry in terms of general wetting trends and mechanisms describing them. However, for a given surface tension the contact angles are generally lower for saturated hydrocarbon chemistry (as seen with surfactant solution advancing contact angles) and drop to lower values more abruptly, at higher surface tensions (as seen with surfactant solution receding contact angles). This is understandable, given that saturated hydrocarbon chemistry results in lower intrinsic contact angles compared to fluorination, which would in turn lead to lower contact angles on SHS.

Saturated hydrocarbon SHS show higher advancing contact angles with surfactant solutions compared to pure liquids of similar surface tension/intrinsic contact angle. This is understood as a result of mechanism 1 (increased intrinsic contact angle) and mechanism 2 (surfactant film formation over the pores/crevices of the SHS). However, saturated hydrocarbon SHS would not be expected to behave well

dynamically, due to their lower and generally less constant receding contact angles (compared to fluorinated surfaces). The receding angle behavior is understood as the result of low intrinsic contact angle, and possibly contact line pinning by surfactant film stretching (mechanism 2) and re-self-assembly (mechanism 3). Mechanism 4 was not required to explain the observed wetting behavior of surfactant solutions on saturated hydrocarbon SHS. It was suggested in Chapter 2 as one of many possibly explanations for the unexpected receding behavior on PTFE.

Considering all of the above, saturated hydrocarbon SDS would therefore be less useful than fluorinated SHS (for the topographies studied) in industrial applications where uniformly high advancing and receding contact angles are desired. However, unlike pure liquids, which show an abrupt switch in wetting state and an accompanying abrupt decline in contact angle, surfactant solutions show a gradual decline in advancing contact angle on saturated hydrocarbon SHS (Figure 3-6 and Figure 3-7). With a change in surfactants allowing a further decrease in surface tension, a switch in wetting might be seen, or at least continued decrease in contact angle. Considering this, in the range tested, saturated hydrocarbon SHS could be used as a sensor for surfactant or impurity concentration, if the response could be suitably calibrated.

3.4 Summary and Conclusions

The wetting of four pure liquids of various surface tensions (~27-73 mN/m) and nine surfactant solutions of various polarities and concentrations was studied on saturated hydrocarbon surfaces with three different topographies. It has been shown that surfactant solutions behave at least as well as pure liquids of similar surface tension on superhydrophobic surfaces (SHS) and also on smooth OTS coated silicon. Results were compared throughout with those for fluorinated surfaces of the same topography.

Smooth surfaces showed higher contact angles with surfactant solutions than with pure liquids of similar surface tension when surface tension was less than ~45 mN/m (intrinsic contact angle less than ~85°). This is interesting as it questions the importance of the autophilic effect; it was also seen in Chapter 2 with fluorinated smooth surfaces.

The observed higher contact angles of surfactant solutions compared to pure liquids of similar surface tension on SHS cannot be explained by consideration of the higher intrinsic contact angle alone. For solutions and pure liquids of similar intrinsic contact angle, surfactant solutions still show higher apparent contact angle on SHS. This suggests that the formation of surfactant films over the pores/crevices of the surface, inhibiting penetration, is also at work. This was also seen with fluorinated SHS [Chapter 2].

Generally, saturated hydrocarbon SHS were seen to show similar behavior to fluorinated SHS, but with lower contact angles (especially at lower surface tensions), and with less consistent receding stages. Saturated hydrocarbon SHS also showed abrupt transitions to advancing and receding contact angles of zero sooner (i.e. at higher surface tensions) than for fluorinated SHS. The receding contact angle of all liquids on uncoated AKD was again zero, as with Teflon™ coated AKD. It is understood as the result of topography and/or chemistry aided pinning of the contact line.

Observations suggest surfactant polarity might play some role on the receding contact angle behavior on SHS. This could be due to the lower intrinsic contact angle of HTAB solutions compared to solutions of other surfactants of similar surface tension. Differences in the receding contact angle on SHS was seen both on fluorinated PTFE in Chapter 2 and OTS coated aluminum in this chapter, with the same surfactant type (HTAB) but at different concentrations. This phenomenon is incompletely understood and is recommended for further study. Other than these two cases, surfactant polarity has little effect on wetting for fluorinated or saturated hydrocarbon surfaces.

In terms of application to industry, the less rough, dual-scale topography of the aluminum (Ra = 0.4 μm), results in higher contact angles and is more repellent than the more rough, sharper topography of the AKD (Ra =

1.248 μm). The OTS coated aluminum does not show the 'metastable' Cassie state wetting for BN and HD as seen for the fluorinated aluminum surface. For industrial application requiring repellency, saturated hydrocarbon SHS are not recommended since fluorinated SHS give better results for the topographies studied. The saturated hydrocarbon SHS show a gradual decline in advancing contact angles for surfactant solutions of increasing concentration, and an abrupt one for receding contact angle with surfactants and all contact angle with pure liquids. Saturated hydrocarbon SHS could therefore be used as sensors or switches in industrial application, as suggested by others [22], or used to tune the absorbent characteristics of SHS for spill cleanup [24].

Table 3-1: AFM, and XPS results for AKD (naturally a saturated hydrocarbon chemistry), electrochemically etched aluminum SHS (OTS coated), and OTS coated silicon as a control sample. Value in parenthesis denotes standard deviation. * For silicon, measurements are in nanometers, not microns.

	AKD	Aluminum	Silicon
Ra (microns*)	1.248 (0.17)	0.40 (0.19)	7.511 (0.02)
Rq (microns*)	1.53 (0.15)	0.50 (0.21)	13.835 (1.32)
Rmax	7.82 (0.18)	3.80 (0.37)	437.05 (92.2)
Wenzel Roughness Factor, *r*	2.85 (0.27)	1.77 (0.15)	Not available
Fractal Dimension (by cube counting)	2.23 (0.06)	2.38 (0.09)	Not available
[C-C] and [C-H]	>80%	58.8%	61.87%

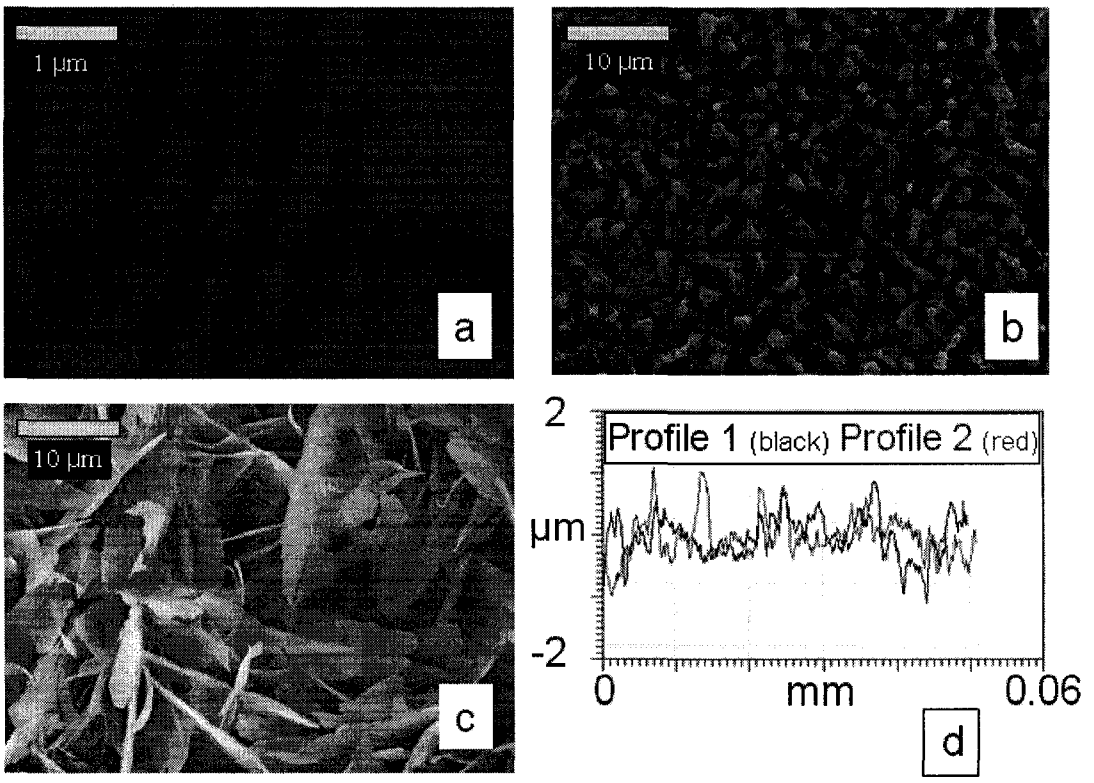

Figure 3-1: SEM images of: (a) OTS coated silicon, (b) OTS coated electrochemically etched aluminum, and (c) uncoated AKD. Scale bar for (a) is approximately 1 micron, scale bars for (b), (c) are approximately 10 microns. (d) Two traces profiles through AFM data of OTS coated aluminum, showing dual scale nature (large fluctuations of height with distance, overlaid with small fluctuations.

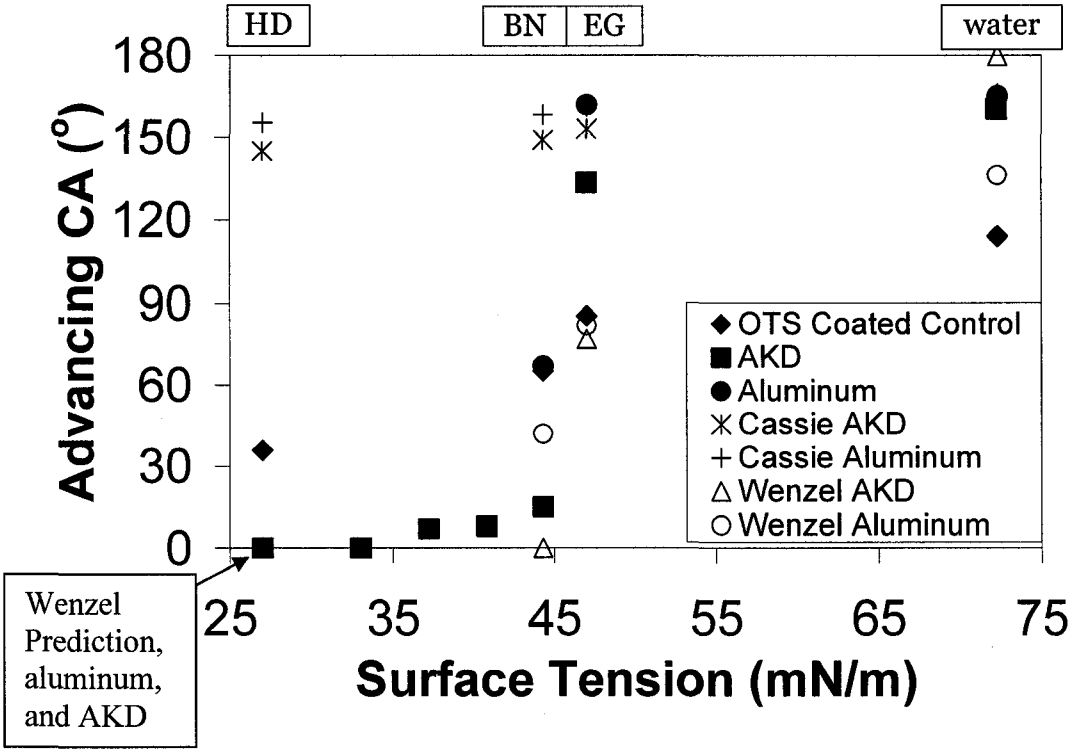

Figure 3-2: Advancing contact angle for water, ethylene glycol, 1-bromonaphthalene, and hexadecane on two topographically modified SHS and one smooth saturated hydrocarbon surface. The pure liquids tested in this thesis are labeled above the graph, with the rest (*cis*-decaline, ethylcinnamate, dibenzylamine) in literature [21]. Standard deviation was calculated for each data point except those from [21], in several cases the value is so low that the error bars are within the symbol itself. The calculated Cassie (f=0.1, 0.05 for AKD and aluminum, respectively) and Wenzel (r=2.85, 1.77 for AKD and aluminum, respectively) predictions are shown using the intrinsic advancing contact angle data from OTS coated silicon. Wenzel predictions above 180° (physically impossible) are shown equal to 180°. Cassie and Wenzel wetting equations describe equilibrium contact angle (between advancing and receding).

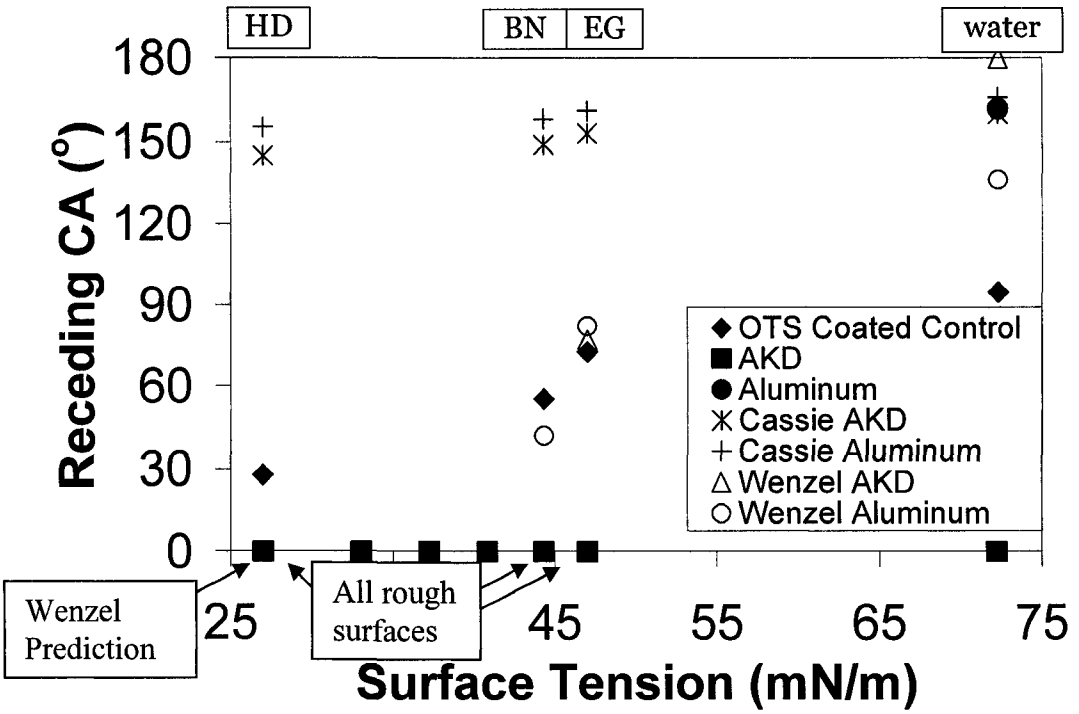

Figure 3-3: Receding contact angle for water, ethylene glycol, 1-bromonaphthalene, and hexadecane on two topographically modified SHS and one smooth saturated hydrocarbon surface. The pure liquids tested in this thesis are labeled above the graph, with the rest (*cis*-decaline, ethylcinnamate, dibenzylamine) in literature [21]. Standard deviation was calculated for each data point except those from [21], in several cases the value is so low that the error bars are within the symbol itself. The calculated Cassie (f=0.1, 0.05 for AKD and aluminum, respectively) and Wenzel (r=2.85, 1.77 for AKD and aluminum, respectively) predictions are shown using the intrinsic advancing contact angle data from OTS coated silicon. Wenzel predictions above 180° (physically impossible) are shown equal to 180°. Cassie and Wenzel wetting equations describe equilibrium contact angle (between advancing and receding).

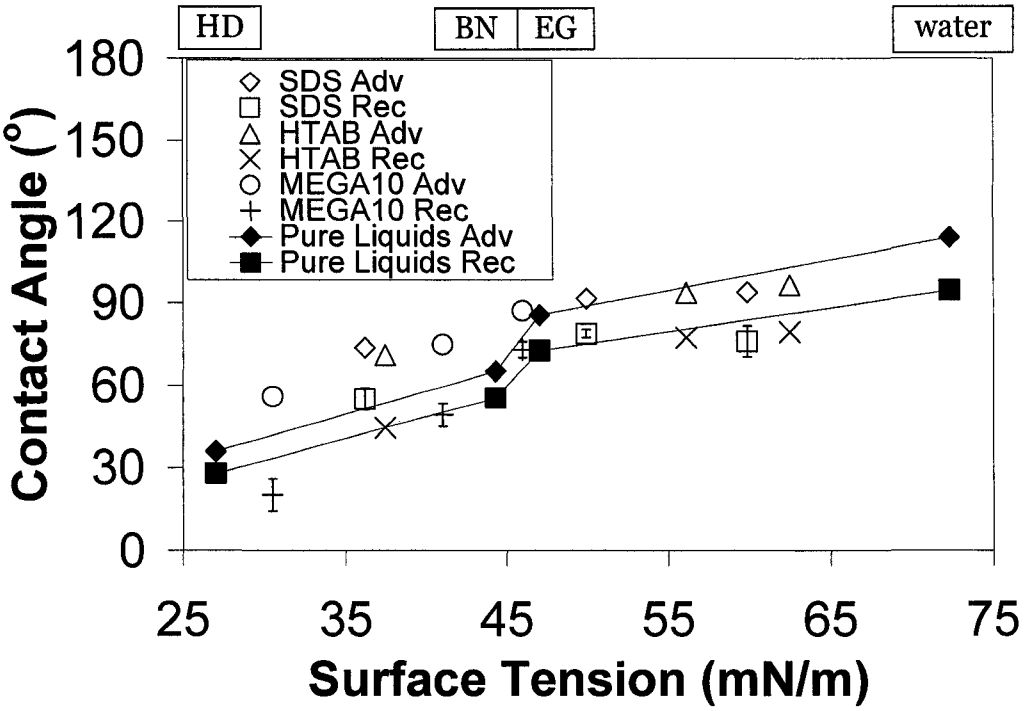

Figure 3-4: Surfactant solution and pure liquid contact angles for OTS coated silicon control surface. Pure liquids are labeled above the graph. Standard deviation was calculated for each data point, in most cases the value is so low that the error bars are within the symbol itself. Lines are to guide the eye.

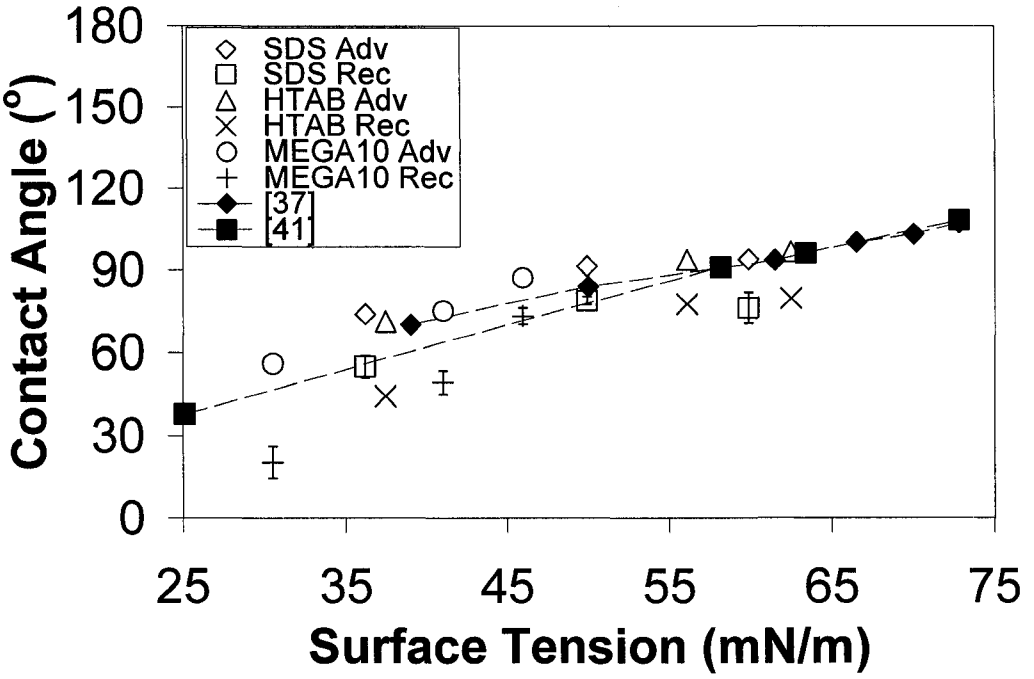

Figure 3-5: Advancing and receding contact angles for surfactant solutions on OTS coated silicon control surface. Standard deviation was calculated for each data point, in most cases the value is so low that the error bars are within the symbol itself. Also plotted are advancing contact angle results for SDS [37] and pure liquids [41] on Parafilm™ (a saturated hydrocarbon smooth surface). Lines are to guide the eye.

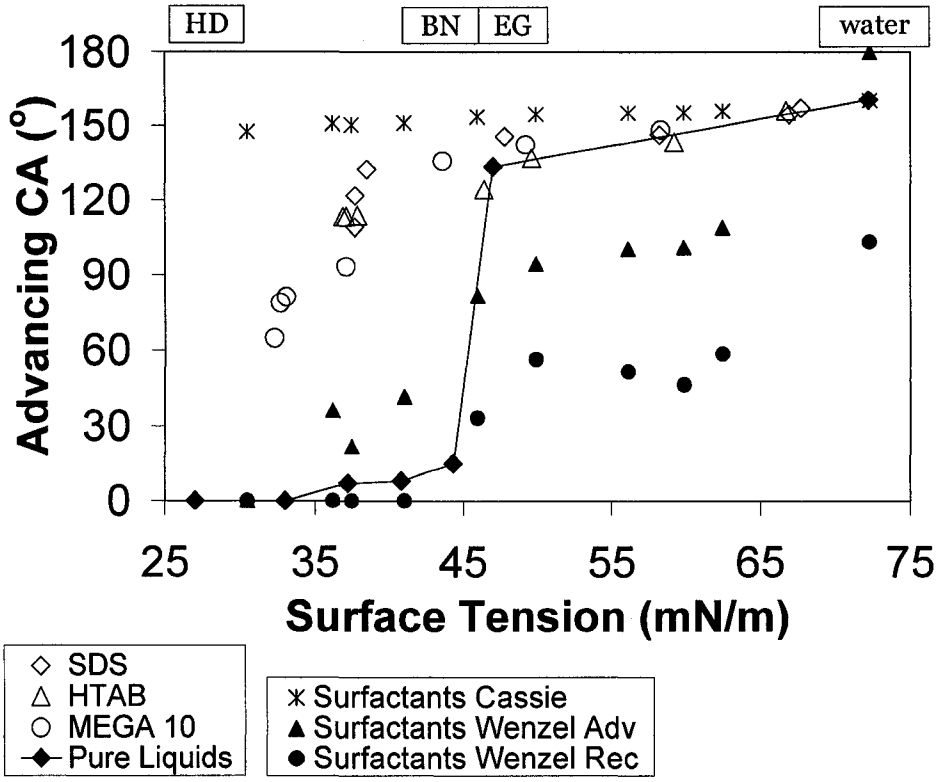

Figure 3-6: Surfactant solution and pure liquid advancing contact angles (CA) for uncoated, naturally rough AKD. Pure liquids are labeled above the graph. Standard deviation is unavailable for this literature data. Lines are to guide the eye. The calculated Cassie (f=0.1) and Wenzel (r=2.85) predictions are shown using contact angle values on OTS coated silicon. Wenzel predictions above 180° (physically impossible) are shown equal to 180°. Calculated Cassie angle based on receding angle is approximately equal to advancing value and is not shown. Two calculations for Wenzel angle (based on advancing and receding contact angle on control surface) are shown and the true value is between them. Strickly speaking, Cassie and Wenzel wetting equations describe equilibrium contact angle (between advancing and receding).

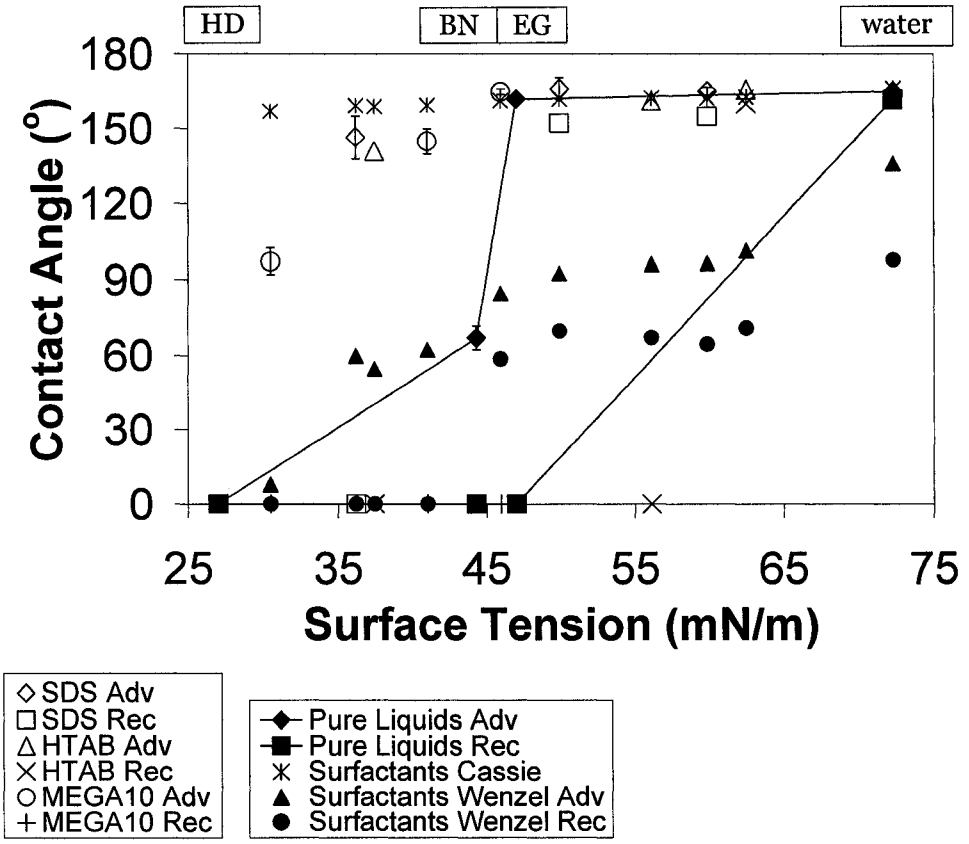

Figure 3-7: Surfactant solution and pure liquid contact angles for OTS coated electrochemically etched aluminum. Pure liquids are labeled above the graph. Standard deviation was calculated for each data point, in most cases the value is so low that the error bars are within the symbol itself. Lines are to guide the eye. The calculated Cassie (f=0.05) and Wenzel (r=1.77) predictions are shown using contact angle values on OTS coated silicon. Calculated Cassie angle based on receding angle is approximately equal to advancing value and is not shown. Two calculations for Wenzel angle (based on advancing and receding contact angle on control surface) are shown and the true value is between them. Strickly speaking, Cassie and Wenzel wetting equations describe equilibrium contact angle (between advancing and receding).

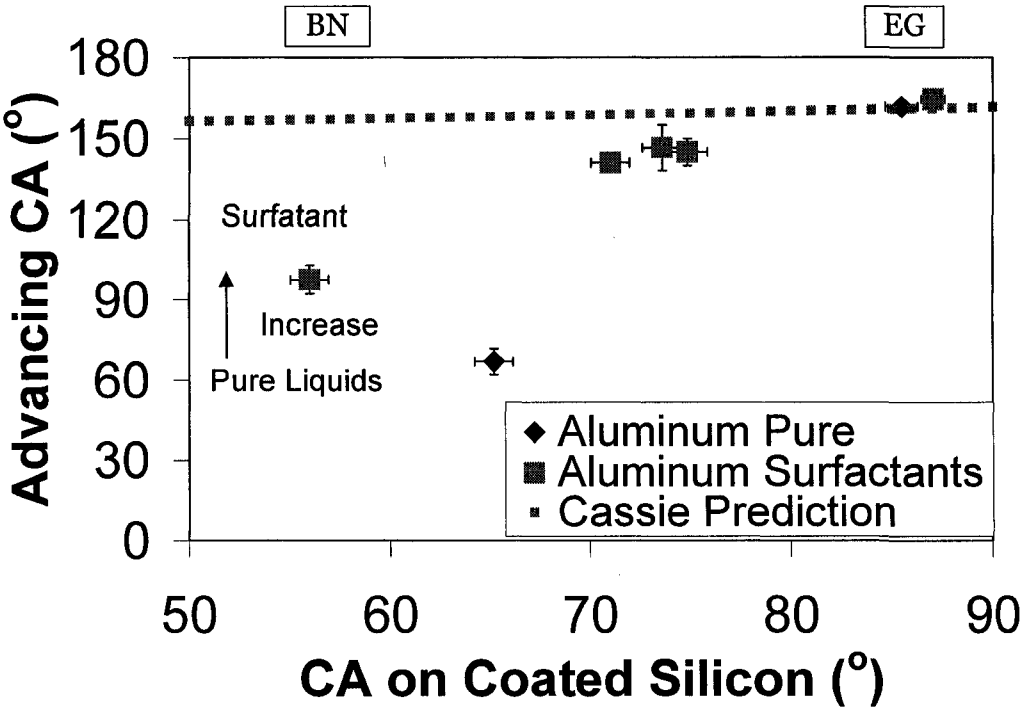

Figure 3-8: Advancing contact angle of OTS coated aluminum versus advancing contact angle of OTS coated silicon for pure liquids ethylene glycol and 1-bromonaphthalene (labeled above the graph) and surfactant solutions of similar intrinsic contact angle. For the Cassie prediction, f is 0.05, and the intrinsic contact angle used in calculation is taken directly from the x-axis.

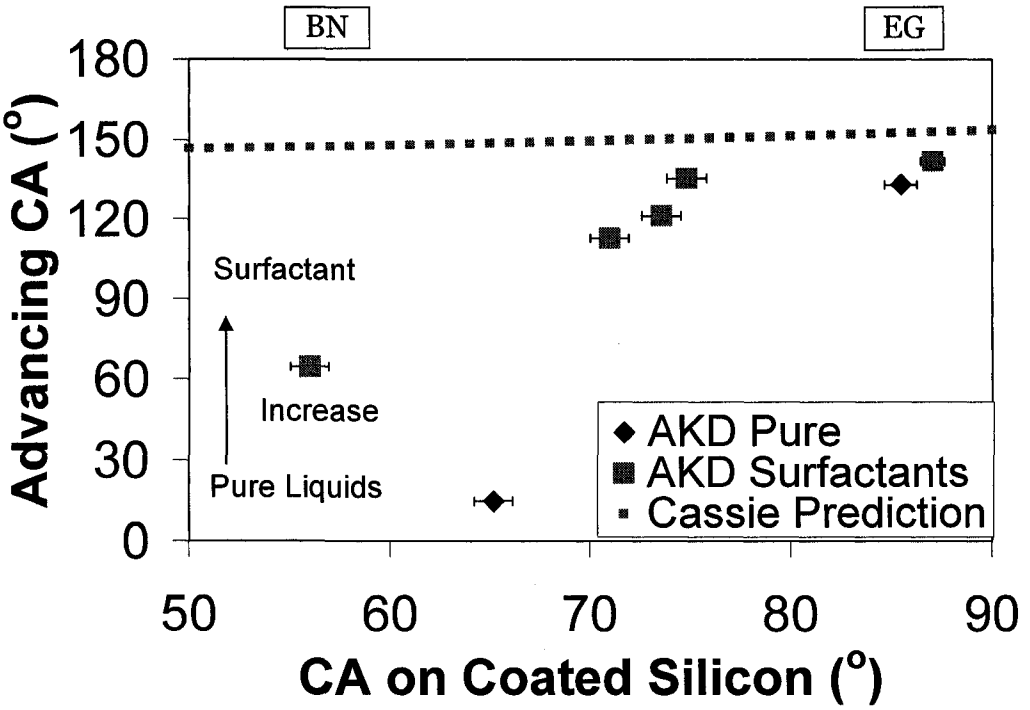

Figure 3-9: Advancing contact angle of uncoated AKD versus advancing contact angle of OTS coated silicon for pure liquids ethylene glycol and 1-bromonaphthalene (labeled above the graph) and surfactant solutions of similar intrinsic contact angle. For the Cassie prediction, f is 0.05, and the intrinsic contact angle used in calculation is taken directly from the x-axis.

References

1. Carman, M. L.; Estes, E. G.; Feinberg, A. W.; Schumacher, J. F.; Wilkerson, W.; Wilcon, L. H.; Callow, M. E.; Callow, J. A.; Brennan, A. B *Biofouling* **2006**, 22, 11.
2. Cheng, Y. T.; Rodak, D. E.; Wong, C. A.; Hayden, C. A. *Nanotechnology* **2006**, 17, 1359.
3. Hoipkemeier-Wilson, L.; Schumacher, J. F.; Carmen, M. L.; Gibson, A. L.; Feinberg A. W.; Callow, M. E.; Finlay, J. A.; Callow, J. A. Brennan, A. B. *Biofouling* **2004**, 20, 53.
4. Shang, H. M.; Wang, Y.; Takahashi, K.; Cao, G. Z.; Li, D.; Xia, Y. N. *J Mat. Sci.* **2005**, 40, 3587.
5. Shang, H. M.; Wang, Y.; Limmer, S. J.; Chou, T. P.; Takahashi, K.; Cao, G. Z. *Thin Solid Films* **2005**, 472, 37.
6. Aussillous, P.; Quéré, D. *Nature* **2001**, 311, 924.
7. Shastry, A.; Case, M. J.; Böhringer, K. F. *Langmuir* **2006**, 22, 6161.
8. Shikida, M.; Ando, M.; Ishihara, Y.; Ando, T.; Sato, K.; Asaumi, K. *J. Micromech. Microeng.* **2004**, 14, 1462.
9. Ren, S.; Yang, S.; Zhao, Y.; Yu, T.; Xiao, X. *Surface Sci.* **2003**, 546, 64.
10. Ren, S.; Yang, S.; Zhao, Y. *Acta Mechanica Sinica* **2004**, 20, 159.
11. Zhai, L.; Berg, M. C.; Cebeci, F. Ç.; Kim, Y.; Milwid, J. M.; Rubner, M. F.; Cohen, R. E. *Nano Lett.* **2006**, 6, 1213.
12. Choi, C.-H.; Ulmanella, U.; Kim, J.; Ho, C.-M.; Kim, C.-J. *Phys. Fluids* **2006**, 18, 087105.

13. Fukagata, K.; Kasagi, N.; Kououtsakos, P. *Phys. Fluids* **2006**, 18, 051703.

14. Gogte, S.; Vorobieff, P.; Truesdell, R.; Mammoli, A.; van Swol, F.; Shah, P.; Brinker, C. J. *Phys. Fluids* **2005**, 17, 051701.

15. Mamur, A. *Langmuir* **2006**, 22, 1400.

16. Ou, J.; Rothstein, J. P. *Phys. Fluids* **2005**, 17, 103606.

17. Extrand C.W. *Langmuir* **2004**, 20, 5013.

18. Extrand C.W. *Langmuir* **2005**, 21, 10370.

19. Extrand C.W. *Langmuir* **2006**, 22, 1711.

20. Li, W.; Amirfazli, A. *Adv. Colloid Interface Sci.* **2007**, 132, 51, 2007.

21. Mohammadi, R.; Wassink, K.; Amirfazli, A. *Langmuir* **2004**, 20, 9657.

22. Shirtcliffe, N. J.; McHale, G.; Newton, M. I.; Perry, C. C.; Roach, P. *Mat. Chem. Phys.* **2007**, 103, 112.

23. Shibuichi, S.; Onda, T.; Satoh, N.; Tsujii; K. *J. Phys. Chem.* **1996**, 100, 19512.

24. Rao, A. V.; Hegde, N. D.; Hirashima, H. *J. Colloid Interface Sci.* **2007**, 205, 124.

25. Fujita, M.; Muramatsu, H.; Fujihira, M. *Japanese J. App. Phys.* **2005**, 44, 6726.

26. Shibuichi, S.; Yamamoto, T.; Onda, T.; Tsujii, K. *J. Colloid Interface Sci.* **1998**, 208, 287.

27. Chen, W.; Fadeev, Y.; Hsieh, M. C.; Öner, D.; Youngblood, J.; McCarthy, T. J. *Langmuir* **1999**, 15, 3395.

28. Ferrari, M.; Ravera, F.; Rao, S.; Liggieri, L. *App. Phys. Lett.* **2006**, 89, 053104.

29. Wenzel, R. N. *J. Ind. Eng. Chem.* **1936**, 28, 988.

30. Cassie, A. B. D.; Baxter, S. *Trans. Faraday Soc.* **1944**, 40, 546.

31. Pierce, E.; Carmona, F. J.; Amirfazli, A. *Colloids and Surfaces A: Physicochemical and Engineering Aspects* **In Press**, DOI: 10.10161/j.colsurfa.2007.09.032.

32. Hennig, A.; Grundke, K.; Frenzel, R.; Stamm, M. *Tenside Surf. Det.* **2002**, 29, 243.

33. Kumar, N.; Varanasi, K.; Tilton, R. D.; Garoff, S. *Langmuir* **2003**, 19, 5366.

34. Starov, V. M.; Kosvintsev, S. R.; Velarde, M. G. *J. Colloid Interface Sci.* **2000**, 227, 185.

35. Starov, V. M. *J. Colloid Interface Sci.* **2004**, 270, 180.

36. Varanasi, K. S.; Garoff, S. *Langmuir* **2005**, 21, 9932.

37. Dutschk V.; Sabbatovskiy, K. G.; Stolz, M.; Grundke, K.; Rudoy, V. M. *J. Colloid Interface Sci.* **2003**, 267, 456.

38. Decker, E. L.; Garoff, S. *Langmuir* **1997**, 13, 6321.

39. Jarvis, N. L.; Zisman, W. A. *Report of NRL Progress* **1965**, Sept., 1.

40. Hoorfar, M., Neumann, A. W. *J. Adhesion* **2004**, 80, 727.

41. Kwok, D. Y.; Neumann, A. W. *Adv. Colloid Interface Sci.* **1999**, 81, 167.

42. Jeong, H. E.; Lee, S. H.; Kim, J. K.; Suh, K. Y.; *Langmuir* **2006**, 22, 1640.

43. Herminghaus, S. *Euro. Phys. Lett.* **2000**, 52, 165.

44. Yu, L. M. Y.; Lu, J. J.; Chan, Y. W.; Ng, A.; Zhang, L.; Hoorfar, M.; Policova, Z.; Grundke, K.; Neumann, A. W. *J. Appl. Physiol.* **2004**, 97, 704.

Chapter 4 - Summary, Conclusions, and Future Directions

Wetting was compared on seven surfaces for four pure liquids of various surface tensions (~27-73 mN/m) and nine surfactant solutions (used to model impure liquid) of various polarities. One fluorinated hydrocarbon surface and one saturated hydrocarbon surface were smooth coatings on silicon wafer. The other five superhydrophobic surfaces (SHS) were electrochemically etched aluminum (fluorinated and saturated, i.e. CH_3/CH_2 chemistries), plasma etched PTFE (fluorinated chemistry) and naturally rough alkyl ketene dimer (AKD, semi-fluorinated and uncoated, saturated chemistries). Wetting depends on the effects of topography and liquid chemistry/purity, as well as the surface chemistry (which can modify the effects of topography).

Saturated hydrocarbon chemistry (CH_3/CH_2) generally shows intrinsic contact angle (measured on coated silicon) ~10° lower than fluorinated chemistry, for all liquids/solutions. SHS pure liquid advancing contact angles remained high for intrinsic contact angles above 90°. Below 90°, advancing contact angle depends strongly on surface topography type and chemistry. PTFE and aluminum fluorinated surfaces give contact angles above 120° for intrinsic contact angles below 90°, due to 'metastable' Cassie wetting. Fluorinated aluminum gives the highest contact angles, understood as the result of its overhanging dual-scale topography. PTFE gives the next highest contact angles. Saturated hydrocarbon aluminum shows a 'metastable' Cassie state for ethylene glycol, but an abrupt drop to

lower contact angles signaling the Wenzel state for lower intrinsic contact angle pure liquids. This shows that the topographic benefits to repellency of pure liquids can be overruled by an unsuitable chemistry. The plate-like microstructure of uncoated and semifluorinated AKD shows similar behavior to the saturated hydrocarbon aluminum with similar explanations.

Receding angle is dependant on chemistry and topography. For saturated hydrocarbon (or semi-fluorinated) chemistry, zero receding contact angle is seen with all pure liquids on AKD (and solutions, a correction to previous work [1]) and all non-aqueous pure liquids on aluminum. For fluorinated chemistries the lower roughness dual-scale aluminum samples give higher, Cassie state receding contact angles compared to the higher roughness single-scale PTFE samples, for pure liquids of surface tension above ~45 mN/m (intrinsic contact angle above 90°). For intrinsic contact angle less than 90°, however, all rough surfaces show zero receding contact angle. Zero receding contact angle is understood as the result of the Wenzel wetting state during the recede. The Wenzel state could be triggered by contact line pinning by heterogeneities and topography causing intrinsic contact angles slightly above 90° to decrease to below 90° during the receding phase.

On smooth hydrophobic surfaces of either chemistry, surfactant solutions show similar contact angles to pure liquids of similar surface tension for

surface tension above ~45 mN/m. Otherwise, surfactant solutions show contact angles greater than those for pure liquids. This type of comparative test on a smooth hydrophobic surface is unreported to date, and the somewhat surprising results on two different surfaces question how autophilicity [2-5] affects wetting by solutions versus pure liquids.

As before [1] surfactant solutions show higher advancing contact angles than pure liquids of similar surface tension on all five SHS. Increased intrinsic contact angle cannot alone explain the higher values but surfactant films inhibiting penetration of solution into the pores and crevices of the SHS (along with the increased intrinsic contact angle) can. Surfactant film stretching and re-self-assembly pinning the contact line may also explain differences seen in the receding behavior of high concentration (low intrinsic contact angle) solutions, but this bears more investigation. Fluorinated aluminum shows the highest advancing contact angle with solutions, but follows the receding behavior of pure liquids (zero for surface tensions below ~45 mN/m). PTFE shows advancing contact angles near those on aluminum, and hydrophobic receding contact angles for some surfactant solutions of surface tensions less than 45 mN/m (receding smooth surface contact angles less than 90° and intrinsic contact angle, i.e. advancing smooth surface contact angle, slightly above 90°). Saturated hydrocarbon aluminum also shows high receding contact angles with some solutions of intrinsic contact angle only slightly above 90°, and zero for other surfactant solutions of similar intrinsic contact

angle and higher surface tension. For both PTFE and OTS coated aluminum, the zero receding contact angle was seen for solutions of HTAB. This suggests that surfactant polarity could play some role in the receding behavior of SHS (possibly manifested in intrinsic contact angle). In most tests however, surfactant polarity was seen to have little effect on the wetting of hydrophobic smooth surfaces or SHS.

Industrial applications must take into account the type of liquid expected, and the level of liquid impurities, as well as the desired wetting behavior. Based on this information, the proper choice of surface topography and chemistry can be made.

4.1 Future Directions

The results of this thesis can be applied and furthered in many ways in the future.

For industrial applications, lessons learned from this thesis suggest that to try to make a SHS repellent for both pure and impure liquids, one could construct a dual-scale surface of sharp features and test if this topography gave repellency for all liquid/solutions. A combination of sharp and bumpy features might also combine the repellent behaviors seen in the aluminum and PTFE samples. To broaden the application of surfactant solution and pure liquid wetting tests on SHS, they should be repeated using other metrics of wettability (e.g. drop impact behavior and drop

adhesion/necessary force for removal by tilting or airflow), to determine if the wetting trends are repeated in more dynamic environments.

For academe, two simple (but possibly time consuming) projects can be started immediately. The first is to pre-treat surfaces with various surfactants to see what effect surfactant adsorption on the solid has on the wetting. The second, considering the results of surfactant solution and pure liquid wetting on smooth surfaces, is to conduct theoretical investigations of surfactant solution interactions on smooth surfaces with an eye toward the comparative wetting by pure liquids and the application of results to rough surfaces. Theoretical investigations might even be possible for ordered topographies, similar to what has been done for pure liquids [6].

On two SHS, HTAB solutions were seen to show somewhat different receding behavior from SDS (and sometimes MEGA 10) solutions. This difference suggests some effect of surfactant polarity, but bears more study to see if the results are repeated on other surfaces, and to determine the mechanism for the effect. Two possible experiments to investigate these questions are suggested below.

In Chapter 2 it was shown that the fluorination of AKD was incomplete, which led to wetting results were quite similar to those on uncoated AKD. This makes it difficult to draw conclusions as to the effect of chemistry on

wetting for this topography. It would thus be interesting to completely fluorinate the AKD surface (either by better coating techniques, or transfer of the AKD topography to PTFE by microfabrication techniques). Depending on the receding contact angles found on the fluorinated AKD topography, chemical or topographical reasons for the zero receding contact angle on uncoated AKD would be determined, and differences (if any) in the receding behavior with HTAB versus other surfactants could also be examined.

Likewise, the topography of PTFE showed interesting results in Chapter 2, especially during the receding phase with high surfactant concentration (low intrinsic contact angle). Some surfactant solutions (HTAB and MEGA 10 maximum concentration) showed zero receding contact angle, whereas solutions of SDS and less concentrated MEGA 10 showed reduced but non-zero contact angle for similar or lower surface tension. If the topography of the PTFE could be given a saturated hydrocarbon coating, it would be interesting to see if/how the receding behavior with surfactant solutions is changed, to examine the effects of chemistry on receding contact angle and to examine surfactant polarity/concentration effects.

Testing of fully fluorinated AKD, and saturated hydrocarbon coated PTFE surfaces would complete the matrix of topography – chemistry – probe liquid combinations tested in this thesis. This would allow one to see if the hypotheses formed in this thesis hold. Other topographies (especially more

ordered ones created by lithography etc.) and chemistries could also be added to the testing matrix, to further try the hypotheses and compare to the theoretical investigation described above. Other impurities (other surfactants, salt, etc) in water or other pure liquids could be used to expand the application of the tests conducted in this thesis.

To directly probe the question of how surfactant solutions give higher contact angles than pure liquids on SHS, three tests are envisioned. If tracers (fluorescent or otherwise) can be added to the solutions, it may be possible to visualize the interface under the drop, and potentially answer if/how surfactants are preventing penetration. It may also be possible to directly probe the interface under the drop by immersion AFM techniques. Finally, a parabolic flight has been scheduled to test SHS of simplified topography with surfactants and pure liquids. The reduced gravity allows the topography scale to be enlarged. It is hoped that the visualization techniques employable for these larger structures will allow direct observation of surfactant effects at the air-liquid interface under the drop.

References

1. Mohammadi, R.; Wassink, K.; Amirfazli, A. *Langmuir* **2004**, 20, 9657.
2. Starov, V. M.; Kosvintsev, S. R.; Velarde, M. G. *J. Colloid Interface Sci.* **2000**, 227, 185.
3. Starov, V. M. *J. Colloid Interface Sci.* **2004**, 270, 180.
4. Kumar, N.; Varanasi, K.; Tilton, R. D.; Garoff, S. *Langmuir* **2003**, 19, 5366.
5. Varanasi, K. S.; Garoff, S. *Langmuir* **2005**, 21, 9932.
6. Li, W.; Amirfazli, A. *Adv. Colloid Interface Sci.* **2007**, 132, 51, 2007.

Appendix A: Experimental Details

Glassware Cleaning

All glassware was cleaned before and after use with chromosulphuric acid in the following manner. First, the glassware was cleaned of particles and impurities visible to the naked eye, using ethanol, water, and paper towels. The final rinse should be with water to avoid spoiling the acid by reaction with excessive organic contamination. Once the glasswear appeared clean it was submerged in chromosulphuric acid. All acid work was performed under a fume hood, wearing a lab coat and gloves. Smaller items, such as syringe barrels or small beakers, were placed within larger beakers, and full strength chromosulphuric acid was poured over them. The larger beakers were filled nearly to the brim and covered with kitchen grade aluminum foil. The beakers were placed in a larger Pyrex™ casserole dish to contain possible spills and the entire set was left inside the fume hood. Glassware was left for at least six hours, often 12 or 16 hours. Following this time, the acid was poured back into its jug. If the acid in an individual beaker had lost potency (denoted by a color change from dark orange/brown to green) the spoiled acid was poured into acid waste and the glassware was cleaned again. Residual acid was rinsed out of the glassware into acid waste using one or two rinses with distilled, de-ionized (DI) water. Subsequent to this, each piece of glassware was filled partially with DI water and agitated by hand for at least 10 seconds. The end of the beakers were covered with a clean gloved hand to allow vigorous water motion across all surfaces of the glass to remove residual acid. This rinsing

was conducted three times. Glassware was then dried either under a heat lamp or in a vacuum chamber (de-pressurized to 0.1 inHg for all drying purposes described in this thesis). Once dry, the glassware was once again covered in aluminum foil until use.

Syringe Cleaning

The syringe used in wetting tests was cleaned in the following way. First the syringe was filled and purged with DI water 10 times. Next, the syringe barrel was cleaned in chromosulphuric acid as described above. The other parts of the syringe (plunger, blunt needle, screw cap and any other connections) could not be cleaned in acid because they would react. The Teflon™ insert of the needle was not cleaned in acid because it was too small and would likely be lost in the cleaning process. After cleaning and rinsing the syringe barrel, all parts of the syringe were placed in a graduated cylinder and submerged in ethanol. The cylinder was covered and placed in a running ultrasonic bath for 30 minutes. The ethanol was then drained, the pieces of the syringe rinsed with DI water, and dried either under a heat lamp or in a vacuum chamber. Once dry, the syringe (with needle) was assembled and wrapped in aluminum foil.

Syringe Use in Surfactant Solution Tests

The syringe was cleaned with chromosulphuric acid and ethanol as described above before and after each set of tests using surfactant solutions. For a given surfactant test (e.g. the three concentrations of SDS)

the syringe was used in the following way. If wettability tests were being conducted with DI water, these would be conducted first. After this, the syringe would be filled and purged 10 times with DI water, and then filled and purged with room air several times to dry the inside of the barrel (drying under a heat lamp or in a vacuum oven is recommended, but was not generally done). Next, the lowest concentration of the surfactant under test was drawn into the syringe. Wettability tests were conducted with this liquid, after which the syringe was filled and purged with water and dried with air as described above in this paragraph. Next the second lowest concentration of the surfactant under test was drawn into the syringe and used for testing. This process of rinsing with DI water and testing with the next highest concentration was continued until all concentrations of a given surfactant were tested. After this, the syringe would be rinsed once more, then disassembled and cleaned with chromosulphuric acid and ethanol as described above.

Syringe Use in Non-Aqueous Pure Liquid Tests

The syringe was cleaned with chromosulphuric acid and ethanol as described above before and after each set of tests with pure liquids. For pure liquid tests the syringe was used in the following way. Note that wettability tests with water were conducted during the tests with surfactant solutions, as described in the previous section. This was done to ensure that the non-aquesous pure liquids would not be contaminated with residual water. So, the syringe was first filled with ethylene glycol,

and used for wettability tests. The syringe was then filled and purged with acetone 10 times, disassembled and placed in a graduated cylinder filled with acetone. The cylinder was covered and placed in a running ultrasonic bath for 30 minutes. The acetone was then drained, the pieces of the syringe rinsed with DI water, and dried either under a heat lamp or in a vacuum chamber. Once dry, the syringe was assembled and filled with hexadecane and used for wettability tests. After this, the cleaning procedure of acetone purge followed by acetone sonication, water rinse and drying was repeated. Finally, the syringe was filled with bromonaphthalene and wetting tests were conducted. After this, the syringe was cleaned once more in the manner described above in this paragraph, then (before drying) it was cleaned with chromosulphuric acid and ethanol as described above.

Pre-Wetting Test Preparation

Before each wetting test with a given liquid, the syringe was cleaned following the applicable procedure described above and then filled with the liquid under test. If the liquid was a surfactant solution, it was placed in a running ultrasonic bath for 10 minutes to ensure a well mixed state before being drawn into the syringe. To fill the needle, it was submerged in the liquid and the plunger drawn back to fill the barrel. Generally, this resulted in a mixture of liquid and trapped air in the syringe. If this was the case, the syringe would be inverted, tapped to bring the bubbles to the top of the liquid column (near the needle), and the plunger would be

driven in to purge the trapped air. The syringe would then be refilled to recover the lost volume, and the process of purging and refilling would continue until a sufficient volume of liquid was in the syringe.

If the liquid was of a sufficiently low surface tension it sometimes drained through the gap between the needle and the hole in the surface during a wetting test. If this occurred, the syringe was removed and the needle dried with a fresh Kimwipe (a commercially available lint free wipe). The needle would then be wrapped in Teflon™ tape, starting from the metal screw cap and proceeding up the needle to cover the entire edge of the needle without obstructing the tip. This served two purposes. First, it decreased the gap between the needle and the hole in the surface. Second, it decreased the surface energy of the needle. These combined effects prevented the low surface tension liquid from draining through the gap between the needle and the hole in the surface, allowing wettability tests to proceed as described above.

Generally, the start of a wettability test involves the fast growth of a small (<15 μl) drop on the surface. This is because the initial phases of drop growth is not thermodynamically relevant as the drop radius is of the same order size as the hole radius. Usually, the initial growth was driven from the mounted syringe. Sometimes, for given surfaces, this proved difficult. If slight heterogeneities exist near the hole edge, the drop can grow in one direction only, having an edge on the edge of the hole, which is undesirable

because the contact line will thus be locally constrained by the hole. If this was the case, the drop was immediately removed by wicking it vertically off the surface with a clean Kimwipe. The surface was then blown dry with nitrogen and a drop of the same liquid was placed by hand using a pipetter, forming a seed drop of <15 μl. This generally resulted in a drop with a lower contact angle (due to vibration of the hand). In this case, the measurements of contact angle were disregarded until the drop grew enough for the contact line to advance.

Surface Tension Measurements

Surface tension was measured in one of two ways. At the Leibniz Institute of Polymer Research, Dresden, Germany (IPF) measurements were conducted for surfactant solutions on a SITA science line t60 tensiometer. This machine measures surface tension by measuring bubble pressure. A capillary was submerged under a dish filled with the surfactant solution to be tested. Air was pumped through the capillary to form bubbles at the capillary tip. The machine recorded maximum bubble pressure (reached when the bubble forms a half sphere on the tip). From this, the surface tension of the liquid can be calculated based upon Laplace's equation of capillarity:

$$\Delta P = \gamma\left(1/r_1 + 1/r_2\right)$$

where ΔP is the difference in pressure across the curved air/liquid interface of the bubble, γ is the unknown surface tension, and r_1 and r_2 are

the radii of curvature of the air/liquid interface (equal to each other and to the capillary radius for the instrument's measurement technique).

Prior to testing, each surfactant solution was mixed by submersion in an ultrasonic bath of water for at least 10 minutes. The machine was run as follows. The capillary tip was cleaned by running air through it into a clean dish of DI water for a minute. The capillary was then raised, wiped dry with a clean Kimwipe and lowered back into the DI water to run for another minute. The capillary was then raised, wiped dry as before with a fresh Kimwipe and the dish was then replaced with a new, clean dish of the lowest concentration of a given surfactant. The capillary was lowered into the surfactant solution and run with a bubble life of approximately 2 seconds (the bubble was controlled to remain in its hemispherical state on the capillary tip for 2 seconds, to observe changes in surface tension due to possible further adsorption of surfactant onto the interface). At least ten measurements were made and then the capillary was raised out of the liquid and wiped dry. The dish was then emptied, rinsed with DI water, wiped dry and filled with the next highest concentration of the same surfactant solution. The measurement process, rinsing, drying, and refilling were repeated for all concentrations of a given surfactant. A new, clean dish was used for each different surfactant type and the capillary tip was cleaned with DI water as described above between measurement of each surfactant type. Temperature of the liquid was, on average 23.2 °C with a standard deviation of 0.7 °C. Surface tension measurements were

averaged for each surfactant concentration and are reported with standard deviation in the text of this thesis.

In Edmonton, surface tension was measured by means of pendant drop analysis, using a First Ten Angstroms FTA-200 dynamic tensiometer. This machine is composed of an inverted disposable syringe with a stainless steel needle attached to the end and mounted to a syringe pump. The syringe is filled with the liquid to be tested, and the pump drives the liquid out until it hangs from the end of the needle but is deformed by gravity (as a tear-drop instead of a spherical shape). The drop is held in this position and imaged by a CCD camera (the drop is back-lit). The drop images are edge fitted and each resulting edge is fitted to a series of polynomials. This analytic equation is used to solve the Laplace equation of capillarity (with the assumption that the drop is axisymmetric about the vertical).

Before calibration and tests with the FTA200, each syringe and needle was dismantled and cleaned by submersion in a covered acetone bath for 30 minutes. Following this, the pieces were rinsed with DI water three times, and dried in a vacuum chamber. The syringes and needles were then reassembled with gloved hands and wrapped in aluminum foil until the surface tension test was made. Prior to testing, each surfactant solution was mixed by submersion in an ultrasonic bath of water for at least 10 minutes. Each surfactant solution was loaded into a separate syringe and mounted in the machine, and one syringe was filled with DI water for

calibration purposes. The machine was operated in the manner described above and each drop was held for about 1 minute, with ~30 images taken of the drop at 2 second intervals. This was to investigate possible time dependent surfactant effects on the surface tension. After this the pump was advanced to detach the drop and run to force another drop out of the syringe until it also dropped. After this, another drop was formed on the syringe and the measurement was made on this drop, giving another ~30 data points. The process of advancing the pump and making another measurement was repeated, to give 3 separate drops with ~30 data points taken for each.

The images of the water test were used to fine tune the magnification calibration of the images. The machine was first calibrated by measuring the needle radius with a digital caliper. The needle was also measured by the machine using edge finding and the internal base calibration. The two measurements were input into the machine to calibrate it. This process was repeated several times yielding successively better calibrations. After the process was complete the surface tension of water was measured on three drops, taking a total of 90 data points. These measurements were averaged and resulted in a value of 73.4 mN/m at approximately 23°C. This measurement and the standard surface tension for water where then input into the machine to fine tune the magnification calibration. The calibration in this final step was changed by only 0.75%, signifying that the initial magnification calibration was very accurate.

After calibration, each of the surfactant drop datasets were analyzed by the machine and the resultant surface tensions averaged and reported with standard deviations.

Surfactant Mixing

Surfactants were mixed in the following manner. A sealed flask was cleaned in chromosulphuric acid as described in the section above on glassware cleaning. After drying the flask, a microbalance was used to measure the required amount of surfactant for the flask volume onto either a glass measuring funnel (in Dresden) or a piece of weighing paper (in Edmonton). This surfactant was carefully washed into the flask with DI water and the flask was filled with DI water to its marked volume. The surfactant solution was then mixed by submersion in an ultrasonic bath of water for at least 10 minutes. In Table A-1, below, nominal concentration, nominal mass for nominal concentration, actual mass measured, actual concentration based on actual mass, and resultant measured surface tension are reported for each surfactant solution used. Standard deviation of surface tension is reported in parenthesis.

Table A-1: Results of surfactant mixing procedure.

Surfactant Type	Nominal Conc. (mM)	Nominal Mass (g)	Actual Mass (g)	Actual Conc. (mM)	Surface Tension (mN/m)
SDS [D]	1	-	-	-	65.8 (0.12)
SDS [D]	4	-	-	-	50.9 (0.06)
SDS [D]	8	0.230704	0.2307	7.99986	38.0 (0.06)
HTAB [D]	0.1	0.0036445	0.0036	0.098779	68.8 (0.14)
HTAB [D]	0.2	0.007289	0.0073	0.2003	66.8 (0.07) 66.9 (0.11)
HTAB [D]	1	0.036445	0.0364	0.99877	39.8 (0.07)
MEGA 10 [D]	0.5	0.0087365	0.0087	0.49791	59.4 (0.13)
MEGA 10 [D]	2	0.034946	0.0349	1.99737	44.7 (0.09)
MEGA 10 [D]	9	0.157257	0.1573	9.00246	30.3 (0.11)
SDS [R]	1	-	-	-	53.0 (0.43)
SDS [R]	4	-	-	-	40.6 (0.94)
SDS [R]	8	-	-	-	36.2 (0.33)
SDS [A]	1	-	-	-	67.3 (0.51)
SDS [A]	2	-	-	-	59.9 (0.97)
SDS [A]	4	-	-	-	49.9 (0.96)
SDS [A]	8	0.230704	0.2318	8.03801	37.1 (0.39)
HTAB [R]	0.1	-	-	-	62.5 (0.41)

HTAB [R]	0.2	-	-	-	56.1 (1.46)
HTAB [R]	1	-	-	-	37.5 (0.23)
MEGA 10 [R]	1	-	-	-	46.0 (0.56)
MEGA 10 [A] June	2	0.0349	0.0352	2.01454	40.1 (0.73)
MEGA 10 [A] Jan	2	-	-	-	41.0 (0.54)
MEGA 10 [A] Jan	9	0.157257	0.1571	8.99101	30.5 (0.53)

D = Surfactant solution mixed and used in Dresden
R = Surfactant solution mixed by Reza Mohammadi in Edmonton for his previous work and reused in the present thesis
A = Surfactant solution mixed by Andrew Milne in Edmonton for testing in the present thesis due to concerns with contamination of solutions mixed by Reza Mohammadi (concerns raised by observed foreign material in surfactant solutions). Contaminated solutions were not used in any wetting tests.
Conc. = Concentration
June = Mixed June 2007 (to replace mixture made in January 2007)
Jan = Mixed January 2007

Mass and concentration data are missing for surfactants mixed by Reza Mohammadi. Surface tension measurements were performed to ensure that solutions were still approximately the correct concentration. Where mass and concentration data are otherwise missing the surfactant solutions were made by diluting a higher concentration surfactant solution by the appropriate amount of DI water.

The surface tension of HTAB 0.1 mM and HTAB 0.2 mM mixed in Dresden was found to be too high and too similar. HTAB 0.2 mM mixed by Reza Mohammadi was used in the place of HTAB 0.2 mM mixed in Dresden by testing on extra fluorinated aluminum samples brought back from Dresden to Edmonton.

Contact Angle Testing Apparatus

Below is a picture and schematic of the apparatus used in Edmonton for contact angle measurements. In Dresden an apparatus of the same schematic layout was used.

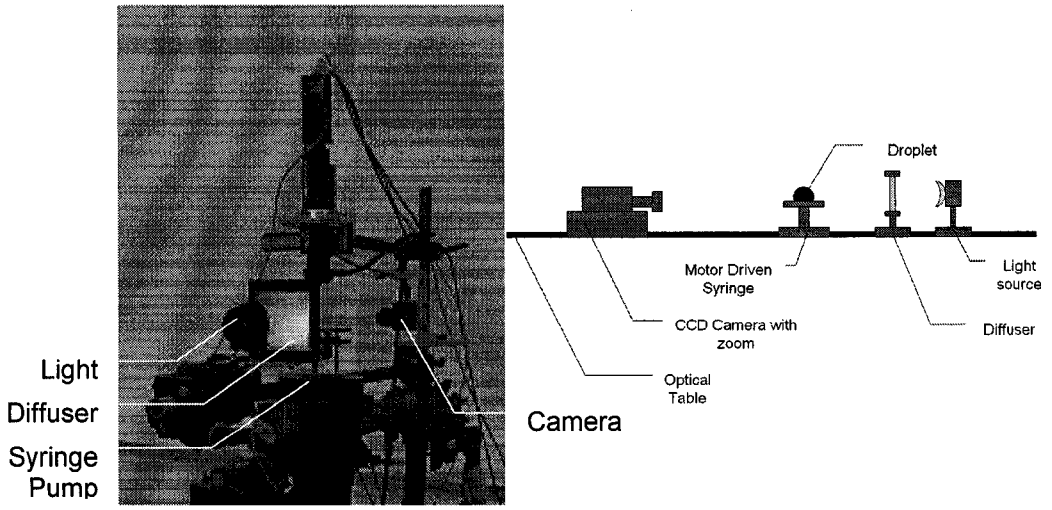

Figure A-1: Picture and schematic of wetting apparatus setup, showing light, diffuser, drop stage, and camera in their relative positions.

XPS Spectra

Below are representative XPS spectra taken for the surfaces under test in this thesis.

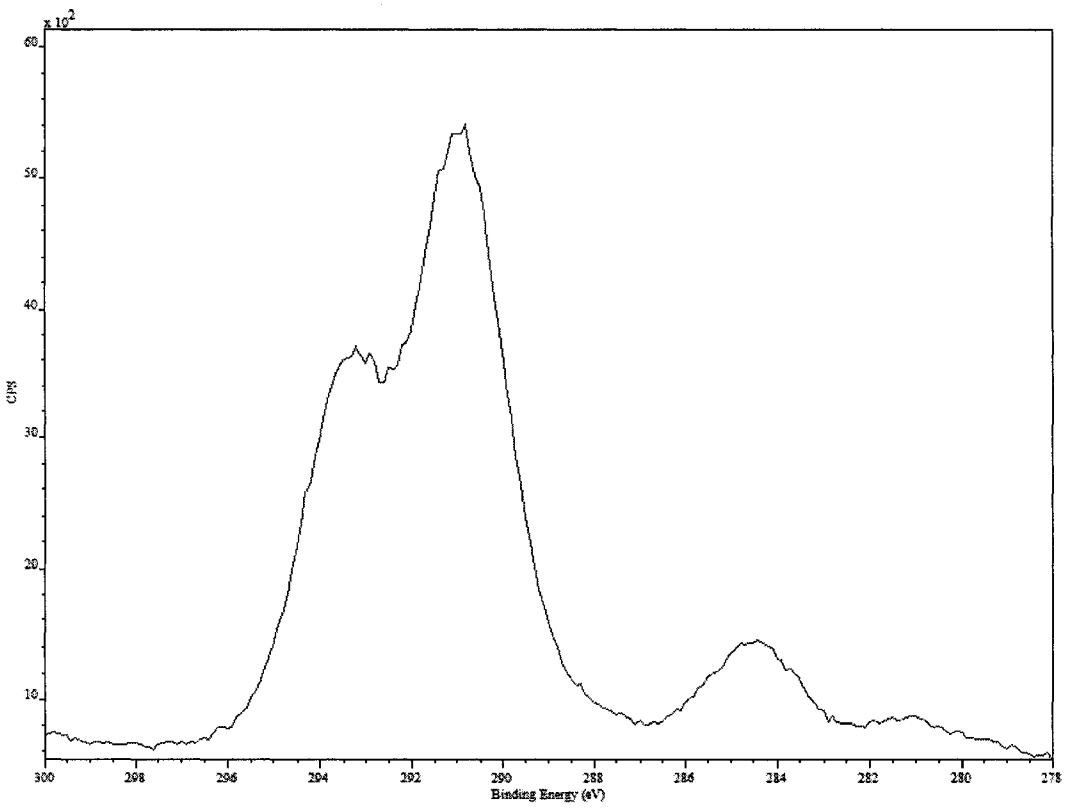

Figure A-2: XPS spectrum of Teflon™ coated silicon wafer. Counts per second (ranging from $6*10^2$ to $60*10^2$) is plotted against binding energy (eV) (ranging from 300 to 278 eV). This spectrum generated by the Alberta Centre for Surface Engineering Science, at the University of Alberta.

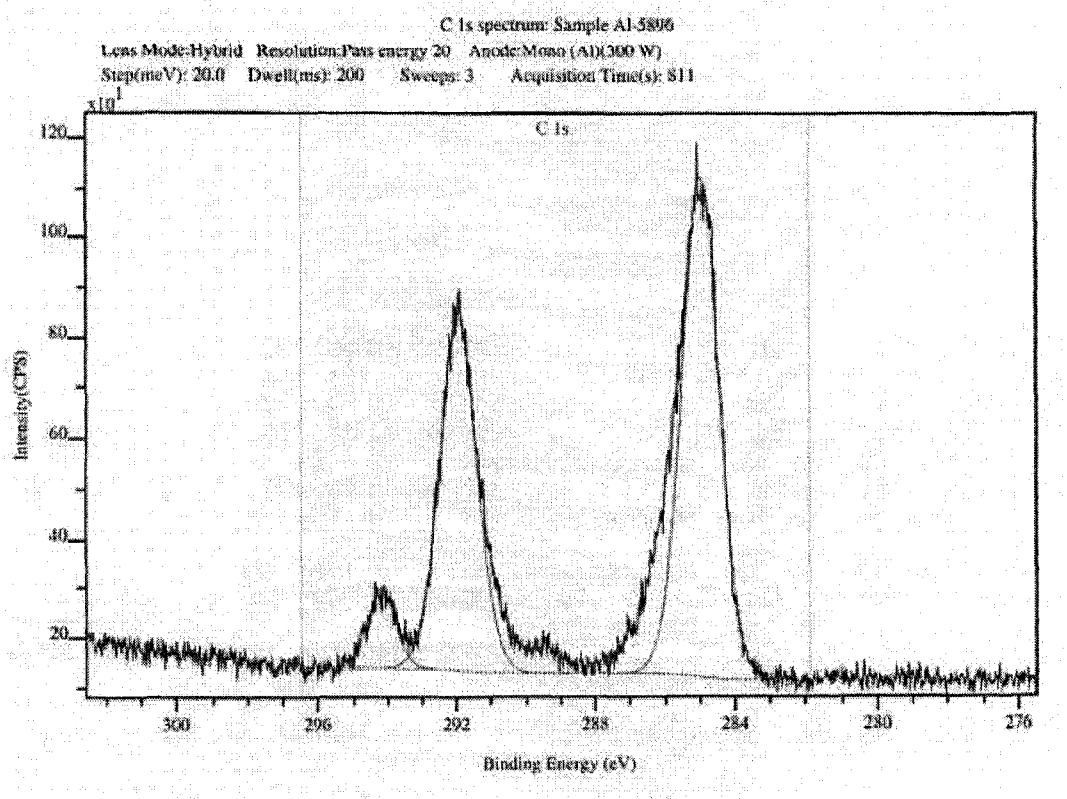

Figure A-3: XPS spectrum of fluorinated aluminum. Counts per second (ranging from $10*10^1$ to $120*10^1$) is plotted against binding energy (eV) (ranging from 302 to 276 eV). This spectrum generated by scientists at the Leibniz Institute of Polymer Research, in Dresden, Germany.

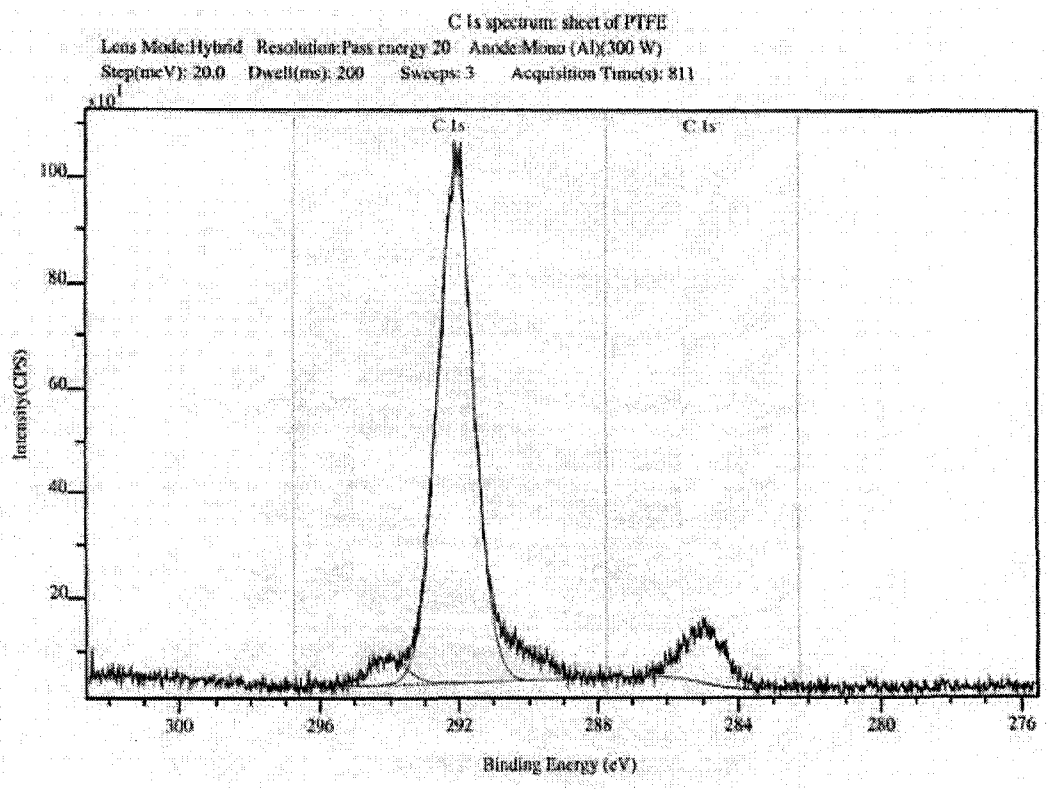

Figure A-4: XPS spectrum of uncoated PTFE. Counts per second (ranging from 0 to $110*10^1$) is plotted against binding energy (eV) (ranging from 302 to 276 eV). This spectrum generated by scientists at the Leibniz Institute of Polymer Research, in Dresden, Germany.

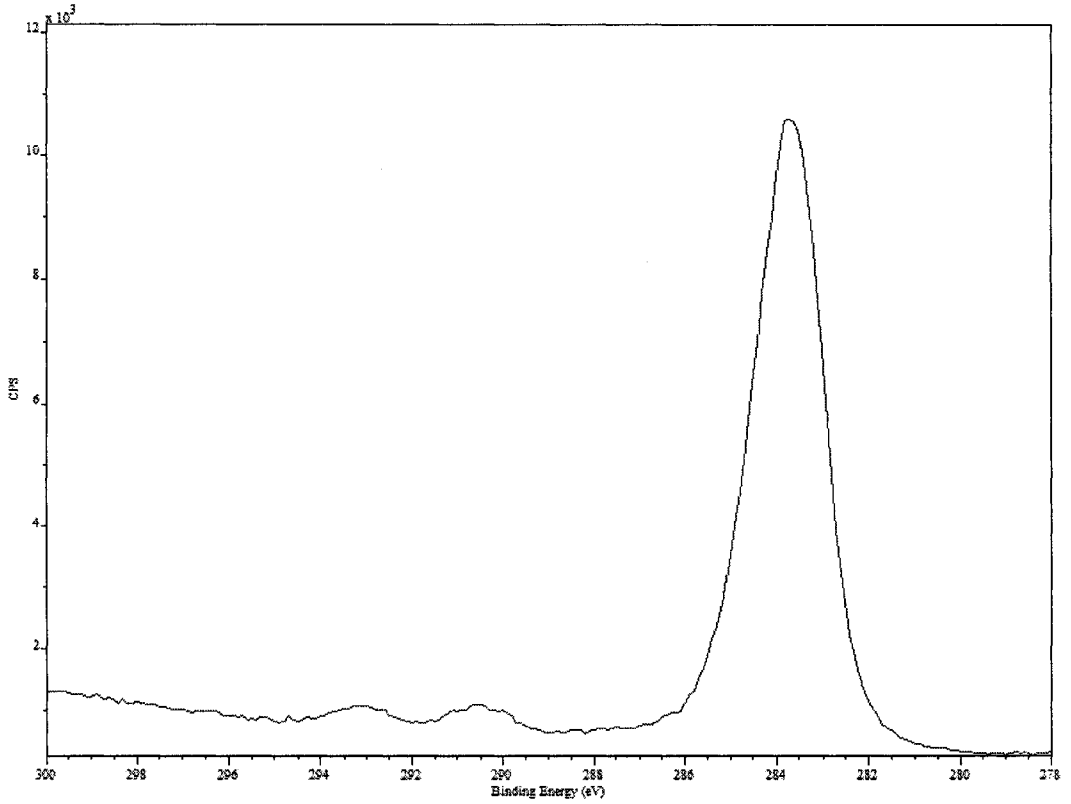

Figure A-5: XPS spectrum of Teflon™ coated AKD. Counts per second (ranging from 0 to $12*10^3$) is plotted against binding energy (eV) (ranging from 300 to 278 eV). This spectrum generated by the Alberta Centre for Surface Engineering Science, at the University of Alberta.

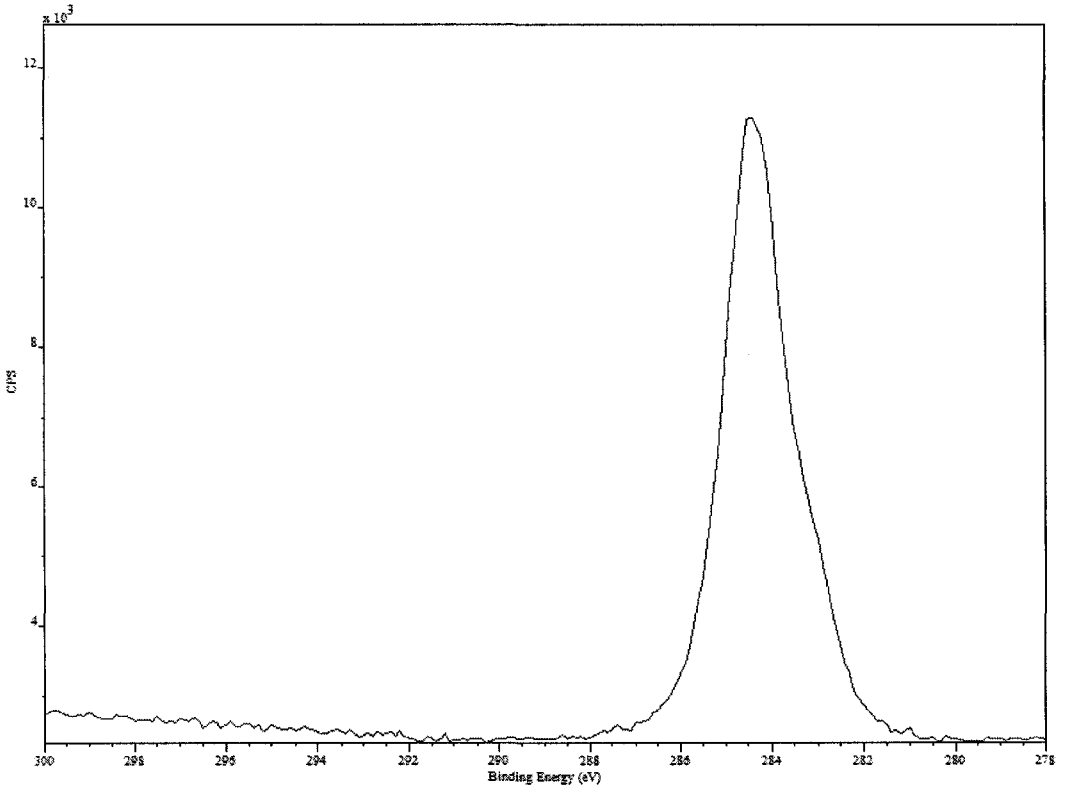

Figure A-6: XPS spectrum of OTS coated silicon wafer. Counts per second (ranging from $2*10^3$ to $12*10^3$) is plotted against binding energy (eV) (ranging from 300 to 278 eV). This spectrum generated by the Alberta Centre for Surface Engineering Science, at the University of Alberta.

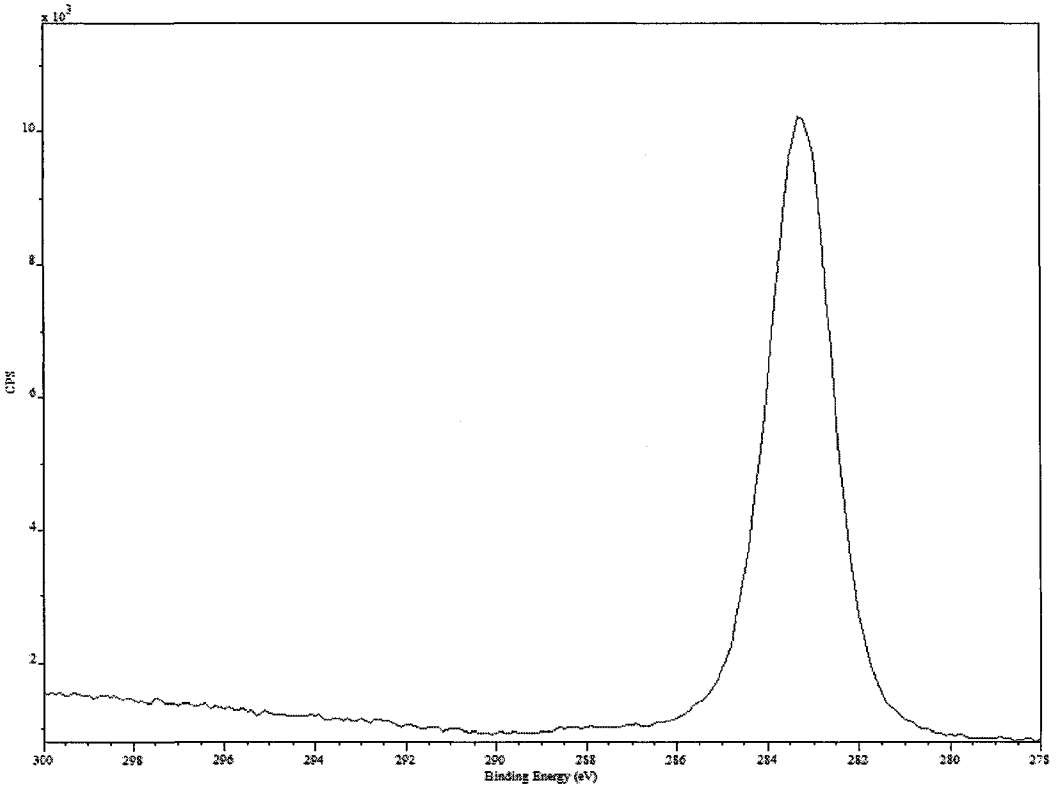

Figure A-7: XPS spectrum of OTS coated aluminum. Counts per second (ranging from $1*10^3$ to $12*10^3$) is plotted against binding energy (eV) (ranging from 300 to 278 eV). This spectrum generated by the Alberta Centre for Surface Engineering Science, at the University of Alberta.

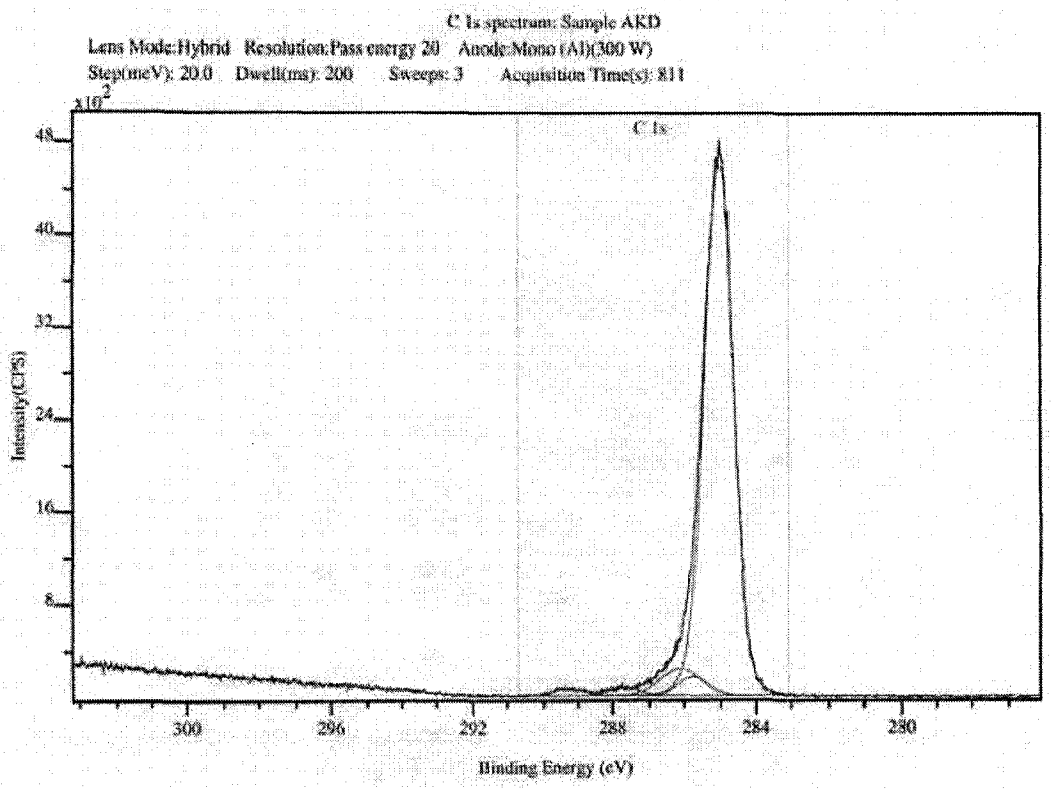

Figure A-8: XPS spectrum of uncoated AKD. Counts per second (ranging from 0 to $48*10^2$) is plotted against binding energy (eV) (ranging from 302 to 276 eV). This spectrum generated by scientists at the Leibniz Institute of Polymer Research, in Dresden, Germany.